SYNTHESIS, PHYSICOCHEMICAL CHARACTERIZATION, AND BIOSENSING APPLICATIONS OF GOLD NANOPARTICLES

A Thesis Submitted to
the Graduate School of Engineering and Sciences of
İzmir Institute of Technology
in Partial Fulfillment of the Requirements for the Degree of

DOCTOR OF PHILOSOPHY

in Chemistry

by
Melek ÜÇÜNCÜ

April 2018
İZMİR

We approve the thesis of **Melek ÜÇÜNCÜ**

Examining Committee Members:

Prof. Dr. Serdar ÖZÇELİK
Department of Chemistry, İzmir Institute of Technology

Prof. Dr. Muhsin ÇİFTCİOĞLU
Department of Chemical Engineering, İzmir Institute of Technology

Prof. Dr. Suna TİMUR
Department of Biochemistry, Ege University

Prof. Dr. Ali ÇAĞIR
Department of Chemistry, İzmir Institute of Technology

Assoc. Prof. Dr. Yeliz YILDIRIM
Department of Chemistry, Ege University

27 April 2018

Prof. Dr. Serdar ÖZÇELİK
Supervisor, Department of Chemistry
İzmir Institute of Technology

Prof. Dr. Ahmet Emin EROĞLU
Head of Department of Chemistry

Prof. Dr. Aysun SOFUOĞLU
Dean of the Graduate School of Engineering and Sciences

ACKNOWLEDGEMENTS

I would like to express my sincere gratitude to many people at İzmir Institute of Technology who have supported me and contributed to my studies during my PhD journey. First of all, I am heartily grateful to my supervisor Prof. Dr. Serdar Özçelik for his guidance, encouragement and valuable scientific advices throughout this study. I cannot imagine thesis have written without his valuable guidance. It was truly an honour for me to work with him.

I would like to thank all old and new members of İYTE Özçelik research group for their friendships and helps. I wish to thank my friends in İzmir for helping me get through the difficult times, and for all the emotional support, camaraderie, entertainment and caring they provided.

Besides my supervisor, I also would like to thanks my thesis committee Prof. Dr. Muhsin Çiftcioğlu and Assoc. Prof. Dr. Ali Çağır for their insightful comments and guidance during all stages of my thesis, and also many thanks to Prof. Dr. Suna Timur and Assoc. Prof. Dr. Yeliz Yıldırım for participating as committee member and for reviewing my work.

Last but not the least, I am deeply and forever indebted to my parents Alirıza and Gülay for their love, support and encouragement throughout my entire life. I am grateful to my sibling Tülay and Zafer who have provided me through emotional support in my life. I would also like to thanks my husband and best friend, Muhammed, for his love, encouragement and editing assistance. This accomplishment would not have been possible without them.

ABSTRACT

SYNTHESIS, PHYSICOCHEMICAL CHARACTERIZATION, AND BIOSENSING APPLICATIONS OF GOLD NANOPARTICLES

Cancer is one of the leading diseases that cause death all around the world. In Turkey, lung cancer is the most common type of cancer type in men and it is the fifth in women. Unfortunately, the percentage of treatment of lung cancer is too low. Gold nanoparticles (AuNPs) are widely used in the biotechnology as imaging, diagnosis, and therapeutic agents because of their unique properties such as plasmon resonance, easy synthesize, biocompatibility, and facile surface modification.

In this study, it is aimed to design gold nanoparticles as biosensors for lung cancer cells. For this purpose, different sizes (5-40 nm) of Au nanoparticles were synthesized and their uptake and distribution into the lung cancer cells were investigated. The results of the study revealed that cellular uptake of gold nanoparticles are high for the size of 20 and 40 nm. The optimal visibility into the cells was achieved by using DIC microscopy in which the particles uptaken into the cytoplasm and localized at around nucleus of cells. In the second part of the study, surfaces of 20 and 40 nm particles were conjugated with RGD peptides and their distribution and light scattering properties were investigated in living cells by using dark-field microscopy. Due to the receptor-mediated endocytosis, RGD-AuNPs showed different distribution within the cells. These results indicate that the RGD conjugated Au nanoparticles exhibits much higher light scattering properties than non-conjugated nanoparticles. In addition to this, synthesized Au nanoparticles were conjugated with nucleus-localized peptide (NLS) and directed to the nucleus of cancerous (A549, H358) and healthy (BEAS2B) lung cells. The nucleus targeting properties of the NLS conjugated particles were also investigated to understand if there is any cell line selectivity. The internalizations of peptide conjugated Au nanoparticles into cell lines were visualized in living cells by using DIC microscopy. NLS conjugated AuNPs internalized into nucleus of A549 and H358 cancer cells. Although NLS conjugated AuNPs present inside the cytoplasm of BEAS2B cells, they did not localize into the nucleus of normal cell lines.

ÖZET

ALTIN NANOPARÇACIKLARIN SENTEZİ, FİZİKOKİMYASAL KARAKTERİZASYONU VE BİYOALGILAYICI OLARAK UYGULAMALARI

Kanser, dünya genelinde ölüme neden olan hastalıkların başında gelmektedir. Kanser türlerinden akciğer kanseri, ülkemizde erkeklerde ilk sırada, kadınlarda ise beşinci sırada görülmektedir ve sağ kalım oranları da diğer kanser türlerine göre oldukça düşüktür. Altın nanotanecikler (AuNPs) yüzey plazmon rezonans özelliği başta olmak üzere, kolay sentezlenebilir olma, yüksek biyouyumluluk, ve yüzey modifikasyonunun kolay olması gibi özelliklerinden dolayı görüntüleme, tanı ve tedavi gibi biyoteknoloji alanlarında yaygın bir şekilde kullanılmaktadırlar.

Bu çalışmada altın nanotaneciklerin akciğer kanser hücreleri için biyoalgılayıcı olarak tasarlanması amaçlanmaktadır. Farklı boyutlarda (5-40 nm) sentezlenen Au nanotaneciklerin akciğer kanser hücrelerine alınımları ve hücre içerisindeki dağılımları incelendi. 20 ve 40 nm boyutundaki taneciklerin hem hücre içerisine alınımlarının yüksek olduğu hem de DIC mikroskobu ile hücre içerisinde daha iyi görüldüğü ve taneciklerin hücrelerin stoplazmasına girip nükleusun etrafında lokalize oldukları belirlendi. 20 ve 40 nm boyutunda ki taneciklerin yüzeyi RGD peptidleri ile konjuge edilip hücre içerisindeki dağılımları ve ışık saçılım özellikleri karanlık alan mikroskobu ile canlı hücrelerde incelendi. RGD konjuge Au nanotanecikler hücre içerisine reseptör aracılığıyla alınıp hücre içerisinde farklı dağılım gösterdikleri için RGD konjüge Au nanotaneciklerin konjüge olmayan nanotaneciklere oranla çok daha yüksek ışık saçılım özelliği gösterdiği belirlendi. Bu Au nanotanecikler nükleus lokalize peptit (NLS) ile konjüge edilip kanserli (A549, H358) ve sağlıklı (BEAS2B) akciğer hücrelerinin çekirdeğine yönlendirildi ve konjüge taneciklerin hücre türüne bağlı olarak çekirdeği hedefleme özelliği incelendi. NLS konjüge Au nanotaneciklerin A549 ve H358 kanserli hücrelerin çekirdeğine girdiği ama BEAS2B sağlıklı hücrenin çekirdeğine girmediği DIC mikroskobu ile canlı hücrelerde alınan görüntüler ile belirlendi.

TABLE OF CONTENTS

LIST OF FIGURES

Figure **Page**

LIST OF TABLES

CHAPTER 1

INTRODUCTION

1.1. Gold Nanoparticles

Gold is the quintessential noble element. It is by nature highly unreactive, so, antique artifacts made of it preserve their exquisite glitter for thousands of years without tarnishing (i.e. oxidation) or degradation. Uses of gold in jewelry, coinage, and electronics are well known in its bulk form. The word "nano", derived from the Greek (*νᾶνος*(*nanos),* meaning dwarf, is used to describe any material or property which occurs with dimensions on the nanometer scale (1–100 nm). Since nanoscale gold can display bright colors (Figure 1.1) unlike bulk- and molecular-scale gold, it has become a very popular study object among chemists, physicists, and recently, biomedical practitioners (Figure 1.2).

Although gold nanoparticles in∼5-200 nm diameter range are large enough to support a conduction band for they are comparable to the mean free path of electrons in the metal at room temperature (∼100 nm), they are so small with respect to the wavelengths of visible light (∼400-750 nm). Irradiation with light at particular frequencies brings about a collective oscillation of electrons known as "plasma oscillations" or "plasmons"(El-Sayed 2001). They are depicted generally as washing over the surface of the particle ("surface plasmons" or "localized surface plasmon resonance", LSPR) (Figure 1.3).The dielectric constant of bulk gold determines the resonance frequency of this plasma oscillation, which is visible light (Willets and Duyne 2007).

The color of the particles in solution (Eustis and El-Sayed 2006, Joshi et al. 2004) is the result of the change in the position of the plasmon band, which in turn is bought about by the alteration in the size, shape and chemical environment of the particles. Relevance of AuNP suspensions from time immemorial to generate color spectrum in stained glass is a consequence of this (Edwards and Thomas 2007). The shape of the nanoparticle is more convenient for fine-tuning the optical properties of AuNPs, though size and chemical setting can too affect the position of AuNP plasma bands. To illustrate, -since the intensity and position of the absorption bands are relatively fixed with merely

a modest shift to red and widening with increased size of the particles, potential for SPR tuning is narrow for spherical AuNPs (Eustis and El-Sayed 2006).

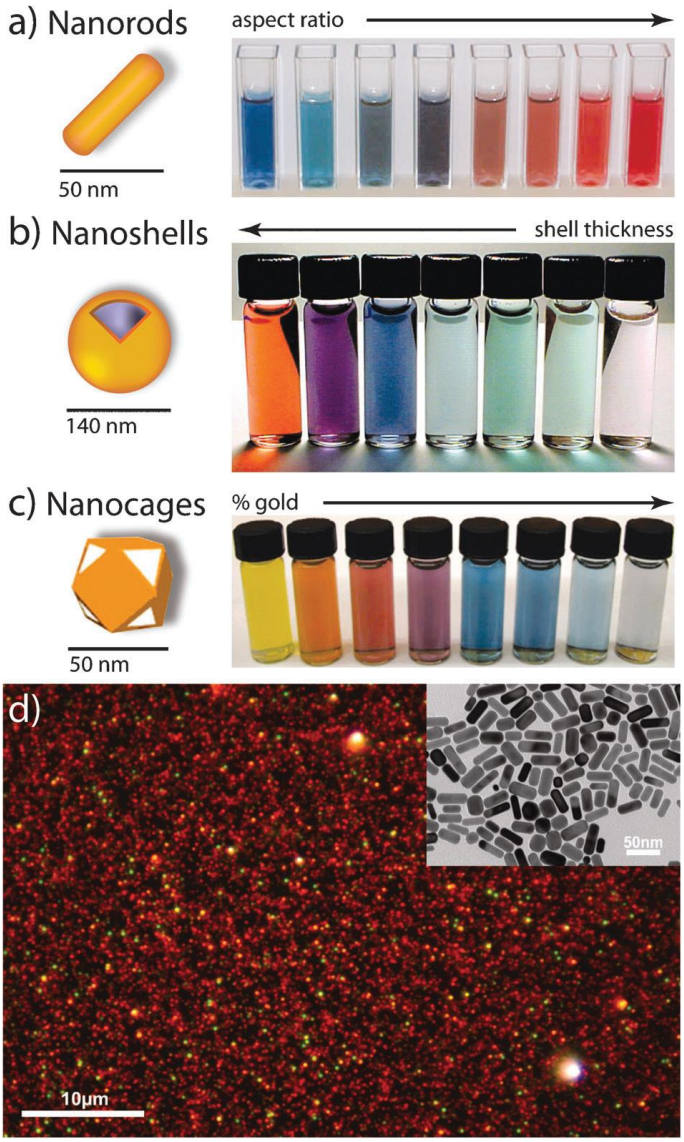

Figure 1.1. a) Gold nanorods, (b) silica–gold core–shell nanoparticles, and (c) gold nanocages. The intense color of these nanoparticles arises from the collective excitation of their conduction electrons, or surface plasmon resonance modes, which results in photon absorption at wavelengths, which varies with (a) aspect ratio, (b) shell thickness, and/or (c) galvanic displacement by gold. (d) Optical dark-field scattering micrograph of gold nanorods (electron micrograph in the inset) showing resonant scattering from their transverse (short-axis) plasmon mode (green) and their lower energy, longitudinal (long-axis) plasmon mode (red)). (Source: Dreaden et al. 2012)

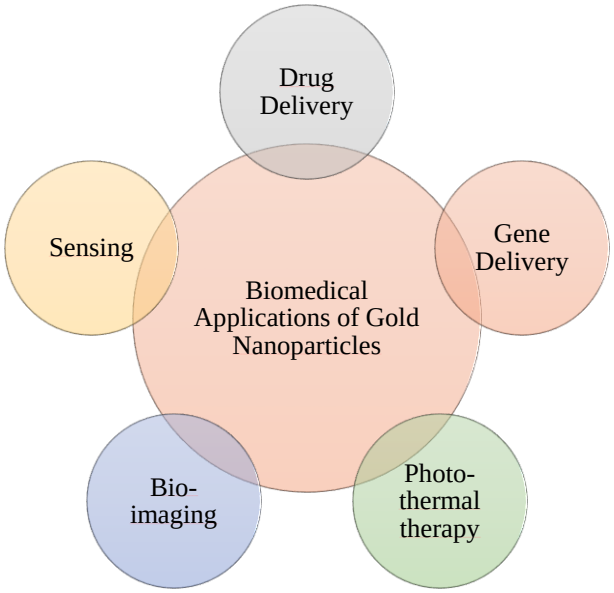

Figure 1.2. Biomedical applications of Gold nanoparticles

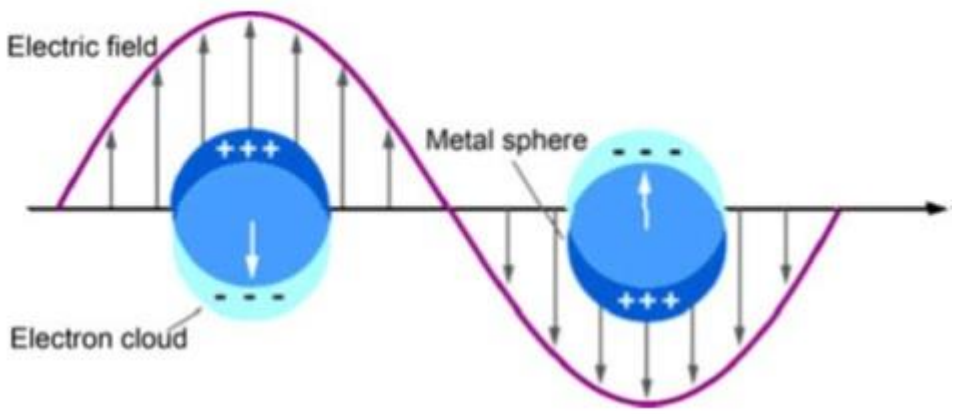

Figure 1.3. Schematic diagrams illustrating a localized surface plasmon (Source: Willets and Duyne 2007).

Principally, the ratio of atoms localized on the particle surface to those confined in the particle increases as the as particle size decreases. New thermal, optical, electrical, magnetic, electronic and catalytic properties are emanated from this (Roduner 2006). Figure 1.4 summarized that the optical properties of gold nanoparticles and their applications.

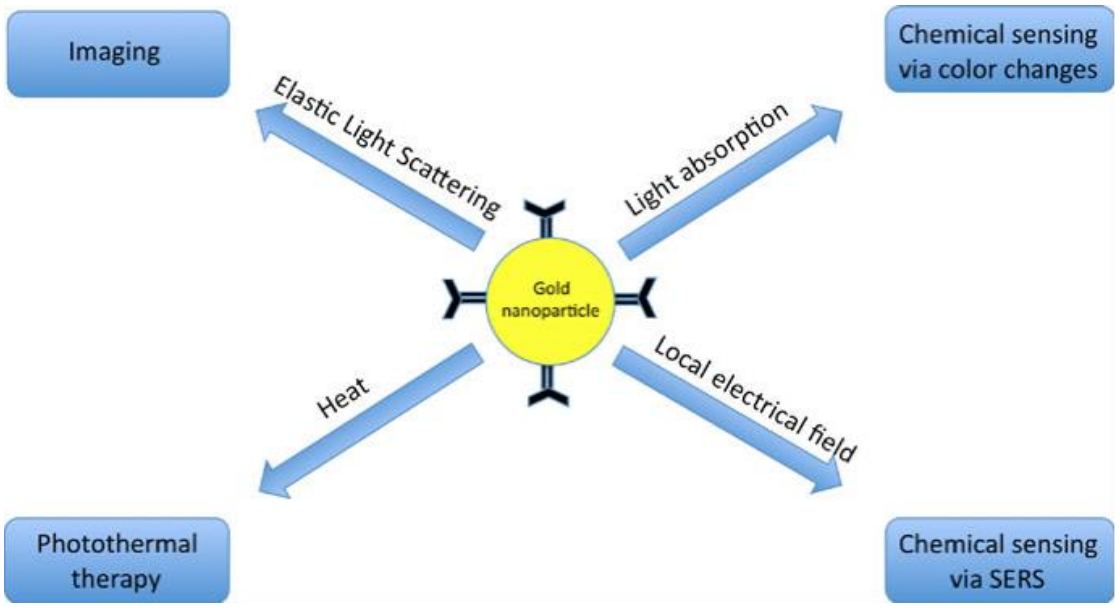

Figure 1.4. Schematic showing of the physical events that occur as a result of satisfying the localized surface plasmon resonance condition, with the corresponding applications. See text for details (Source: Roduner 2006).

The plasmon frequency is delicately susceptible to the dielectric nature of its interface (refractive index with the medium) since nanoparticles have a high surface area to volume ratio. Therefore, colorimetric shifts in dispersions occur due to changes in the surroundings (surface modification, aggregation, medium refractive index, etc.) (Kelly et al. 2003, Burda et al. 2005).

Different from conventional dyes, AuNPs have a tunability of their optical properties thanks to the resulting effects of these changes in the shapes, sizes and compositions (Huang et al. 2007). In this way, the absorption and scattering cross-section of AuNPs are better than those of conventional dyes. The absorption cross-section of AuNPs is four to five orders of magnitude larger than that of strongest absorbing rhodamine-6 G dye molecules (Huang et al. 2007, Radwan and Azzazy 2009). Moreover, the light scattering from 80 nm AuNPs is 10^5 times higher than the light emission from fluorescein molecules. Besides, contrary to molecular fluorophores, badly affected by photobleaching and can be detected by only a few techniques, AuNPs are not sensitive to photobleaching (Rosi and Mirkin 2005, Jain et al. 2006a). Furthermore, AuNP-based probes surmount some limitations of conventional organic dyes, like poor hydrophilicity and photostability, low quantum yield and detection sensitivity, insufficient stability in biological systems, and weak multiplexing capability (Jain et al. 2006b, Radwan and Azzazy 2009, 2007).

1.2. Synthesis of Gold Nanoparticles

Colloidal gold had been synthesized long before scientific literature grown mature, but the first scientific reporting of the colloidal gold nanoparticles is attributed to Michael Faraday, who in 1857 wrote that the ‘‘fine particles’’ formed from the aqueous reduction of gold chloride by phosphorus could be stabilized by the addition of carbon disulfide, resulting in a ‘‘beautiful ruby fluid’’ (Faraday 1857). The approaches for most colloidal syntheses to produce gold nanoparticles (Figure 1.5a) today are similar in that solvated gold salt is reduced in surface capping ligands that saves the particles from aggregation by electrostatic and/or physical repulsion. Particle size can be manipulated by altering the gold ion: reducing agent or gold ion: stabilizer ratio, with larger sizes (and typically less monodisperse) acquired from larger ratios.

In 1908, Mie showed that the intensity of colors in Faraday’s gold solutions are the result of the absorption and scattering of light by spherical gold nanoparticles in those solutions (Mie 1908). Using electron microscope, invented in 1932 by Knoll and Ruska, (Knoll and Ruska 1932), Turkevich et al. studied the structure of gold nanoparticles under different synthetic conditions in 1951 (Turkevich, Stevenson, and Hillier 1951). Frens studied Turkevich’s procedures of mediation by citrates methodically in 1973. Those procedures give 16-150 nm-diameter monodisperse spherical gold nanoparticle (Frens 1973).

20 nm gold spheres are produced throughout the reaction in which $HAuCl_4$ boils at a point where a trisodium citrate dihydrate solution is added. The reaction that takes place in the methods used by Turkevich and in most other *in situ* spherical AuNP synthesis schemes has two major phases, viz. nucleation and growth that seem to occur concurrently. In the first stage, citrate is oxidized and dicarboxyacetone is composed as Au^{3+} ions are reduced to Au^{1+}. Generation of gold atoms constitutes the second step in which the disproportionation of aurous chloride molecules allowing gold ions to adsorb on the surface to make aggregates. Numerous researchers have adapted this synthesis to accommodate the adjustment of size. Teams came to scene thereafter have developed a variety of methods (Frens 1973). Numerous groups observed the effects of citrate over the final surface of gold nanoparticles since the Turkevich method of spherical AuNP synthesis has been extensively used. In dealing with further surface functionalization,

scientists suffer from the effects of the negative charge of the citrate coating on the interactions of the particles with other species.

Under ambient conditions, sodium borohydride and alike which are stronger reducing agents provide a seemingly instant reduction of gold ions under ambient conditions, yielding smaller and less polydisperse particles compared to those achieved by sodium citrate.

New ways other than the size-controlled AuNPs synthesis of Frens' to adjust size were needed since polydispersity in particles larger than 30 nm was considerable. As characterized by Schmid, seed mediated growth (originally, ''germ-growth") is employed in another procedure for the enlargement of gold nanoparticles (Schmid 1992). In this way, small-scale AuNPs serve as nucleation zones for developing larger ones. Adjusting three factors, the final size of a particle can be determined — the diameter of the original seed particles, the seed amount included in the solution, and the ionic gold amount in the solution. Since the seed particle size determines the size of the resulting particles, it is of paramount importance.

That even smaller (1.4 ±0.4 nm diameter) phosphine-stabilized gold particles could be obtained from the reduction of PPh3AuCl by diborane in benzene, yielding $Au_{55}(PPh_3)_{12}Cl_6$ was shown by Schmid et al in 1981 (Schmid et al. 1981). According to Hutchison, gold clusters of 1.4–10 nm diameter could be produced through ligand exchange and that these particles could be similarly obtained under ambient conditions without the need for diborane gas (Weare et al. 2000). In 1994, applying a two-stage procedure in which gold chloride was solvated in toluene via a phase-transfer reagent (tetraoctylammonium bromide), Brust et al. investigated the synthesis of thiol-stabilized gold clusters (Brust et al. 1994). In this system, as reducing sodium borohydride was added to the aqueous stage, dodecanethiol was used as a stabilizer for gold clusters formed in the organic phase.

In 1990s, shape controlled synthesis of gold nanoparticles was studied by same researchers. Colloidal growth method was developed by Murphy et al. (Jana, Gearheart, and Murphy 2001) and Nikoobakht and El-Sayed (Nikoobakht and El-Sayed 2003), by which monodisperse gold nanorods in high yield based on seeded growth is obtained (Figure 1.5c). In this method, single-crystal seed particles with diameters of approximately 1.5 nm, which were produced from the reduction of chloroauric acid by borohydride in the presence of CTAB, are aliquoted into Au(I) growth solution formulated with moderate reduction of chloroauric acid by ascorbate and inclusion of

$AgNO_3$ and CTAB. Using this method, gold nanorods as long as 300 nm with diameters of approximately 10–20 nm can be formed in relatively high yield, thus their subsequent biomedical use (Sau and Murphy 2004). Aspect ratio for these nanorods can be adjusted by the seed/gold salt ratio or by the relative concentration of additive impurity ions.

Liz-Marza´n and coworkers demonstrated that by using poly(vinylpyrrolidone) (PVP) functionalized gold nanorods as seeds for the ultrasound-induced reduction of chloroauric acid by N,N-dimethylformamide (DMF) in the presence of PVP (Carbo-Argibay et al. 2007), spherically-capped colloidal gold nanorods can be modified into single-crystal octahedra. In their study, the subsequent morphology changed from sharpened (octagonal) rods to tetragons to octahedra (Figure 1.5d) by increased ratio of gold salt to nanorod seeds.

Because of their impressive optical characteristics and various biomedical applications, silica-gold core–shell nanoparticles, or gold nanoshells (Figure 1.5e), have recently had an appeal among researchers. According to the 1951 prediction of Aden and Kerker (Aden and Kerker 1951), concentric spherical particles could exhibit tunable plasmon resonance changing as a function of the shell thickness to core radius ratio. In 1998, Halas and his colleagues demonstrated that preparation of near-infrared absorbing gold nanoshells can be achieved by adsorption of small gold nanoparticles to the surfaces of silica nanoparticles electrostatically and as a result, additional gold onto the structures to form a conformal shell is reduced (Oldenburg et al. 1998). Other similar structures like asymmetric ‘‘nanoeggs’’ and quadruply concentric ‘’nanomatryoshkas’’ that reveal unique optical characteristics have been obtained as well (Wang et al. 2007).

Xia and colleagues have developed gold nanocages and nanoframes (Figure 1.5f) which have numerous potential uses in biomedicine thanks to their optical properties and hollow structures seemingly capable of holding cargo (Chen et al. 2006, Skrabalak et al. 2008). A process called galvanic replacement, which lets more noble metal ions (e.g. Au, Pt) spontaneously oxidize the surface atoms of a less noble metal (e.g. Ag, Cu) with concomitant reduction of the more noble metal, allows formation of these structures. For drug loading/delivery and photothermal therapy applications, gold nanoparticles that are near-infrared absorbing (spherical) hollow (Figure 1.5g) have been developed as well. Hollow gold nanospheres were produced by Caruso and coworkers through calcination or dissolution of polystyrene–gold core–shell nanoparticles (Liang, Susha, and Caruso 2003). In this process, polystyrene nanospheres were coated in polyelectrolyte multilayer films and tiny, 4-(dimethylamino) pyridine (DMAP) stabilized gold nanospheres (6 nm

diameter) were adsorbed to the polyelectrolyte surface electrostatically. After that, to finish a virtually conformal gold shell, hydroxylamine was used to further reduce chloroauric acid onto the seed-coated polystyrene spheres. Then, to obtain hollow gold spheres with diameters of about 650 nm, the polystyrene cores were pulled out via dissolution in tetrahydrofuran (THF) or calcination at 310 ^{0}C.

That more geometrically complex gold nanostructures (100–300 nm in size) could be produced through a polyol process variation was shown in 2004 by Yang, et al. (Figure 1.5h) (Kim et al. 2004). Tetrahedra, cubes, octahedra, and icosahedra were obtained in high yield with good monodispersity by using ethylene glycol as a solvent/reducing agent and PVP as a particle stabilizer. According to the findings of the authors, the subsequent nanoparticle morphology depends profoundly on the gold concentration in the solution, with tetrahedra formed at high concentrations and icosahedra (with a few octahedra) at lower concentrations. Gold nanocubes were obtained, too, by adding a small amount of silver nitrate during the reaction.

According to Niu and coworkers, new complex gold nanostructures can be obtained in high yield (over 96%) through a related seeded growth method (Niu et al. 2009) where CTAB-capped gold nanorods were amplified in a Au(III)/CTAB solution and functionalized with cetylpyridinium chloride (CPC) to serve as single-crystalline seeds (with a diameter of approximately 40 nm) for the following rhombic dodecahedral, octahedral, and cubic gold nanocrystal growth from Au(I). The authors curiously saw that the CPC surfactant preferentially stabilized {100} > {110} > {111} facets, just in contrast to their typically observed surface free energies (i.e. > {100} > {111}). They also saw a rhombic dodecahedral morphology (Figure 1.5i) when CPC-Au{100} (and to a lesser extent, -Au{110}) association was dominant and octahedral geometries (Figure 1.5j) when CPC-Au{111} association was found to dominate.

More recently, Mirkin, et al. proposed a production method for monodisperse gold nanocubes in high yield (Figure 1.5k) that includes a seeded growth technique similar to the one used to obtain nanorods. But Mirkin and coworkers used the chloride analog of CTAB: cetyltrimethylammonium chloride, CTAC (Zhang et al. 2010). The authors observed that it is possible to adjust the size of the nanocubes by simply changing the seed quantity in the growth solution, subsequently getting cubes with edge lengths ranging from 38 ±7 nm to 269 ±18 nm with yields of as high as 95%.

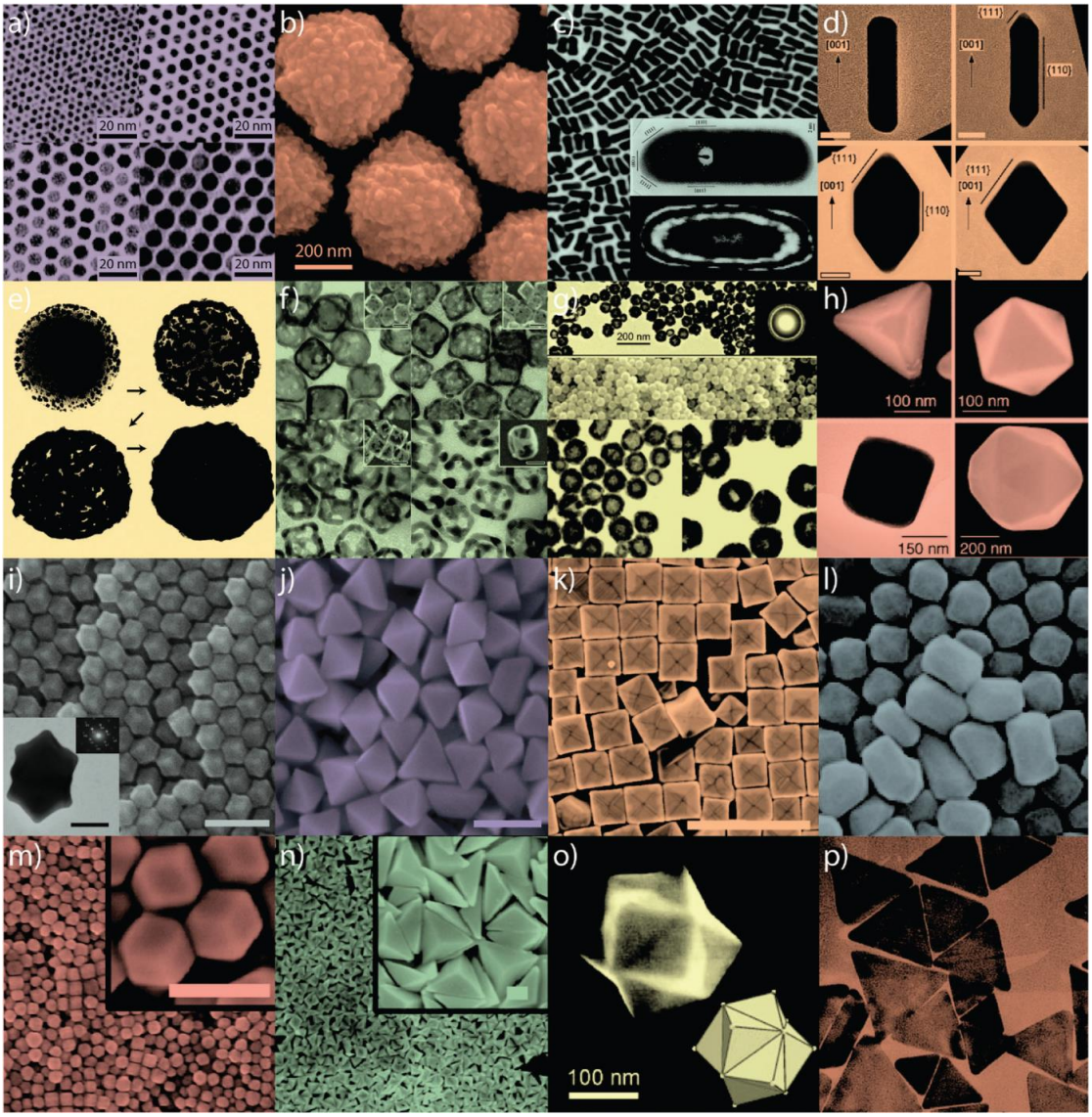

Figure 1.5. Gold nanoparticles of various size and shape with potential applications in biomedicine. Small (a) (Source: Shimizu et al. 2003) and large (b) (Source: Pong et al. 2007), (c) nanorods (Source: Wang et al. 1999, Sau and Murphy 2004), (d) sharpened nanorods (Source: Carbo-Argibay et al. 2007), (e) nanoshells (Source: Oldenburg et al. 1998), (f) nanocages/frames (Source: Lu et al. 2007), (g) hollow nanospheres (Source: Liang et al. 2005), (h) tetrahedral/octahedral/cubes/icosahedra (Source: Kim et al. 2004), (i) rhombic dodecahedra (Source: Niu et al. 2009), (j) octahedral (Source: Niu et al. 2009) (k) concave nanocubes (Source: Zhang et al. 2010), (l) tetrahexahedra (Source: Ming et al. 2009), (m–n) rhombic dodecahedra-obtuse triangular bipyramids (Source: Personick et al. 2011), (o) trisoctahedra (Source: Ma et al. 2008), and (p) nanoprisms (Source: Millstone et al. 2005).

Before this, structurally-related, near-infrared absorbing tetrahexahedral gold nanoparticles enclosed by 24 {037} facets were produced by Ming et al. by using a related synthetic approach involving CTAB (>95% yield) (Figure 1.5l) (Ming et al. 2009).

According to the study of Personick et al., rhombic dodecahedra (Figure 1.5m) and obtuse triangular bipyramids (Figure 1.5n) can be produced by a seeded (7 nm diameter) growth involving CTAC and dilute Ag+ concentrations, obtaining the sole {110}- faceted bipyrimidal gold nanostructures reported yet (31 ±5 nm and 270 ±26 nm edge length, respectively) (Personick et al. 2011).

By aqueous reduction of chloroauric acid, some interesting compositions like gold trisoctahedra can be produced (Figure 1.5o) (Ma et al. 2008). These nanostructures with diameters of 100–200 nm and enclosed by 24 {221} facets were formed by the ascorbic acid reduction of chloroauric acid in the presence of CTAC (a yield of ca. 85%) as shown by Zheng et al.

Some methods including photoreduction, seed mediated growth, plasmon-driven synthesis, and biosynthesis deliver triangular, or prismatic nanoparticles. Sastry and colleagues first produced gold nanoprismatic structures in fair yield (ca. 200–500 nm in size, 45% yield) from the aqueous reduction of chloroauric acid by lemongrass extract (Shankar et al. 2004). According to the authors, this transformation was the result of the reducing capacity of aldose sugars present in the plant extract, with shape-directing formation due to the crystallographically preferential adsorption of aldehydes/ketones present in the extract. That similar gold nanoprisms (144 ±30 nm edge length) could be synthesized in high yield using a seeded growth method (Figure 1.5p) was shown later by Schatz and coworkers (Millstone et al. 2005).

1.3. Surface Functionalizations of Gold Nanoparticles

To impart biological compatibility and specificity to gold nanoparticles, chemical adjustment of the surface of the nanoparticle is essential. Studies of Nuzzo and Whitesides on the formation of self-assembled monolayers (SAMs) of molecules on planar gold (Bain et al. 1989, Love et al. 2005) and later by Bard (Hu and Bard 1998) and Murray (Hostetler, Templeton, and Murray 1999, Sardar et al. 2009, Templeton, Wuelfing, and Murray 2000) in studying the dynamics and conformations of these assemblies by electrochemical, scanning probe, and mass spectrometric methods constitute the basis for the functionalization of gold nanoparticles for biomedical applications. A wide spectrum of functional molecular linkers and passivating agents are presently used for the

conjugation of gold nanoparticles utilized in biomedical applications. Yet, the anchoring groups employed for fixing these molecules onto the surface of gold usually include: thiolate (Brust et al. 1994, Martin et al. 1999, Walter et al. 2008), dithiolate (Hou, Dasog, and Scott 2009), dithiocarbamate (Zhao et al. 2005), amine (Daniel and Astruc 2004), carboxylate (Daniel and Astruc 2004), selenide (Yee et al. 2003), isothiocyanate (Martin et al. 1999, Daniel and Astruc 2004), or phosphine (Schmid et al. 1981, Walter et al. 2008) moieties. While labile applications often employ amine or carboxylate surface anchors, non-labile ones often use thiol-based anchoring groups. To illustrate, the study by Burda et al. has demonstrated that therapeutic results of gold nanoparticle-mediated delivery of photodynamic therapy agents benefits immensely from the use of more labile amino linkers with respect to stronger thiol groups because of the vesicular sequestration of particle-bound drug molecules (Cheng et al. 2010, Cheng et al. 2011).

Surface adsorption in room temperature for most alkanethiols is spontaneous, taking place over milliseconds to minutes (Love et al. 2005). Although monolayer packing/reordering can take several hours, for optimal results, overnight particle-ligand incubation with additional sonication or gentle heating is usually sufficient.

While the bond strength between anchoring groups and the gold surface have a crucial place in determining the subsequent functionality, packing density and surface energetics present equally important contributions. Although dithiolates are generally regarded as preferable to their mono-thiolate counterparts because of multivalent binding avidity, these molecules are actually more inclined to oxidative desorption due to inefficient packing (Hou, Dasog, and Scott 2009). According to the studies of Cima et al., thiolates, whose most common use is in non-labile biomedical applications where they are employed for attachment to gold nanoparticles, can remain stably adsorbed for up to 35 days under physiologic conditions (Flynn et al. 2003). This suggests that for attachment of biological molecules to gold surfaces in various biomedical applications, thiolates might be a preferred functional group.

The need for sufficient stabilization in biological environments containing high serum concentrations and high ionic strengths is common among most applications of gold nanoparticles in biomedicine. The most commonly employed surface ligand used with biomedical gold nanoparticles is thiolated poly(ethylene glycol), PEG–SH. Its hydrophilicity, which has been documented comprehensively, allows the aqueous dispersion of gold nanoparticles conjugated with a wide range of lipophilic molecules (Dreaden et al. 2009) and increases circulatory half-life (Dickerson et al. 2008) by

blocking adsorption of serum proteins and opsonins that help uptake and clearance by the reticuloendothelial system (RES) (Harris and Chess 2003, Zheng, Davidson, and Huang 2003, Niidome et al. 2006, von Maltzahn et al. 2009).

Various biofunctional molecules can be used for conjugation with gold nanoparticles by simple physical methods like hydrophobic–hydrophobic interaction (Figure 1.6a) and charge pairing (Figure 1.6b). Highly hydrophobic molecules (e.g. chemotherapeutics such as paclitaxel and doxorubicin) can be labily bound to biomedical gold nanoparticle conjugates via the use of amphiphilic ligands as demonstrated by Rotello et al. (Kim et al. 2009). Classical cross coupling reagents can also be used for the non-labile conjugation of a wide variety of biofunctional targeting, therapeutic, and imaging contrast agents (Figure 1.6c).

Most applications involving amine-containing molecules/proteins employ classical carbodiimide cross coupling (carboxylate+amine-amide) with some commercial manufacturers producing ready-made N-hydroxysuccinimide (NHS)-activated heterobifunctional polymers and ligands (Gibson, Khanal, and Zubarev 2007, Gole and Murphy 2008). In a number of gold nanoparticle conjugation strategies, Huisgen cycloaddition (click, or azide–alkyne coupling) has been similarly employed (Gole and Murphy 2008). Inorganic complexes like cisplatin or its prodrug forms can also be datively bound to gold nanoparticle ligands by way of appropriate ligands (Figure 1.7a) (Brown et al. 2010). Mirkin and coworkers were first to utilize oligonucleotide-functionalized gold nanoparticles, employing thiolated ssDNA as surface linkers to which targeting ligand-, biomolecule-, and/or imaging contrast agent-tethered complementary ssDNA could be hybridized (Figure 1.7b) (Rosi et al. 2006, Seferos et al. 2007). Recently, Rotello and colleagues have shown the synthesis, gold nanoparticle conjugation, and phototriggered release of the cytotoxic thymidylate synthase inhibitor 5-fluorouracil (5-FU) via a photocleavable, o-nitrobenzyl PEG–SH linker, demonstrating significant toxicity following UV exposure and diminished cytotoxicity drastically in its absence (Figure 1.7c) (Agasti et al. 2009).

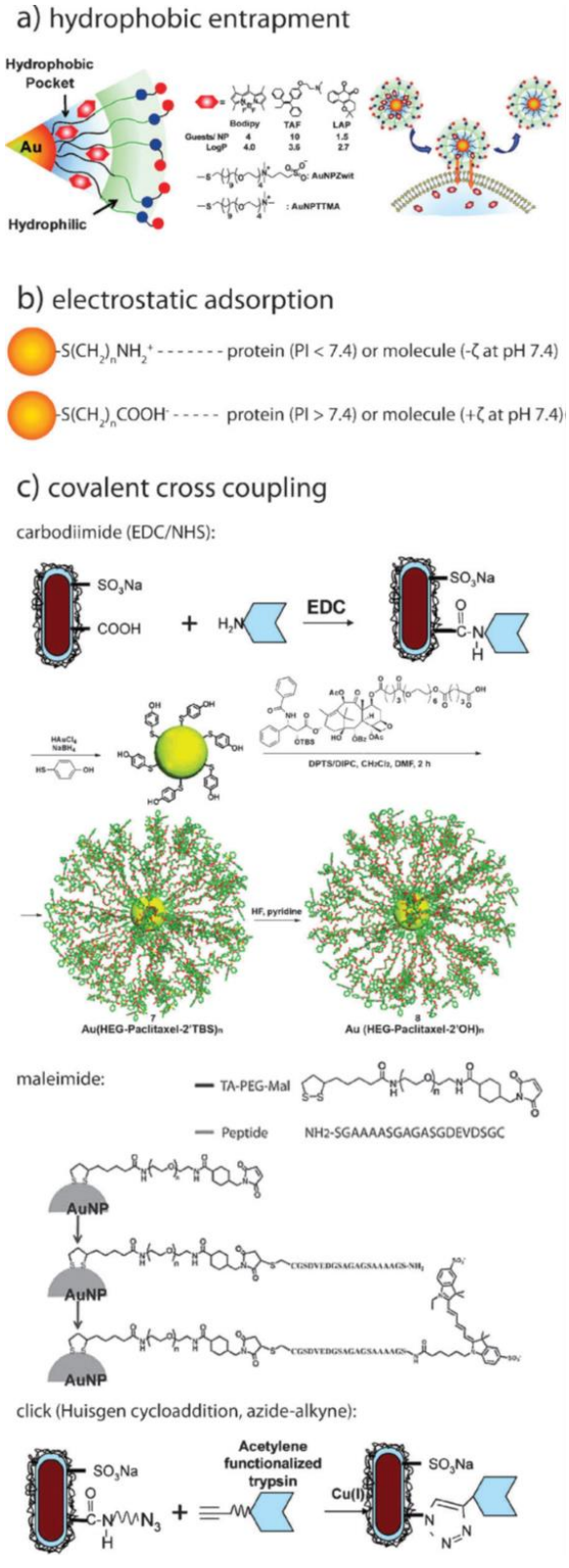

Figure 1.6. Schematics illustrating various methods by which gold nanoparticles can be conjugated with biofunctional molecules. (a) hydrophobic entrapment (Source: Kim et al. 2009), (b) electrostatic adsorption, and (c) covalent cross coupling by carbodiimide, maleimide, and click chemistry (Source: Gibson, Khanal, and Zubarev 2007, Gole and Murphy 2008, Oh et al. 2010).

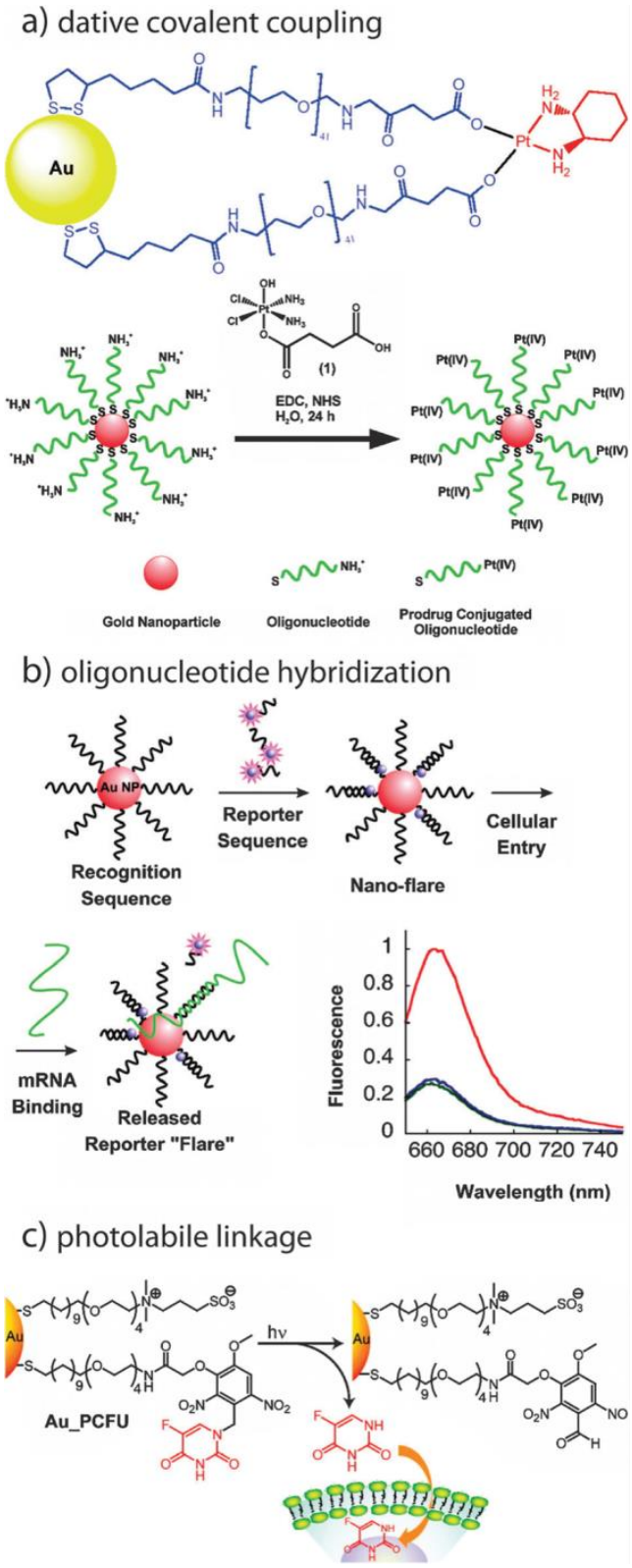

Figure 1.7. Schematics illustrating additional methods by which gold nanoparticles can be conjugated with biofunctional molecules. (a) dative covalent bonding (Source: Brown et al. 2010, Dhar et al. 2009), (b) oligonucleotide hybridization (Source: Seferos et al. 2007), and (c) and photolabile linkage (Source: Agasti et al. 2009).

The resulting nanoparticles showed adjustable surface charge and permitted the proteins to be adsorbed electrostatically (see Figure 1.6b) over a large spectrum of isoelectric points and solvent pH values.

1.4. Optical Imaging of Gold Nanoparticles

Since far-field optical imaging techniques does not require any contact with the samples and do not interfere with the biological processes, they are particularly important for this purpose. Because most unstained biological samples either show low contrast or are utterly invisible under optical microscopes, researchers often tag specific molecules with a label, such as a fluorescent dye. For their versatility as a labeling platform, nanoparticles have become an increasingly important alternative to fluorescent dyes in biological and medical applications. Besides, they show unique optical and chemical properties with a large functionality palette, which includes targeted drug/gene delivery, cellular imaging, in vivo biosensing, and biomedical diagnostics and therapies (Love, Marquis, and Haynes 2008, Sperling et al. 2008, Murphy et al. 2008, Wax and Sokolov 2009).

For live-cell optical imaging, non-fluorescent nanoparticles come to the fore. Fluorescent molecules and quantum dots suffer from photostability-associated problems, though they are used extensively in biological research. Besides, quantum dots have cytotoxicity effects that hinder their use over a long period (Hardman 2006). Most non-fluorescent nanoparticles, on the other hand, show good photo-stability, thus allowing the particles to be observed for an indefinitely long time without bleaching. In addition, individual nanoparticles can be localized with high spatial and temporal resolution. Only the total number of photons that can be collected per unit time limits the precision in localization of an isolated particle or a single fluorophore. Because of their large optical cross-sections that enable super-localization in short integration times, nanoparticles are superior in this regard.

Gold nanoparticles can scatter light at their plasmon wavelengths strongly, that is, 10^5–10^6 times stronger scattering cross-sections than that of the emission from a fluorescent dye molecule (Yguerabide and Yguerabide 1998a, b, Jain et al. 2006b). As presented theoretically and experimentally, larger gold nanoparticles and nanorods with

higher aspect ratios show stronger scattering efficiencies than their smaller counterparts (Mie 1908, Yguerabide and Yguerabide 1998a, b, Jain et al. 2006b, Orendorff et al. 2005, Lee and El-Sayed 2005).

As a result of the exclusion of the unscattered beam from the image in dark-field microscopy (both light and electron), the field around a specimen, where there is no specimen to scatter the beam, is usually dark. Dark-field, an illumination technique used to sharpen the contrast in unstained samples in optical microscopy, works by illuminating the sample with light that will not be collected by objective lens, thus will not form part of an image. Thereby some bright objects are seen on a dark background.

Thanks to their high scattering cross-sections at or near their plasmon frequencies, noble metal particles are attractive optical labels for dark-field SPT (single-particle tracking). At reasonable illuminating intensities, they neither photo-bleach nor optically saturate. With adjustment of the particle size and shape, the plasmon resonance absorption and scattering can be brought out of the visible and into the near-infrared (NIR) region, where biological tissues are relatively transparent. This attribute elevates noble metal particles to a high position for optical probe in biological imaging.

The absorption and scattering of light by a homogeneous dielectric sphere was first reported by Gustav Mie in 1908 (Mie 1908). In the limit of particle sizes smaller than the wavelength of the illuminating light, the cross-sections s are given by the following equations:

$$\sigma_{absorption=} \frac{8\pi^2}{\lambda} R^3 Im\left\{\frac{m^2-1}{m^2+2}\right\} \tag{1.1}$$

$$\sigma_{scattering} = \frac{128\pi^5}{3\lambda^4} R^6 \left|\frac{m^2-1}{m^2+2}\right|^2 \tag{1.2}$$

where l is the wavelength; R is the radius of the particle; m is the ratio of refractive indices of the particle and the medium; Im is the imaginary part of the complex number. Rayleigh scattering decreases with the sixth power of the particle radius. Under ideal conditions, it is possible to detect particles as small as 4 nm, depending on the particle material and the design of the dark-field microscope, but in complex biological environments, the minimum size for a particle to be detected rises to 20 nm.

As touched upon to some degree above, low light levels seen in the final image is the main limitation of dark-field microscopy. Bringing a risk of damaging the sample, a strong illumination is required. Here, the high scattering features of AuNPs can enhance

contrast in dark-field imaging. Not only intracellular uptakes of AuNP is widely determined by dark-field microscopy analysis (Figure 1.8) (Heo et al. 2012), but also single AuNP as real-time optical probes for the detection of NADH-dependent intracellular metabolic enzymatic pathways (Zhang et al. 2011).

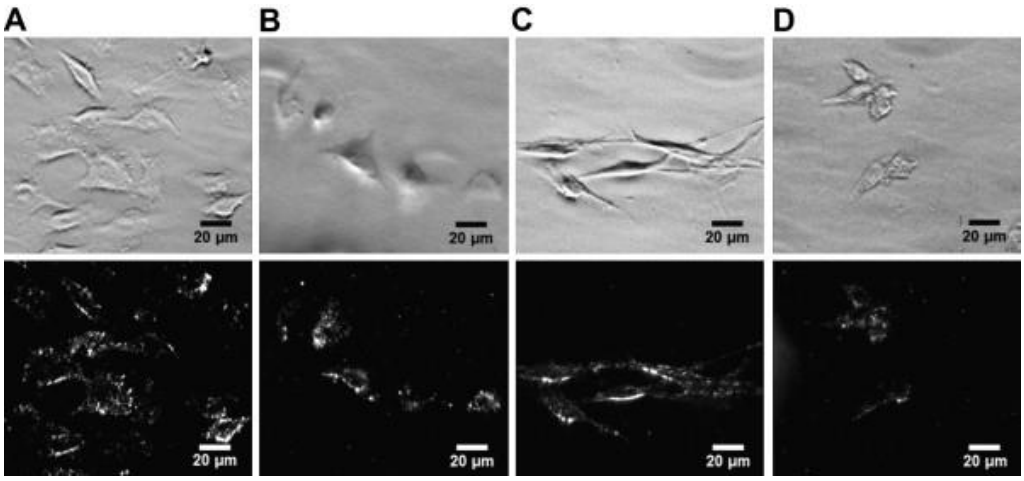

Figure 1.8. Dark-field microscopy images of (a) HeLa, (b) A549, (c) MG63 and (d) NIH3T3 cells involved with AuNP-3 (Source: Heo et al. 2012).

Dark-field microscopy was used for the successful selective detection of cancerous cells by El-Sayed et al. (El-Sayed, Huang, and El-Sayed 2005), who conjugated 35-nm AuNPs with anti-EGFR antibodies to target two malignant epithelial cell lines. This is also helpful in monitoring the targeted delivery of nanorods conjugated with transferrin or cell-penetrating peptides (Oyelere et al. 2007). Dark-field microscopy can support multiplex labeling, as shown by the simultaneous detection of nanorods with different aspect ratios, targeted toward separate cell-surface biomarkers on human breast epithelial cells (Yu, Nakshatri, and Irudayaraj 2007).

Bright-field microscopy relies on transmitted light for illumination of the sample. The objects that strongly absorb light will appear as dark spots on a bright, non-absorbing background. It has some limitations such as low contrast for weakly absorbing samples and low optical resolution due to the blurry appearance of out-of-focus material. In order to make biological samples visible under a bright-field microscope, usually staining is required.

Very small structures as small as 20 nm became visible with the development of video-enhancement techniques in the 1980s. This improvement brought about the rapid development of bright-field *in vivo* single particle tracking for receptor-mediated

endocytosis, motion of cell surface molecules, and intracellular transport studies (De Brabander et al. 1986).

Since colloidal gold nanoparticles have large absorption and scattering cross sections, they constitute an excellent choice for labeling in bright-field microscopy. The minimum detectable diameter is 15 nm, and typically a diameter of 30–40 nm is used to maintain a good signal-to-noise ratio at video rate (30 Hz) (Saxton and Jacobson 1997). Organelles are practically invisible in these studies, because gold nanoparticles absorb and scatter light far more effectively than organelles.

Bright-field microscopy has not been used as frequently as dark-field microscopy in recent studies because of its high background levels and low spatial resolution.

DIC microscopy that works on the principles of interference to determine optical path length gradients of the specimen was first introduced by Nomarski in the 1950s. Today, most DIC microscopes have a two-prism configuration in which the incident light is split by a first Nomarski prism into two orthogonally polarized illumination beams mutually shifted by a small (typically sub-wavelength) distance. The two shifted beams are projected onto the sample, generating two identical bright-field images behind the microscope objective. Then, these images are laterally shifted and overlaid by a second Nomarski prism to generate an interference pattern of the final DIC image (Tsunoda, Isailovic, and Yeung 2008).

Suitability to the employment of full objective and condenser apertures that provides the user with the highest lateral resolution and at the same time the shallowest depth of field constitutes one major advantage of DIC microscopy. Besides, it has a better z-resolution than what is achievable with bright-field and dark-field microscopies since contrast is generated primarily within the thin focal plane with minimal influence from objects outside of the focal plane.

To be able to make a comparison of the three techniques, Tsunoda et al. imaged the same live cell in 3D with DIC, bright-field, and dark-field microscopy. In the dark-field mode, the edges of the cell produced intense scattering, and this strongly interfered with the observation of organelles inside the cell. Scattered light from the points of interest in the cell could easily be distorted by the presence of objects along the optical path. In the case of bright-field microscopy, some of the cell's features could be revealed, but the images were affected by interference with other organelles from outside of the focal plane. The best performance for imaging thin vertical sections of live cells was that

of the DIC microscopy, for it allowed observing the cell features in the focal plane without significant interference from other points in the cell.

Another major advantage of DIC microscopy is simultaneous imaging of nanoprobes and live cells for several hours without the need for staining, thereby enabling researchers to observe biological systems directly while minimizing intrusion level on the system. To monitor the entire endocytosis process of mesoporous silica nanoparticles (MSN) into live A549 human lung cancer cells, without staining the sample, Sun and colleagues used a DIC microscope (Sun et al. 2008). In a recent study, the entire endocytosis process of 40 nm gold nanospheres by a HeLa cell was recorded at video rate (Sun et al. 2009). Nanoparticles and cellular structures were clearly visible in the images. In this way, determination of the relative position of nanoprobes in relation to cell features has become possible with DIC microscopy.

Surface-enhanced Raman scattering (SERS) (Kneipp et al.), computed tomography (CT) (Kim et al. 2007), magnetic resonance imaging (MRI) (Vartholomeos et al. 2011), optical coherence tomography (OCT) (Zagaynova et al. 2008, Oldenburg et al. 2009), photoacoustic imaging (PAI) (Yang et al. 2009, Kim et al. 2011) and two-photon microscopy (TPL) (Wang et al. 2005, Durr et al. 2007, Nitin, Javier, and Richards-Kortum 2007) are also used for cancer imaging .

OCT has become a prominent biomedical tissue-imaging technique by which three-dimensional micrometer-resolution images from within optical scattering media such as a biological tissue can be captured. Depth penetrations in low millimeter range, axial resolutions on the order of 10 mm and lateral resolutions in the low micron range (Zysk et al. 2007, Fujimoto et al. 1995) are possible with it. Besides, OCT is noninvasive and analogous in several respects to ultrasound imaging, except that reflections of NIR light are detected rather than sound. Studies using OCT methods can benefit highly from NIR-active contrast agents like Au-nanorods (NRs) (Oldenburg et al. 2006, Troutman, Barton, and Romanowski 2007).

Gold nanocrystals, particularly gold nanorods, are detectable at single particle levels under femtosecond NIR laser excitation for they have enhanced two-photon luminescence (TPL) (Boyd, Yu, and Shen 1986, Bouhelier, Beversluis, and Novotny 2003, Imura, Nagahara, and Okamoto 2004, Wang et al. 2005, Loumaigne et al. 2010). TPL can be used in single particle tracking to study the mechanisms of cellular uptake of the targeted gold nanorods (Huff et al. 2007). Due to the high contrast associated with TPL imaging, cellular localization of the nanorods could be clearly differentiated. For

comparison, TPL imaging of an Au nanorod is 100 times stronger than the emission of single fluorescein isothiocyanate molecule (Li and Gu 2010).

Laser-induced heating of materials constitutes photothermal (PT) and photoacoustic (PA) imaging where the former relies on the direct detection of heat, the latter on the detection of acoustic waves generated by the thermal expansion of air surrounding the materials. Because of their strong light absorption properties (extinction coefficients of ~10^9 M^{-1} cm^{-1}), gold nanocrystals are very promising contrast agents for PT and PA imaging (Zheng, Davidson, and Huang 2003). Since the optical absorption of a metal nanoparticle decreases as the third power of its diameter while scattering decreases as the six power of diameter, absorption prevails over scattering below a certain size. Therefore, PT imaging is often best suited for small gold nanoparticles (down to 2 nm) while larger gold nanoparticles give stronger PA signals (Boyer et al. 2002, Brusnichkin et al. 2007).

PAI, as an emerging noninvasive imaging technique, is based on photoacoustic effects where non-ionizing laser pulses are delivered into biological tissues (when radio frequency pulses are used, the technology is referred to as thermoacoustic imaging) (Sun and Diebold 1992). There are two types of PAI systems, photoacoustic tomography (PAT) and photoacoustic microscopy (PAM). A typical example of the former employs an unfocused ultrasound detector to acquire photoacoustic signals, and the image is reconstructed by solving the photoacoustic equations inversely. A latter, on the other hand, uses a spherically focused ultrasound detector with 2D point-by-point scanning and does not require any reconstruction algorithms.

1.5. Targeting of Gold Nanoparticles to Cancer cells

Medically known as a malignant neoplasm, cancer manifests itself as cell growth in an unregulated manner and can metastasize to other parts of the human body. It is still among the prominent causes of mortality throughout the world, with new cases exceeding 10 million every year, despite substantial advances in cancer studies (Balmain, Gray, and Ponder , Hanahan and Weinberg 2000, Ponder 2001). For early detection and treatment of cancer, it is critical to search for advanced diagnostic and therapeutic methods. To curb the mortality of cancer, as well as to reduce materiel costs, a simple and rapid diagnosis

tool for early detection is desirable. Measuring in between 100 and 1 nm (Jing et al. 2012), NP sizes are around one hundred to ten thousand times smaller than those of human cells. Therefore, they can interact unprecedentedly with biomolecules both on the surface of and inside the cells, promising progress in cancer diagnosis and treatment (Dupuy and Goldberg 2001, Goldberg 2001, Mirza et al. 2001, Ahmed, Fessi, and Elaissari 2012). NPs that are mostly used for cancer studies include gold nanoparticles (AuNPs) polymers, dendrimers, liposomes, perfluorocarbons, quantum dots, iron oxides, nanotubes, and nanowires (Cai et al. 2008). There are potential applications of the AuNPs in cancer diagnosis and treatment due to some unique properties. There are many subtypes of AuNPs based on their size, shape, and physical properties like colloidal gold, gold nanospheres, gold nanorods, gold nanoshells and gold nanocage (Cai et al. 2008).

AuNPs offer extraordinary potential for targeting, imaging at the cellular and molecular level (Peer et al. 2007, Davis, Chen, and Shin 2008, Li et al. 2012) based on some features including their selective recognition of cancer cells (Mirkin et al. 1996), their optical properties controlled by the geometry and size of AuNPs, and their further advantage of biocompatibility (Bardhan et al. 2011).

1.6. Toxicity and Cellular Uptake of Gold Nanoparticles

While bulk form and micron size or larger gold are generally thought to be non-catalytic, stable, inert, and biocompatible, uptake and toxicity of nano-sized gold is a much more complex issue (Khlebtsov and Dykman 2011). Researchers have begun to improve to result matrices with important variables such as synthesis, size and shape of nanoparticles, cell type and end point studied (Beddoes, Case, and Briscoe 2015).

As functional assays relate to a specific metabolic pathway or function performed by the cell to a quantifiable level of cell viability, they are frequently employed. For example, tetrazolium-based assays such as MTS [3- (4,5-dimethylthiazol-2-yl)-5-(3-carboxymethoxyphenyl)-2-(4-sulfophenyl)-2H-tetrazolium] and MTT [3-(4,5-dimethylthia zol-2-yl)-2,5-diphenyltetrazolium bromide] (Monteiro-Riviere, Inman, and Zhang 2009), as well as alternatives such as the Presto Blue metabolic assay (Jokerst et al. 2012), and Neutral Red assays (Male et al. 2008) can be mentioned in this context. Since only tetrazolium salts possess the mitochondrial activity required to cleave a

tetrazolium ring thus creating formazan these cells can identify metabolically active cells selectively. Formazan formation brings about a purple color appearing only in viable cells, thus increasing the detectability of the amount of viable cells colorimetrically (Monteiro-Riviere, Inman, and Zhang 2009).

The ability of cultured cells to uptake gold nanoparticles is well-studied and it is widely agreed that cellular uptake of gold nanoparticles is a function of size, shape, surface functionality/charge, aggregation state of nanoparticles, concentration of nanoparticles, the type of cell, incubation conditions, and type of culture media.

The way gold NP size, shape, and surface charge effect their cellular uptake and toxicity using cell cultures has been the focus of many studies regarding gold NPs *in vitro* behavior (Alkilany and Murphy 2010). Generally, a suspension of gold NPs in cell culture media acts as a delivery mechanism for gold NPs. A mix of ultraviolet-visible absorbance spectroscopy (UVvis) and inductively coupled plasma mass spectrometry (ICP-MS) is used for GNP uptake measurement. For gold, the latter is a very sensitive analytical technique, which can detect 60 parts per trillion gold atoms. This means, depending on the size of the nanoparticle, concentrations are in femtomolar to attomolar order (Murphy et al. 2008).

Both qualitative and quantitative analytic tools like transmission electron microscopy (TEM) (Marquis et al. 2009, Alkilany and Murphy 2010), scanning electron microscopy (SEM) (Peckys and de Jonge 2011), atomic force microscopy (AFM) (Shukla et al. 2005, Muñoz Javier et al. 2006), dark-field optical microscopy (El-Sayed, Huang, and El-Sayed 2005, Alkilany et al. 2009), differential interference contrast (DIC) microscopy (Ryan et al. 2007, Gu et al. 2011), and photothermal heterodyne imaging (Berciaud et al. 2004, Leduc et al. 2011) have been used for monitoring gold nanoparticle cellular uptake.

Same measurements demonstrated that the gold core is benign and biologically inert. However, since the surface of the gold nanoparticles shows unusual chemical reactivity for sizes under 2 nm, this is not always true when the gold core size drops below this threshold (Alkilany and Murphy 2010). To illustrate, gold nanoparticles with a diameter of 1.4 nm (a cluster of 55 gold atoms) can act as an efficient chemical catalyst due to their high surface reactivity at this size (Turner et al. 2008), and because of this reason, they can be an undesired source of reactions or side effects in biological systems, too. To give a specific example, gold nanoparticles with a diameter of 1.4 nm show

significant toxicity to culture cells through induction of oxidative stress and mitochondrial damage (Pan et al. 2009).

Many reports suggest that gold nanoparticles are ‘’nontoxic’’. Using a human leukemia cell line, Connor et al. found that gold nanospheres with diameters of 4, 12, and 18 nm, and capping agents, namely citrate, cysteine, glucose, biotin, and cetyltrimethylammonium bromide were nontoxic based on the MTT assay (Connor et al. 2005).

On the other hand, gold nanoparticles are ‘’toxic’’ according to some other groups. For example, Goodman et al. demonstrated that cationic gold nanospheres with a diameter of 2 nm are toxic at certain doses, but the same nanoparticles with a negatively charged surface found to be not toxic at the same concentration and in the same cell line (Goodman et al. 2004). Goodman et al. explained this finding by the ability of the cationic nanoparticles to interact with the cellular membrane with a negative charge and the resultant membrane disruption. In 2009, Pan and colleagues observed necrosis, mitochondrial damage, and induced an oxidative stress on all examined cell line emanated from 1.4-nm gold nanospheres (Table 1.1) (Pan et al. 2009). On the other hand, for 15-nm gold nanospheres with the same surface group they found no evidence of a cellular damage, thus deducing of a possible size-dependent toxicity of gold nanoparticles (Pan et al. 2009). Turner et al. summarized these in 2008 that gold nanoparticles with diameters under 2 nm show evidence of chemical reactivity that does not occur at larger sizes (Turner et al. 2008).

Table 1.1. Summary of toxicity and uptake of gold nanoparticles

AuNP shape	**AuNP size (nm)**	**Surface properties**	**Cell line**	**Dose**	**Conclusions**	**Referance**
Spheres	2	Quaternary ammonium, carboxylic acid	COS-1 mammalian cells, red blood cells, E. coli	0.38–3 μM	Cationic nanoparticles found to be toxic where anionic not	(Goodman et al. 2004)
Spheres	3.5 ± 0.7	Lysine, poly(lysine)	RAW 264.7 mouse macrophage	10–100 μM	Nanoparticles are not toxic and not immunogenic	(Shukla et al. 2005)
Spheres	4, 12, 18	CTAB, citrate, cysteine, glucose, biotin	K562 human leukemia	0.001–0.25 μM	All nanoparticles were not toxic	(Connor et al. 2005)
Spheres	13.1	Citrate	Human dermal fibroblast	0–4 mM	Nanoparticles decreased cell proliferation rate, adhesion, and motility	(Pernodet et al. 2006)
Spherical cluster	1.4	Triphenylphosphine monosulfonate	MV3 and BLM (Metastatic melanoma)	Up to 0.4 μM	100% cell death at 0.4 μM compared to 10% cell death for cisplatin at same concentration	(Tsoli et al. 2005)

(cont. on next page)

Table 1.1. (Cont.)

AuNP shape	AuNP size (nm)	Surface properties	Cell line	Dose	Conclusions	Referance
Rods	65 x 11	CTAB, PEG	HeLa	0.09–1.45 μM	Replacing CTAB with PEG on the surface of nanorods reduced the toxicity	(Takahashi et al. 2006)
Spheres	33	CTAB and citrate	BHK21, Hep2G, A549	0–120 nM	Nanoparticles are not toxic to Hep2G and BHK21 but to A549 cell line	(Patra et al. 2007)
Spheres	18	Citrate	HeLa	0.2–2 nM	Nanoparticles are not toxic and did not change geneexpression patterns	(Khan et al. 2007)
Spheres	0.8, 1.2, 1.4, 1.8, 15	Triphenylphosphine mono and tri Sulfonate	HeLa, SK-Mel-28, L929, j774A1	Up to 5.6 μM	(a) 1.4 nm: Most toxic size; (b) 0.8, 1.2, 1.8:4–6 fold toxicity compared to 1.4 nm; (c) 15 nm: completely non-toxic; (d) toxicity is not cell line dependent	(Pan et al. 2007)

(cont. on next page)

Table 1.1. (Cont.)

AuNP shape	AuNP size (nm)	Surface properties	Cell line	Dose	Conclusions	Referance
Rods	40 X 18	CTAB, PSS, PDADMAC	HeLa	10–150 μM	Polyelectrolyte coating of nanorods are not toxic compared to the CTABcapped nanorods and no gene expression abnormalities were observed	(Hauck, Ghazani, and Chan 2008)
Spheres	10	Citrate	Dendritic cells from C57BL/6 mice	0.5 mM	Nanoparticles were not toxic and did not induce dendritic cell activation	(Villiers et al. 2010)
Spheres	1.4 and 1.5	Triphenylphosphine monosulfonate, GSH	HeLa	5.6 mM	(a) The 1.4 nanoparticles induced necrosis by oxidative stresses where the 15 nm particles were found to be not toxic; (b) GSH-capped nanoparticles were less toxic than TPMS capped nanoparticles	(Pan et al. 2009)

(cont. on next page)

Table 1.1. (Cont.)

AuNP shape	AuNP size (nm)	Surface properties	Cell line	Dose	Conclusions	Referance
Spheres	3.7	PEG	HeLa	0.08–100 μM	Nanoparticles entered nucleus and did not induce toxicity	(Gu et al. 2009)
Rods	65 x 15	CTAB, PAA, PAH	HT-29	0.6 nm	Nanorods are not toxic, excess CTAB is. Overcoating the CTABcapped rods with either negatively or positively charged polymers reduces toxicity and affects their uptake	(Alkilany et al. 2009)

Chan et al. studied the cellular uptake of antibody-functionalized spherical gold nanoparticles with sizes varying in between 2–100 nm (Chithrani, Ghazani, and Chan 2006, Jiang et al. 2008) and found that 40-50 nm sized nanoparticles enter cells more efficiently than both smaller and larger ones (Jiang et al. 2008) since antibody-functionalized nanoparticles have the maximum interaction with the receptors at the surface of the cell, thus enter via receptor-mediated endocytosis. The shape of a nanoparticle, too, seems to have an effect in its cellular interactions and uptake. When Chan and colleagues compared the cellular uptake of gold nanorods (14 ± 74 nm) with gold nanospheres (either 14 or 74 nm in diameter) (Polizzi, Stasko, and Schoenfisch 2007),they found that cells take 500 and 375% fewer nanorods than 74 and 14 nm spheres, respectively (all particles had citrate surface capping) (Chithrani, Ghazani, and Chan 2006).

Chithrani and coworkers studied the relationship of the size and shape of gold NPs with cellular uptake by preparing libraries of gold nanoparticles with d core 14-100 nm and gold nanorods with aspect ratios 1.5-5.0. (Chithrani and Chan 2007). According to their study, 50 nm gold NPs and are more rapidly taken up in cell cultures than other gold NPs, and positively charged gold NPs are taken up more rapidly than other gold NPs. Although debatable, it appears that positively charged GNPs associate more quickly with negatively charged cell membranes, resulting in a faster rate of uptake (Goodman et al. 2004, Verma and Stellacci 2010).

Cellular uptake of a gold nanoparticle is profoundly affected by its surface chemistry and net charge. Albeit still arguable, many reports claimed that size and shape being the same, cationic nanoparticles enter cells much more efficiently than anionic ones (Ghosh et al. 2008, Hauck, Ghazani, and Chan 2008, Alkilany et al. 2010, Kim et al. 2010). An efficient interaction between the negatively charged cell membrane and the cationic NPs is the simplest explanation for this but it is not so clear when the attitude of the NPs in biological environments where they will develop new surfaces and an adsorbed protein corona is taken into account (Cedervall et al. 2007, Lynch et al. 2007, Lundqvist et al. 2008, Lynch and Dawson 2008). Besides, according to some studies, cationic nanoparticles are not ‘‘cationic’’ in biological medium containing proteins which are negatively charged and can exhibit electrostatic affinity for the surface of gold (Alkilany et al. 2009, Cho et al. 2010, Doorley and Payne 2011). To illustrate, when mixed with cell growth media containing 10% bovine serum albumin (zeta potential 20 mV) cationic gold nanorods (zeta potential +40 mV) become anionic. Despite the negative net charge

of the cell membrane, there are positively charged and non-charged domains. charge distribution in cell membranes is largely heterogeneous and contains domains that can bind cationic, anionic, or both macromolecules (Ghitescu and Fixman 1984).

Alkilany and Murphy compiled in 1020 a comprehensive review of over results of other groups on the toxicity and cellular uptake of gold NPs (Alkilany and Murphy 2010). Although generally groups studied spherical and rod shaped particles, some chemical stabilizers were employed such as citrate (most common), CTAB, various amino acids, and PEG both *in vitro* and *in vivo*. There was no clear conclusion to draw on the toxicity of AuNPs, for there were conflicting results among results. The final conclusion of these analyses is that particle uptake, distribution and toxicity largely depend on the interaction between the particle surface and the biological environment (Magnussen 2002, Alkilany and Murphy 2010).

Wang et al. also studied the uptake and toxicity of various sized gold nanospheres (synthesized without CTAB) and gold nanorods (synthesized with CTAB) (Wang et al. 2008). They found a radical increase in toxicity from all gold nanorods while there was no toxic effect from nanospheres they tested.

Effects of prismatic AuNPs on various human and animal cells have also been studied albeit in a modest level. Using fresh lemon grass extract, an example of one of the many biogenic synthesis methods developed to provide shape control, Singh et al. (Singh et al. 2011) synthesized gold nanoprisms. Negating potential issues with sample purity, the nanotriangles that eliminated the potential sample purity problems were tolerated by cancerous and non-cancerous cell lines, with 80% cell viability at doses of up to 800 μM. Although prismatic particles did not enter the nucleus, the cells take up them and they remain in the cytoplasmic space according to additional imaging studies.

Even though ligand-mediated uptake of gold nanoparticles is thought to be the normal path for cellular entry, gold nanoparticles with particular surface structures can enter cells by direct penetration as Verma and colleagues demonstrated in 2008 (Verma et al. 2008) by using 5 nm-diameter gold nanospheres with two capping molecules (anionic and hydrophobic, with alternating positions on the surface). Without harming the membrane in an action similar to the cell-penetrating peptides, the nanospheres entered the cells directly (endocytosis-independent entry).

Gold nanoparticles cannot enter the nucleus though they can enter cells and are trapped in vesicles (Shukla et al. 2005, Pernodet et al. 2006, Chithrani and Chan 2007, Khan et al. 2007, Alkilany et al. 2009). Nativo and coworkers showed by using TEM that

16 nm citrate-capped gold nanoparticles enter cells readily (incubation time 2 h) and are trapped into endosomes. There were no free nanoparticles in the cytosol or the nucleus, but by modifying the nanoparticles with cell-penetrating and nuclear-localizing peptides, they were able to deliver these to the cytosol and nucleus (Nativo, Prior, and Brust 2008). Nevertheless, nuclear penetration for gold nanoparticles without special surface functionalization could occur according to other reports. For instance, gold nanoparticles with 1.4 nm diameter were able to enter the nucleus in metastatic melanoma cells and bind DNA with high efficiency (24.5% of the total internalized gold nanoparticles bound to DNA) (Tsoli et al. 2005). In another study using citrate-capped gold nanospheres with 5 nm diameter, 25% of the internalized gold nanoparticles were able to enter the nucleus in HeLa cells without any surface functionalization. When the nanoparticles were functionalized with a nuclear-penetrating peptide, this fraction was doubled (Ryan et al. 2007).

Conclusions that can be drawn from studies are still pristine. Each research group uses different cell lines, different sizes of nanoparticles, different surface groups, different doses, different time points, and in contrast to qualitative visualization, those groups may not have quantitative data on nanoparticle uptake and toxicity of cells.

CHAPTER 2

SYNTHESIS AND CHARACTERIZATIONS OF GOLD NANOPARTICLES AND INVESTIGATIONS OF THEIR TOXIC EFFECT, CELLULAR UPTAKE AND LOCALIZATION INTO HUMAN LUNG CANCER CELLS

2.1. Aim of the Study

It is great importance to develop and understanding of cellular uptake and distribution of gold nanoparticles in living system. Most of the studies have shown that both uptake and removal mechanisms are dependent on the size, shape, and surface properties of nanoparticles.

The aim of this study is to synthesize and characterize gold nanoparticles, which are obtained in different sizes by using NaBH4, L-ascorbic acid and Tri-sodium citrate as a reducing agent, and investigate of their toxic effect, cellular uptake, and cellular distribution into human lung cancer cells. We synthesized gold nanoparticles with diameters of 5, 10, 20 and 40 nm and compared their uptake end intracellular distribution in A549 and H358 lung cancer cells.

2.2. Introduction

Particles, which have two or more dimensions in the size range 2-100 nm, are defined as nanoparticles. Plasmonic nanoparticles have been utilized in biomedical field due to their small size and unique physical, optical and chemical properties. The absorption features of noble metal nanoparticles are characteristic based on their size, shape, and composition of the particles in solution. Gold nanoparticles have been become important for cancer research in recent years because of their easy synthesis and surface modification, enhanced and tunable optical properties as well as excellent biocompatibility properties.

Gold has been used from ancient times to today as household goods, and coinage. The first colloidal gold have discovered by Faraday in 1881, which he called it as beautiful ruby fluid. Timeline of gold nanoparticle synthesis is shown in Figure 2.1. Turkevich et al. provided the first structural studies of gold nanoparticles in 1951 and in 1973, Frens performed systematic studies of Turkevich's citrate-mediated growth method, producing monodisperse spherical gold nanoparticles 16–150 nm in diameter (Turkevich, Stevenson, and Hillier 1951, Frens 1973). In 1994, Brust et al. investigated the synthesis of thiol-stabilized gold clusters using a two-phase system in which gold chloride was solvated in toluene by way of a phase-transfer reagent (Brust et al. 1994). Here, dodecanethiol was used as a stabilizer for gold clusters formed in the organic phase as reducing sodium borohydride was added to the aqueous phase. Halas and coworkers showed in 1998 that near-infrared absorbing gold nanoshells could be prepared by electrostatically adsorbing small gold nanoparticles to the surfaces of silica nanoparticles and subsequently reducing additional gold onto the structures to form a conformal shell (Oldenburg et al. 1998). In 2001, Murphy and El-Sayed demonstrated a colloidal growth method to produce monodisperse gold nanorods in high yield based on seeded growth. In this method, small (1.5 nm diameter) seed particles, produced from the reduction of chloroauric acid by borohydride in the presence of CTAB, are aliquoted into Au(I) growth solution prepared from the mild reduction of chloroauric acid by ascorbate and the addition of AgNO3 and CTAB (Jana, Gearheart, and Murphy 2001). The synthesis of gold nanocages, which were developed by Xia and coworkers, is based on a phenomenon known as a galvanic replacement, whereby more noble metal ions (Au, Pt) spontaneously oxidize the surface atoms of a less noble metal (Ag, Cu) with concomitant reduction of the more noble metal (Chen et al. 2006).

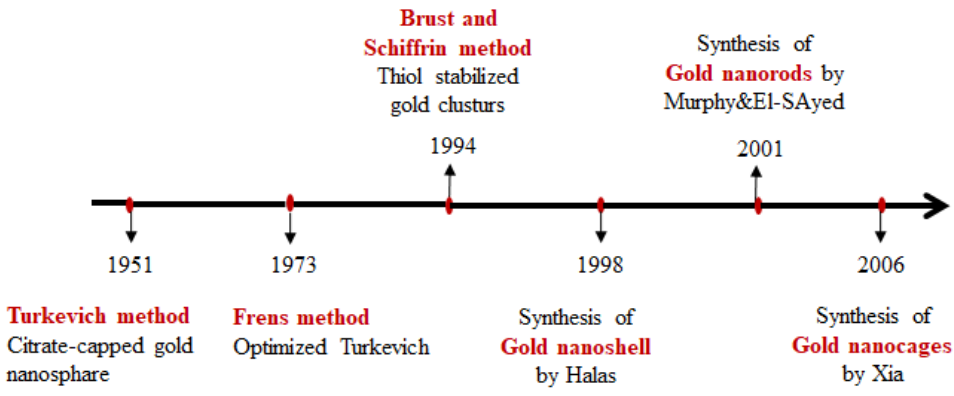

Figure 2.1. Timeline of gold nanoparticle synthesis.

It is possible to synthesize gold nanoparticles in different sizes and shapes with high quality and high efficiency. In this study, we used three different reducing agent, sodium borohydride, ascorbic acid and trisodium citrate for reduction. $NaBH_4$ is one of the most classic reductants in organic and inorganic chemistry, and it is used to reduce transition metal salts to metal (0) NPs in the presence of a stabilizer. Small gold nanoparticles (2-5 nm) are synthesized from the reduction of aqueous chloroauric acid by sodium borohydride (Prado et al. 2014, Deraedt et al. 2014, Ackerson et al. 2010). Ascorbic acid is a mild reducing agent and ascorbic acid plays an important role in the synthesis of advanced nanomaterials. The most popular method developed by Frens for controlling the size of the gold nanocrystals by citrate reduction. This method based on varying the ratio of the initial concentration of sodium citrate to gold, which may ensure the size control. Gold nanospheres (≥10) are synthesized from the reduction of aqueous chloroauric acid by citrate (Turkevich, Stevenson, and Hillier 1951, Frens 1973).

The development of nanotechnology requires quantitative and qualitative study on the cellular uptake and toxicity of nanoparticles according to their size and shape. Literature studies related to the cellular uptake and toxicity of gold nanoparticles depending on their size, shape, and surface chemistry have been described in detail in part 1.6.

Inorganic nanoparticles are widely used as a contrast agent in same applications, especially molecular imaging such as computed tomography, positron emission tomography, magnetic resonance imaging, optical imaging, and ultrasound. Among these techniques, differential interference contrast (DIC) microscope is the most prominent method for the detection of gold nanoparticles under the light microscope. Nomarski first introduced DIC microscopy that works on the principles of interference to determine optical path length gradients of the specimen in the 1950s. Suitability to the employment of full objective and condenser apertures that provides the user with the highest lateral resolution and at the same time the shallowest depth of field constitutes one major advantage of DIC microscopy. Gold nanoparticles give the best contrast under DIC microscope. Sun and colleagues used a DIC microscope to investigate the entire endocytosis process of 40 nm gold nanospheres by a HeLa cell was recorded at video rate.(Sun et al. 2009). Gu and co-workers indicate the endocytosis process of gold nanoparticles by using DIC microscope. In other studies of this group, the movement of gold nanorods was investigated on living cells and cell membranes and rotational movement of these nanorods were determined with DIC microscope (Gu et al. 2011).

The graph in Figure 2.2 was prepared by International Agency for Research on Cancer in 2014. This graph demonstrates the incident and mortality of different cancer types in Turkey for males and females.

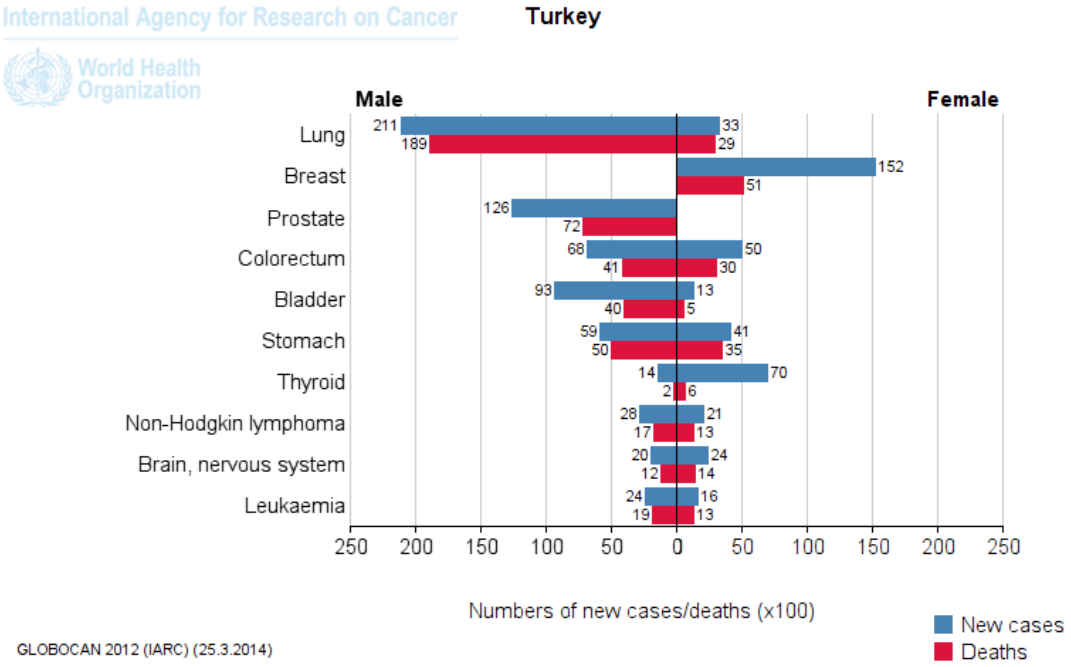

Figure 2.2. Number of new cancer cases and deaths by sex in Turkey, 2012.

According to Figure 2.2, lung cancer is the leading cancer type with respect to mortality and incidence. For this reason human lung cancer cells, which are A549 cancer (a human lung carcinoma epithelial cell lines) and H358 cancer (human lung/bronchiole carcinoma epithelial cell lines) cell lines were chosen this study. Figure 2.3 shows optical imaging of human lung cancer cell lines. Optical images of cell lines were obtained from ATCC website.

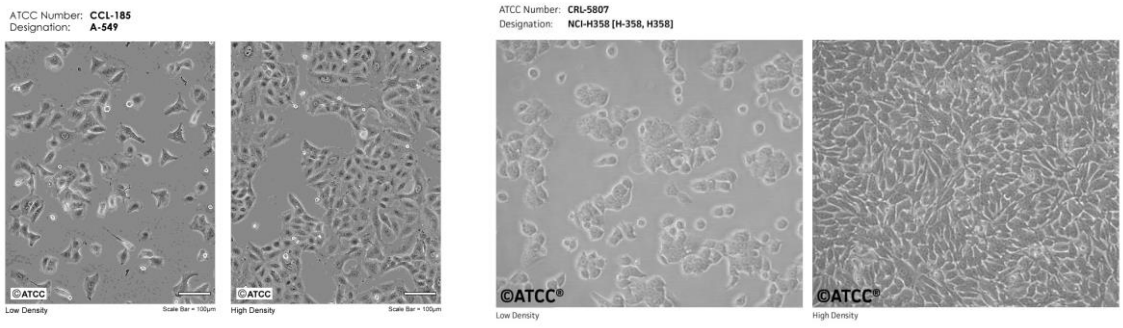

Figure 2.3. Optical images of A549 (right) and H358 (left) cell lines.

2.3. Experimental

2.3.1. Materials

All chemicals -hydrogen tetrachloroaurate (III) trihydrate $HAuCl_4.3H_2O$, 99%), sodium borohydride ($NaBH_4$, 98%), L-ascorbic acid (99%), trisodium citrate dehydrate, sodium dodecyl sulfate- used for the synthesis of gold nanoparticles were purchased from commercial supplier Sigma Aldrich. Ultrapure water was obtained from Millipore instrument for solution preparation. Cell mediums DMEM/F-12 (Dulbecco's Modified Eagle Medium/Nutrient Mixture), RPMI 1640 (Roswell Park Memorial Institute) and other required solutions FBS (Fetal Bovine Serum), L-glutamine, Pen-Strep (penicillin-streptomycin,), trypsin EDTA were purchased from Biological Industries (BI).

2.3.2. Instrumentation

Synthesized AuNPs were characterized by using optical and structural techniques. UV-Visible absorption spectra were recorded on a Varian Cary 50 UV-Vis Spectrometer. Size distribution and zeta potential measurements were performed by using Dynamic Light Scattering (DLS, Malvern ZETASIZER-ZS) instrument. Scanning electron microscopy (SEM) for structural characterizations of particles were performed by field emission scanning electron microscope (FEI QUANTA 250 FEG) operating at 15.0 kV. The concentrations of nanoparticles were analyzed by inductively coupled plasma- mass spectroscopy (ICP-MS) on an Agilent 7500ce. Cell images were taken by a spinning disc confocal microscope (Andor Revolution) equipped with a DIC (differential interference contrast) lens and 100X oil-immersion objective.

2.3.3. Synthesis of 5 nm Gold Nanoparticles ($AuNP_{5\ nm}$)

The 5 nm AuNPS were prepared by the reduction of Au (III) precursor to AuNP by using $NABH_4$ as a reducing agent. In this strategy, $NaBH_4$ (100 μL, 0.6M) was added to a 0.75 mM aqueous solution of $HAuCl_4$ (30 mL) at room temperature and stirred for an hour. The obtained nanoparticles were purified by centrifugation.

2.3.4. Synthesis of 20nm ($AuNP_{20\ nm\text{-}ascorbic}$) and 40 nm ($AuNP_{40\ nm\text{-}ascorbic}$) Gold Nanoparticles

In another approach, gold nanoparticles were synthesized by using ascorbic acid as a reducing agent. To an aqueous solution of $HAuCl_4$ (0.75 mM, 30 mL) of ascorbic acid solution (100 μL) at different concentration were added and stirred at room temperature. The size of gold nanoparticles were adjusted by molar concentration of ascorbic acid depending on Ascorbic acid/$HAuCl_4$ ratio (2 and 4 for 40 nm and 20 nm, respectively). Synthesized AuNPs was purified by centrifugation (6 000 rpm, 15 minutes).

2.3.5. Synthesis of 10 nm ($AuNP_{10\ nm\text{-}citrate}$), 20 nm ($AuNP_{20\ nm\text{-}citrate}$) and 40 nm ($AuNP_{40\ nm\text{-}citrate}$) Gold Nanoparticles

Turkevich method was another approach to synthesize AuNPs in 10 nm, 20 nm and 40nm sizes. Briefly, 50 mL of 0.25 mM $HAuCl_4$ was added to a 100 mL beaker on a stirring hot plate and heated to boiling temperature (110 ^{0}C). 1ml (for 10 nm), 0.5 ml (for 20 nm) and 0.3 ml (for 40 nm) 1% solution (by mass) of trisodium citrate was added to this rapidly stirred boiling solution. The color of the solution turns red in 10 minutes. Synthesized AuNPs was purified by centrifugation (6 000 rpm, 15 minutes).

2.3.6. Cell Culture

In this study, A549 cells (a human lung carcinoma epithelial cell lines) and H358 cells (human lung/bronchiole carcinoma epithelial cell lines) were used to investigate cellular uptake and distribution of synthesized AuNPs. A549 and H358 cell lines were obtained from the ATCC (American Type Culture Collection) and maintained in DMEM/F-12 and RPMI 1640, respectively. Basal mediums were supplemented with %10 FBS (fetal bovine serum), %1 penicillin and %1 L-glutamine. Cell cultures were kept at 37 ^{0}C in a 5 % CO_2 humidified incubator.

2.3.7. Cytotoxicity Assay

In this study, the viability of gold nanoparticle treated H358 and A549 cell lines were determined by using colorimetric MTT assay. For MTT assay, 100 000 cell/ml were initially seeded in 96 well plates. After the overnight incubation, cell medium was removed and replaced with 1 ml of complete medium treated with different concentration of AuNPs. To investigate their cytotoxicity with time, nanoparticle added cells were incubated for further 24, 48, and 72 h. Then, the medium was aspirated, cells washed three times with PBS. MTT solution (15µl, 5 mg/mL) was added to each well plate and incubated for 4 hours. After then, MTT medium was removed and DMSO was added which also used as positive control. The absorbance of each well was measured by spectrophotometry at 540 nm. Three replicates for each experiment were performed.

2.3.8. Cell Fixation

Cell fixation experiments were performed by following procedure. Each well of the 6 well plate was equipped with a sterile glass. Then, cells were seeded in each as 10^5 cells in 2 ml complete medium. After the overnight incubation, cells are treated with 25 µM AuNPs for further 24 h. The medium was removed and washed with PBS and DAPI was added as nuclei stain dye. Then, 4 % paraformaldehyde (PFA) in PBS was added to cells and incubated with PFA for 10 minutes at room temperature. PFA was removed and

cell was washed three times with PBS solution. Finally, ethanol was added to fix the cells and the fixed cells were taken from solution, dried and pasted on microscope slide.

2.3.9. Cellular Uptake of Gold Nanoparticles

Spectroscopic methods was used to determine the percentage and amount (nanoparticles/cell) of nanoparticles taken by A549 and H358 cells. The cells were grown in 96 well plates for overnight. Then, the grown media was removed and new media including AuNPs (50 μM) was added and incubated for further 24 hours. After this time, the culture media was taken into a new 96-well culture plate and optical density was measured at 519 nm, 524 nm and 530 nm by using microplate reader. Concentration of gold nanoparticles were calculated from the change in the absorption value of gold nanoparticles in the cell medium. Then, to calculate the number of nanoparticles per cells counting was performed as in the following procedure. Cells were washed with PBS and were digested with trypsin. After the detachment, cells were collected into centrifuge tube and centrifuged at 1200 rpm for 5 min. The supernatant were decanted and cells were dispersed with medium for counted with the hemocytometer. Cell counting was performed via an inverted optika microscope with 10x objective. The number of AuNPs that were uptaken by cells was determined from optical density of cellular media before and after incubation and calculated both percentage and amount as number of AuNPs per cell.

2.3.10. Imaging Study

A549 and H358 cells were seeded on glass putted in 6 well plate then, incubated overnight for the attachment on surface of plate. Cells were incubated with synthesized gold nanoparticles (6 different type) at concentration of 25 μM for 24 h. After the incubation time, fixation procedure was applied and DAPI was used to visualize nuclei of cells. Spinning disc confocal microscope (Olympus IX71) equipped with DIC nomarski lens was used for cell imaging. 100X oil immersion objective (1.2 NA) was used for fixed cell.

2.4. Results and Discussion

In general, size of nanoparticles are adjusted by using reducing agents with different reducing power. In this study, three different reducing agents -sodium borohydride, ascorbic acid and trisodium citrate- were used to obtain gold nanoparticles within the 5nm to 100 nm size range. To obtain the smallest sized particles (5nm) NaBH4 was used. Because of the strong reducing power the reaction was carried at room temperature and particles formed within short reaction time. Another used reducing agent was ascorbic acid which has intermediate reducing power and allowed to synthesize AuNPs in larger sizes. In both approaches, sodium dodecyl sulfate (SDS) was used as a stabilizing agent. In the third approach, sodium citrate was used to obtain largest particles within the range between 10nm to 100nm in size. The size distribution was achieved by varying the concentration of citrate buffer. In this synthesis, citrate acted as both reducing and stabilizing agent that eliminated the any need for stability additives. It is also worth to mention, sodium citrate was the weakest reducing agent in this study and required high reaction temperatures (boiling temperature) and elongated reaction times. After all work-up procedure, purified nanoparticles were characterized optically and structurally by using UV-vis spectrophotometer, Dynamic Light Scattering (DLS) measurement, Transmission Electron Microscope (TEM) and Scanning Electron Microscope (SEM).

One of the most important characteristics of gold nanoparticles are their specific absorptions that centered at around 510 nm to 540 nm. Optical characterizations of synthesized AuNPs was performed by benefiting from this distinguishing property using UV-Vis spectrophotometer. The reaction of $HAuCl_4$ with $NaBH_4$ in water under ambient conditions provides small AuNPs. The optical and structural characterizations of the AuNPs (5 nm) which synthesized with $NaBH_4$, were shown in Figure 2.4. As seen in UV-vis spectrum, AuNPs (5 nm) has their characteristic absorbance peak at 515 nm. The structural characterization was also performed for all synthesized particles by using Transmission electron microscope (TEM). As shown in Figure 2.4.c, the size of gold nanoparticles is 5 nm and they have spherical shapes. These results were also supported by DLS measurements. The hydrodynamic size distribution of particles are 5 nm (Figure 2.4.b). In addition to these, surface potential of the particles were determined as – 30 mV by using Zeta sizer.

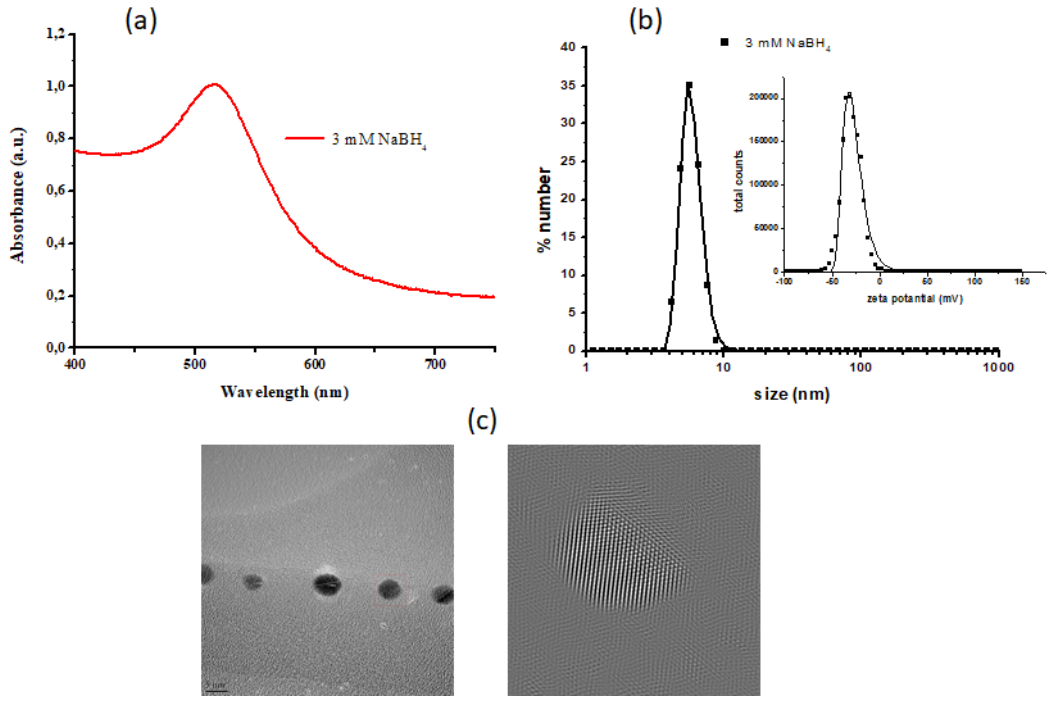

Figure 2.4. Characterizations of 5 nm gold nanoparticles UV-Vis spectrum (a) and TEM images (c) of AuNP. Right graph shows the size distribution and insert graph shows the zeta potential distributions of gold nanoparticles obtained from DLS measurements (b).

The same optical and structural characterization methods were performed for other particles prepared by using ascorbic acid and citrate reducing agents. The characterization of ascorbic acid reduced AuNPs are shown in Figure 2.5. As it mentioned before the concentration of ascorbic acid effects the size distribution of particles. It was seen in Figure 2.5 (a) the particles prepared by using 3 mM of ascorbic acid has maximum absorbance at 525 nm whereas other batch of particles prepared by using 1.5 mM of ascorbic acid has maximum absorbance at 530 nm. The results showed that increasing concentration of ascorbic acid resulted in a decrease in particle size. In general, blue shift is observed in characteristic absorption of gold nanoparticles when the size decreases. In addition to UV-Vis results, DLS and SEM measurements supported the formation of spherical shaped uniform particles (Figure 2.5 (b), Figure 2.5 (c)). From DLS measurements, the synthesized particles were distributed uniformly in 20nm and 40nm sizes with respect to used ascorbic acid concentration. Additionally, surface potentials of synthesized gold nanoparticles were measured and found as -40 and -35 mV for 20 nm and 40 nm, respectively.

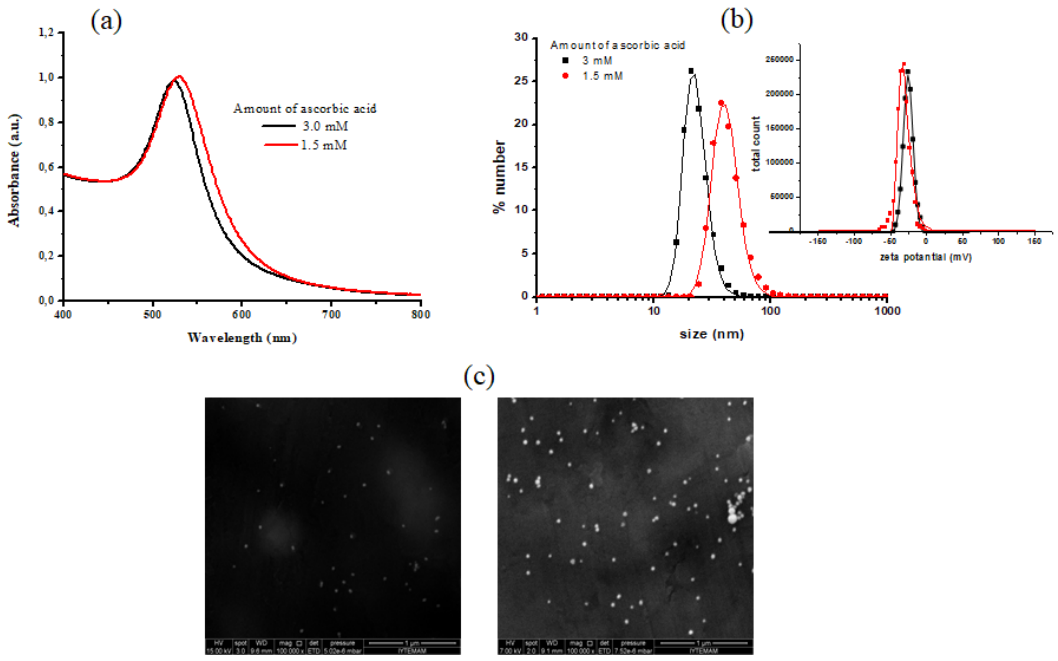

Figure 2.5. Characterizations of synthesized 20 nm and 40 nm gold nanoparticles. UV-vis spectrum (a), size distribution (b) and insert graph shows the zeta potential distributions of gold nanoparticles obtained from DLS measurements. SEM images (c) of AuNPs of size 20 nm (left) and 40 nm (right).

The characterization results of sodium citrate reduced gold nanoparticles were summarized in Figure 2.6. Citrate is a weakly reductant, so that required temperature rise in the synthesis process to increase reduction efficiency. Due to citrate has a good stabilize ability, not surfactant require for this process. Similar to ascorbic acid reduction to tune the diameter of particles varying concentrations of citrate was used. As shown in Figure 2.6 (a), increasing concentration of trisodium citrate resulted in blue shift in characteristic absorbance of gold nanoparticles. Here, similar trend was achieved in which smallest sized particles obtained by using higher concentration of reducing agent. UV-Vis absorption spectrum represent that maximum absorption peak shift from 530 nm to 519 nm with the increasing the amount of trisodium citrate. To support UV-Vis results, DLS measurements were also performed. Size distribution graph proved that size of gold nanoparticles are 40 nm, 20 nm and 10 nm with respect to trisodium citrate amount, which corresponds to 0.25 ml, 0.50 ml and 1.00 ml, respectively. Increasing the amount of trisodium citrate volume results the smaller nanoparticles.

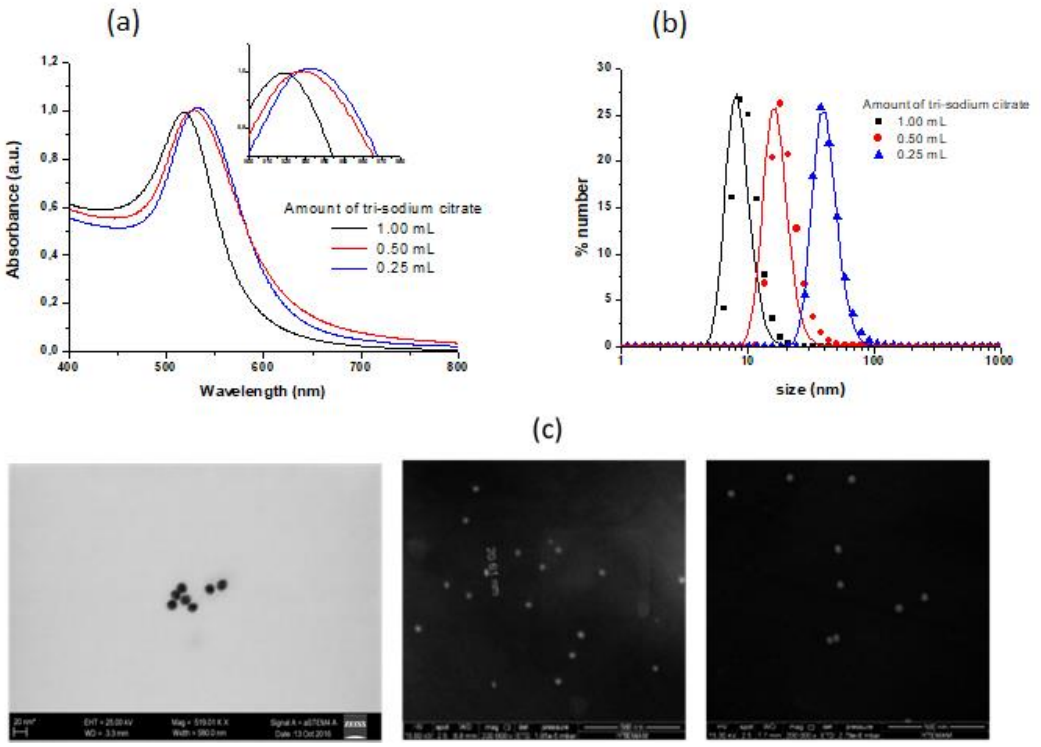

Figure 2.6. Characterizations of synthesized gold nanoparticles. (a) UV-vis spectrum of gold nanoparticles. (b) Size distribution and insert graph shows the zeta potantial distributions of gold nanoparticles obtained from DLS measurements. (c) Electron microscopy images of AuNPs.

The morphology and size of synthesized gold nanoparticles were investigated by using transmission electron microscope (TEM) and scanning electron microscope (SEM) image (Figure 2.6 (c)). The images of gold nanoparticles obtained by 1.00 ml of trisodium citrate taken by TEM (left) were shown in left. In the TEM images, it is clearly seen that the size of AuNPs are 10 nm and their shapes are spherical and monodisperse. Electron microscopy images of AuNPs synthesized with 0.50 ml (centre) and 0.25 ml (right) of trisodium citrate were taken by using SEM. According to SEM images, the sizes of nanoparticles are 20 nm (centre) and 40 nm (right) and the shapes are spheres and have narrow size distribution. These results were consistent with DLS measurements. The particle size was decreased by the increase in the trisodium citrate amount.

Table 2.1. Characteristics of gold nanoparticles

	Size d.nm	λ_{max} nm	Zeta mV	ICP mg/L	Number of AuNPs/mL	Yield %
5 nm-Na	5±2	515	-38±10	82	2.20×10^{14}	80
20nm-as	20±6	525	-40±10	113	1.80×10^{12}	97
40nm-as	40±10	530	-35±13	98	2.30×10^{11}	94
10 nm-cit	10±2	519	-35±10	26	5.00×10^{12}	80
20 nm-cit	20±3	525	-28±14	33	6.00×10^{11}	86
40 nm-cit	40±8	530	-33±15	34	0.75×10^{11}	88

All characterization results of synthesized gold nanoparticles are summarized in Table 2.1. The concentration of synthesized gold nanoparticles and conversion of Au^{3+} to Au^0 were determined by ICP analysis. The amount of conversion of Au^{3+} to Au^0 were determined from the results obtained by ICP analysis. The minimum conversion of Au^{3+} to Au^0 was found as 80% and the maximum conversion was 97%. The lowest conversion were obtained in synthesis of 5 nm and 10 nm sizes of AuNPs. Based on the conversion results, the number of gold atoms (N_T) in the reaction solution were calculated. The average number of gold atoms (N) for each type of nanospheres were calculated by equation 2.1.

$$N = \frac{\pi}{6} \times \rho \times \frac{D^3}{M} = 30.89602 D^3 \quad (2.1)$$

ρ is the density for FCC gold (19.3 g/cm^3), M is atomic weight of gold (197 g/mol). The average number of gold nanoparticles in solution were calculated by dividing the N_T/N. The AuNPs/mL results of synthesized gold nanoparticles were shown in Table 2.1.

The cytotoxicity of gold nanoparticles were also examined. The cytotoxicity of synthesized bare AuNPs was assessed in two human lung cancer cell lines (A549 and H358) by using an MTT (3-(4,5-Dimethylthiazol-2-yl)-2,5-Diphenyltetrazolium Bromide) assay (Figure 2.4 and Figure 2.5). The cells were incubated with different concentrations (0.05, 0.5, 5, 25, 50, 100 μM) of gold nanoparticles for 24, 48 and 72 hours.

A549 cells treated with synthesized Au nanoparticles with varying concentrations ranging from 0.05 to 100 μM. Then, cytotoxicity of these nanoparticles was measured with MTT assay. The MTT results of A549 cell lines were given in Figure 2.7. According to the graphs obtained from the MTT assays, AuNPs do not show any significant toxic effect on A549 cell lines even when the concentrations of gold nanoparticles increased up to 100 μM.

The similar experiments were also performed for H358 cell line to determine cytotoxicity of bare AuNPs. The results of the cytotoxicity of 6 different gold nanoparticles with varying concentrations of AuNPs ranging from 0.05 to 100 μM are shown in Figure 2.8. MTT results showed, AuNPs at concentrations 0.05, 0.5 and 5 μM had no significant effect on cell viability of H358 cell lines. However, the viability of H358 cells decreased by 50% after treatment with higher concentrations which were 25, 50 and 100 μM. It was clearly seen in Figure 2.7 and Figure 2.8, the H358 cell lines exhibited a 50% loss of viability while the A549 cell lines exhibited only 10%-20% loss of viability at 25 μM and over doses.

Whether the material added to the cell will exhibit toxic effects depends on the cell type as well as on the material. In this study, synthesized gold nanoparticles showed different toxic effects on two different types of lung cancer cells.

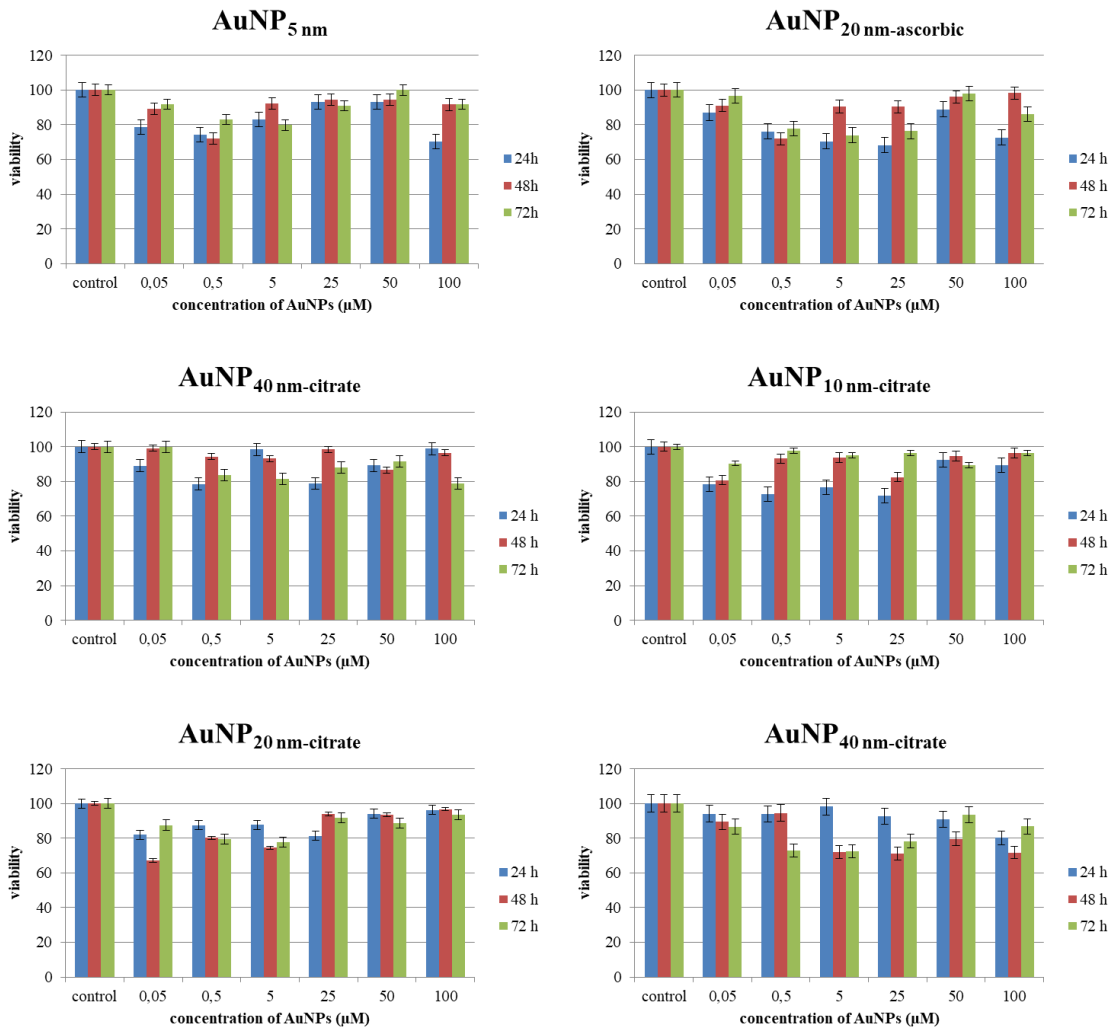

Figure 2.7. Viability of A549 cells after 24 hours incubation with various concentration of synthesized AuNPs.

After examination of cytotoxicity, the cellular uptake efficiencies of different type of AuNPs were scrutinized by quantifying them using UV-Vis spectrophotometry. Firstly, A549 and H359 cells were treated with 25 µM gold nanoparticles and incubated for 24 hours in complete medium. In addition, the concentrations of AuNPs were equalized before the incubation of cells with AuNPs in all experiments. As explained in the experimental section, cell medium was taken another well plate and UV-Vis spectrum measured to determine the concentration of AuNPs, which remained in cell medium. Then, trypsin was added to the each well to detach cells at 37 ^{0}C for 5 min. After the allotted time, cells were detached from well plate surface and counted with hemocytometer. Thus, the count of cells in each well and amount of AuNPs inside the cell were determined for this method.

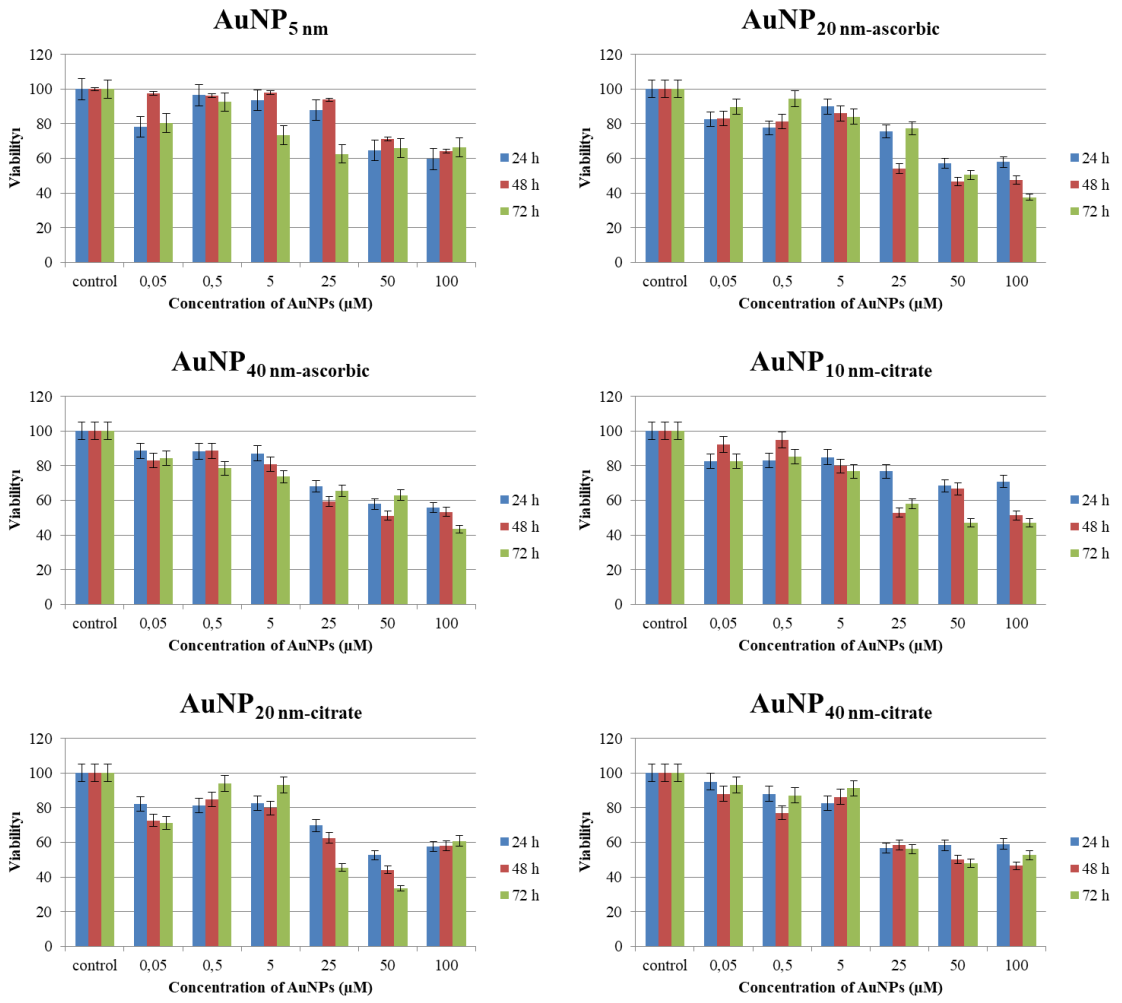

Figure 2.8. Viability of H358 cells after 24 hours incubation with various concentration of synthesized AuNPs.

In Figure 2.9, the graphs which drawn as the number of gold nanoparticles versus different type of gold nanoparticles showed the cellular uptake of particles with different sizes. For A549 cell line, the maximum number of AuNPs with the size of 5 nm, 20 nm-ascorbic, 40 nm-ascorbic, 10 nm-citrate, 20 nm-citrate and 40 nm-citrate were uptaken by amount as $0.15x10^6$, $0.28x10^6$, $0.38x10^6$, $0.20\ x10^6$, $0.30x10^6$ and $0.49x10^6$ particles/cell, respectively. According the graph, the maximum uptake by the A549 cells ensured with the nanoparticle size of 40 nm. Figure 2.9 indicates an increase in cellular uptake around 70% of 40 nm citrate and ascorbic acid reduced gold nanoparticles. For these samples, the number of nanoparticles in a single cell were approximately $0.49x10^6$ and $0.38x10^6$ particles/cell. A quantitative comparison in between 20 nm and 40 nm AuNPs clearly showed that the cellular uptake was greater for 40 nm of AuNPs than 20

nm ones. Additionally, the cellular uptake of 10 nm of gold nanoparticles was greater than 5 nm of gold nanoparticles.

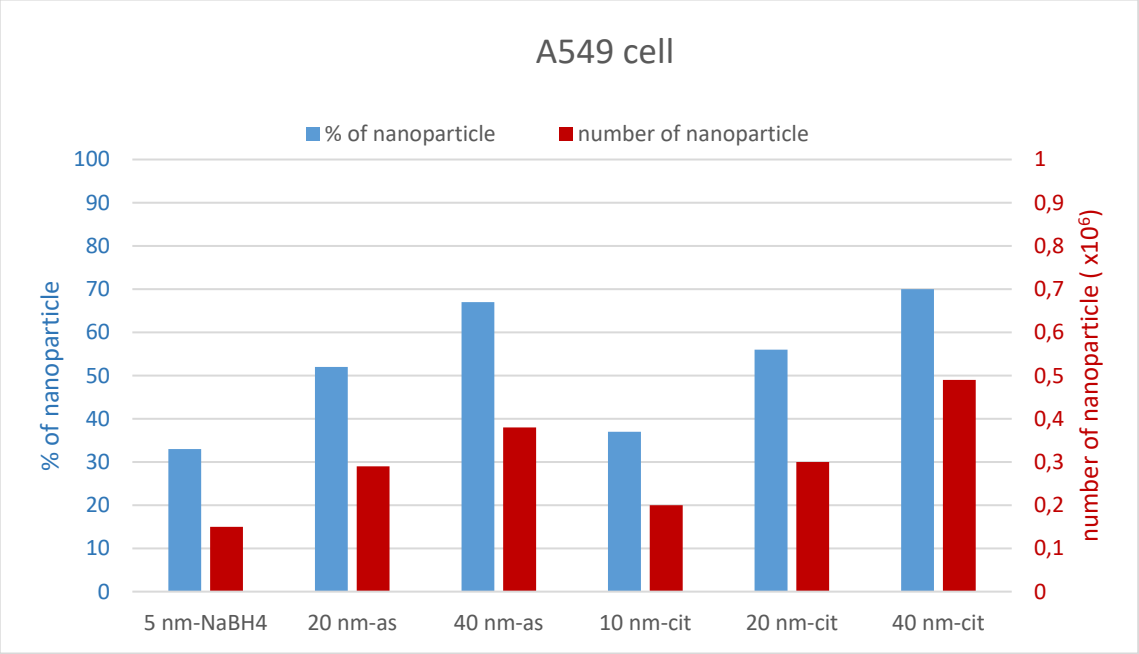

Figure 2.9. Quantitative analysis of cellular uptake of A549 cells treated with synthesized AuNPs after 24 hours

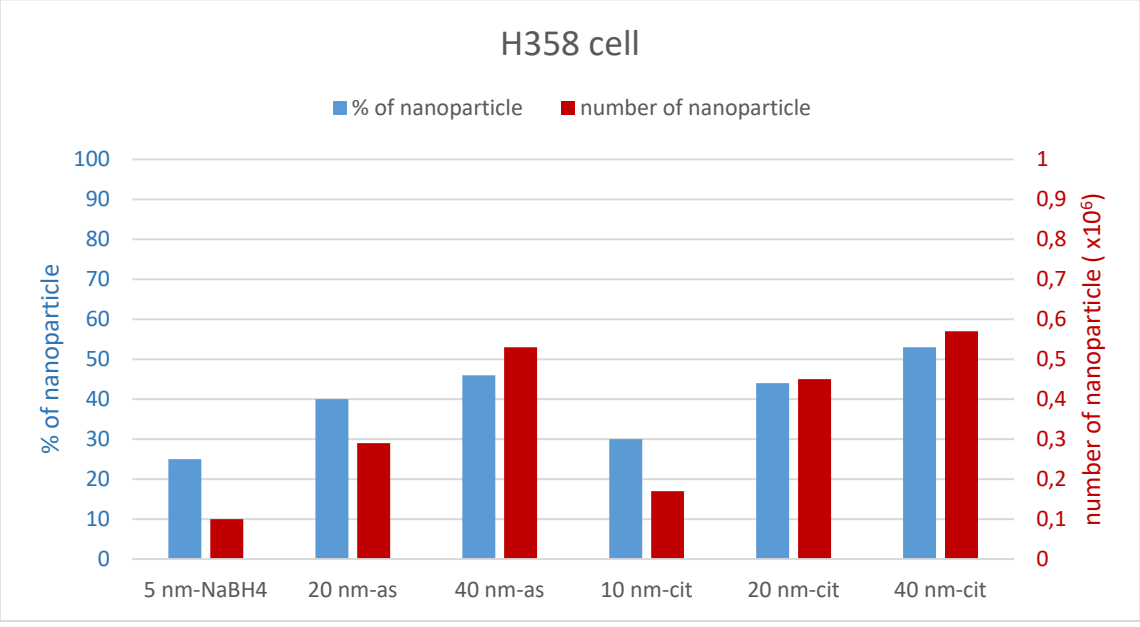

Figure 2.10. Quantitative analysis of cellular uptake of H358 cells treated with synthesized AuNPs after 24 hours

The same experiment was performed to determine cellular uptake of different sizes of gold nanoparticles into H358 cells (Figure 2.10). Almost the same results were obtained for the uptake of AuNPs by H358 cell lines. The maximum number of AuNPs that sized as 5 nm, 20 nm-ascorbic, 40 nm-ascorbic, 10 nm-citrate, 20 nm-citrate and 40 nm-citrate uptaken in H358 cancer cells were $0.10x10^6$, $0.28x10^6$, $0.53x10^6$, $0.17x10^6$, $0.45x10^6$ and $0.57x10^6$ particles/cell, respectively. It is indicated in Figure 2.10, there is a %50 increase in cellular uptake of 40 nm citrate and ascorbic acid reduced gold nanoparticles in which the number of nanoparticles in a single cell were calculated as approximately 0.6 $x10^6$ particles/cell. Moreover, intracellular concentration of 20 nm sizes ascorbic acid and citrate reduced AuNPs in H358 cell lines were estimated to reach $0.3x10^6$ particles/cell based on optical spectroscopic analysis. As shown in Figure 2.10, uptake concentration of 5 nm AuNPs were different than for 10 nm AuNPs. As in the case of A549 cell lines, the lowest uptake of gold nanoparticles into cells were observed in 5 nm sized particles.

For fixed cell imaging study, cells were cultured on glass coverslips and incubated overnight to allow adhesion. A549 and H358 cells, which treated with 25 μM AuNPs, were incubated for 24 hours before images were taken by using confocal microscope. To image of cells, culturing medium was removed and cells were washed with 1X PBS. DAPI was added to cell to stain their nuclei at 37 ^{0}C for 10 min. After the incubation, coverslips were washed with PBS and fixed with 4% paraformaldehyde.

Olympus IX71 spinning disc confocal microscope equipped with DIC Nomarski lens were used to observed the internalization of different AuNPs by A549 and H358 human lung cancer cell lines. Cell nuclei were stained by DAPI and synthesized AuNPs were captured in DIC to evaluate internalizations.

When we looked at the control cells of A549 and H358 that did not include any particles (Figure 2.11 (a) and Figure 2.12 (a)), no black dots were observed into cells. The images were also taken for cells that were treated with gold nanoparticles with six different sized and incubate for 24 hours.

It was clearly seen in Figure 2.11, AuNPs with sizes between 5 nm and 40 nm were shown as black dots inside the cytoplasm of treated A549 cells. However, the particles were localized in cytoplasm and did not enter into nuclei of cells, which were stained with DAPI.

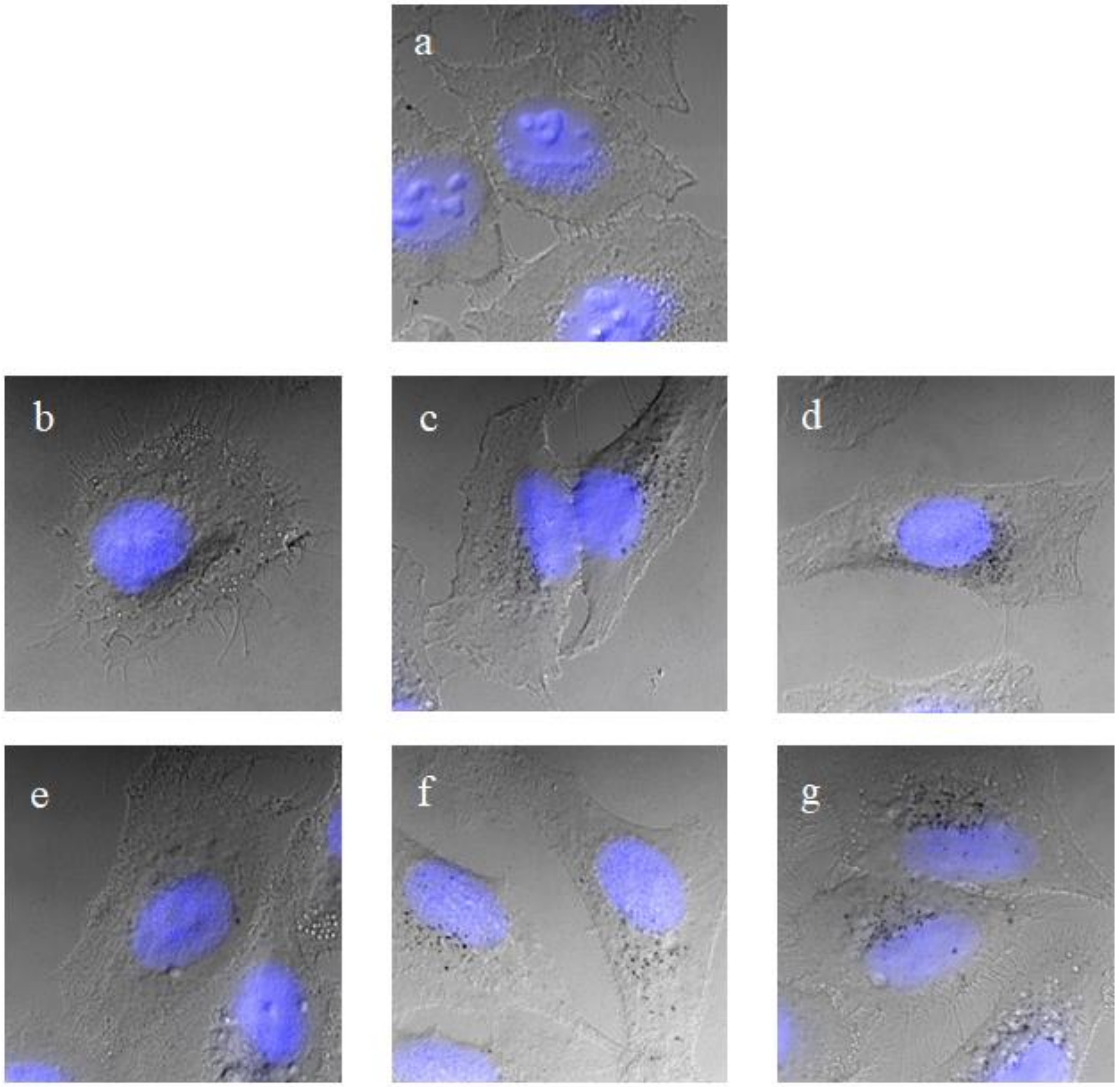

Figure 2.11. Cellular uptake of synthesized AuNPs in A549 cells. Confocal images of fixed A549 cells treated with 25 μM of AuNP for 24 h. a) control cells b) $AuNP_{5nm\text{-}Na}$, c) $AuNP_{20nm\text{-}as}$, d) $AuNP_{40nm\text{-}as}$, e) $AuNP_{10nm\text{-}cit}$, f) $AuNP_{20nm\text{-}cit}$, g) $AuNP_{40nm\text{-}cit}$. Images obtained by using DIC microscopy at 100X oil immersion objective (1.2 NA). DAPI was used for nucleus staining.

In addition, DIC microscope was used at 40X objective to capture the fixed cell images to understand the overall distribution of gold nanoparticles into cytoplasm of A549 cells. Figure 2.12 shows the 40X DIC images of A549 cells treated with AuNPs and stained with DAPI (nuclei staining dye as a blue color). According the 40X DIC images, gold nanoparticles efficiently penetrated through the cell membranes and localized at around the nuclei of the cells. Also morphology of cell did not change after treatment of AuNPs for 24 h.

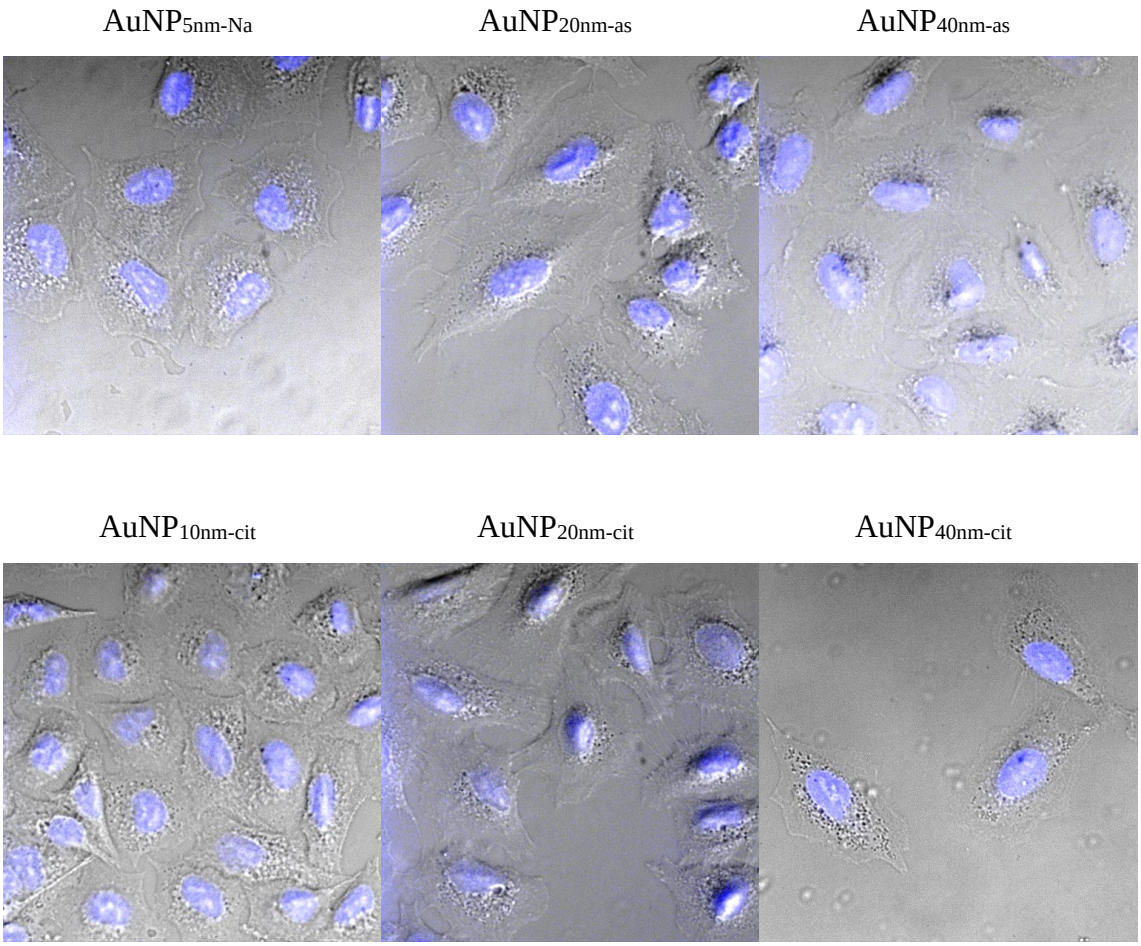

Figure 2.12. Confocal images of different AuNPs acquired after 24 hours incubation in A549 cells. DIC images represent with incubation 25 μM AuNPs obtained by using 40X objective. DAPI was used for nucleus staining.

The distribution of synthesized gold nanoparticles into H358 cells were shown in Figure 2.13. As similar case with A549 cell line, untreated control cells did not include any black dot structure that may interfere the observation of gold nanoparticles in next experiments. After the treatment of H358 cancer cells with AuNPs for 24 h, it was obviously seen that particles entered to the cell membrane and located into the cytoplasm.

To observe the overall distribution of gold nanoparticles into cytoplasm of H358 cells, fixed cell images were taken by DIC microscope at 40X objective (Figure 2.14). According to DIC images, gold nanoparticles internalized into cytoplasm and localized at around nuclei of H358 cells.

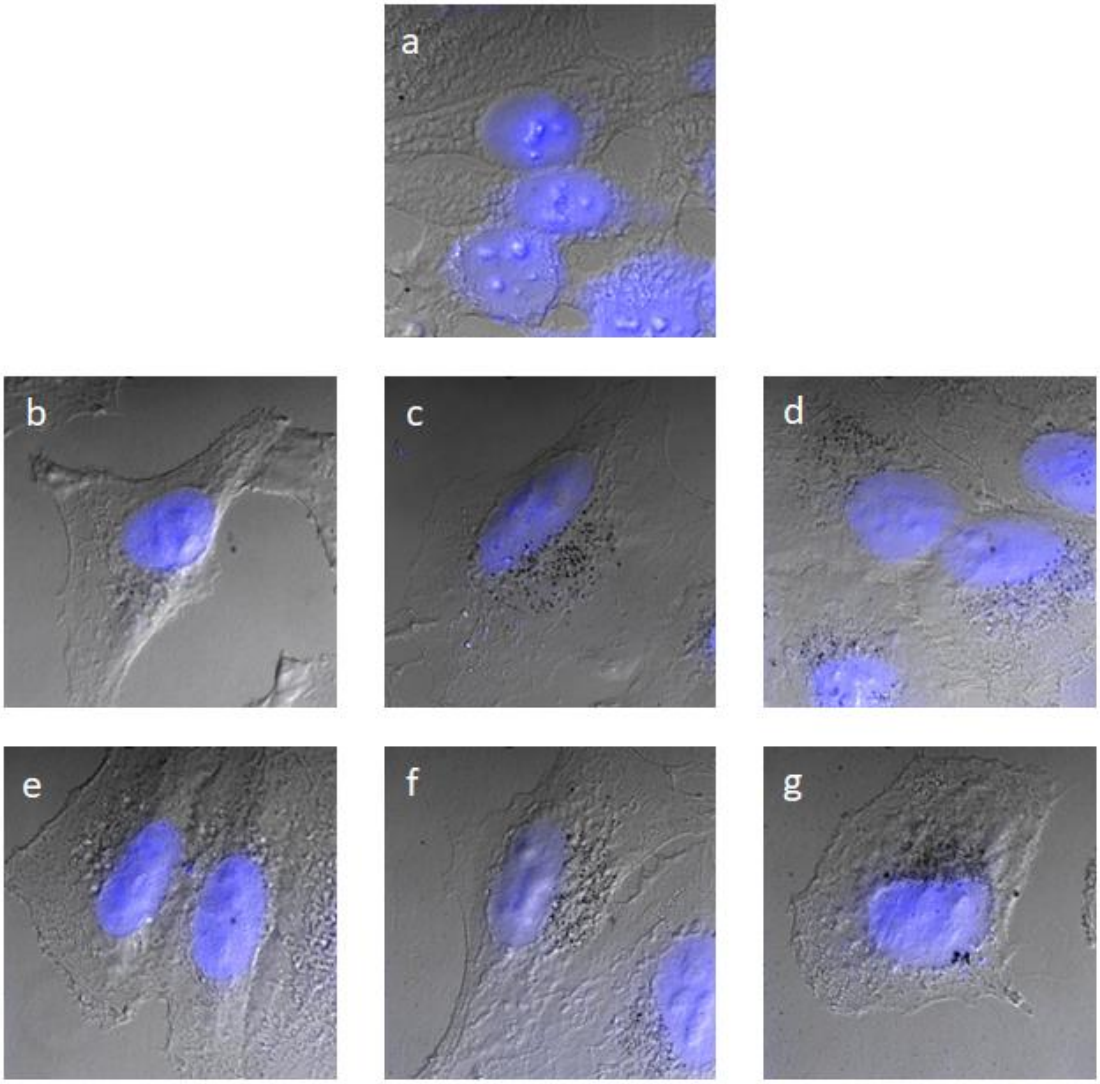

Figure 2.13. Cellular uptake of synthesized AuNPs in H358 cells. Confocal images of fixed H358 cells treated with 25 μM of AuNP for 24 h. a) control cells b) $AuNP_{5nm\text{-}Na}$, c) $AuNP_{20nm\text{-}as}$, d) $AuNP_{40nm\text{-}as}$, e) $AuNP_{10nm\text{-}cit}$, f) $AuNP_{20nm\text{-}cit}$, g) $AuNP_{40nm\text{-}cit}$. Images obtained by using DIC microscopy at 100X oil immersion objective (1.2 NA). DAPI was used for nucleus staining.

According to DIC images of A549 and H358 cells, it can be said that the visibility and amount of 20 nm and 40 nm sized gold nanoparticles were higher than 5 nm and 10 nm. This is because of two reasons; first, the particle size plays an important role DIC contrast of gold nanoparticles. The contrast increases with increasing size of gold nanoparticles. Smaller nanoparticles cross the cytoplasmic membrane more easily, but their scattering light cross-section is smaller than larger nanoparticles. Second reason of observed results is that gold nanoparticle sized with 40 nm and 20 nm entered into cells more efficiently than 5 nm and 10 nm size of gold nanoparticles. The results of DIC images supported the cellular uptake study.

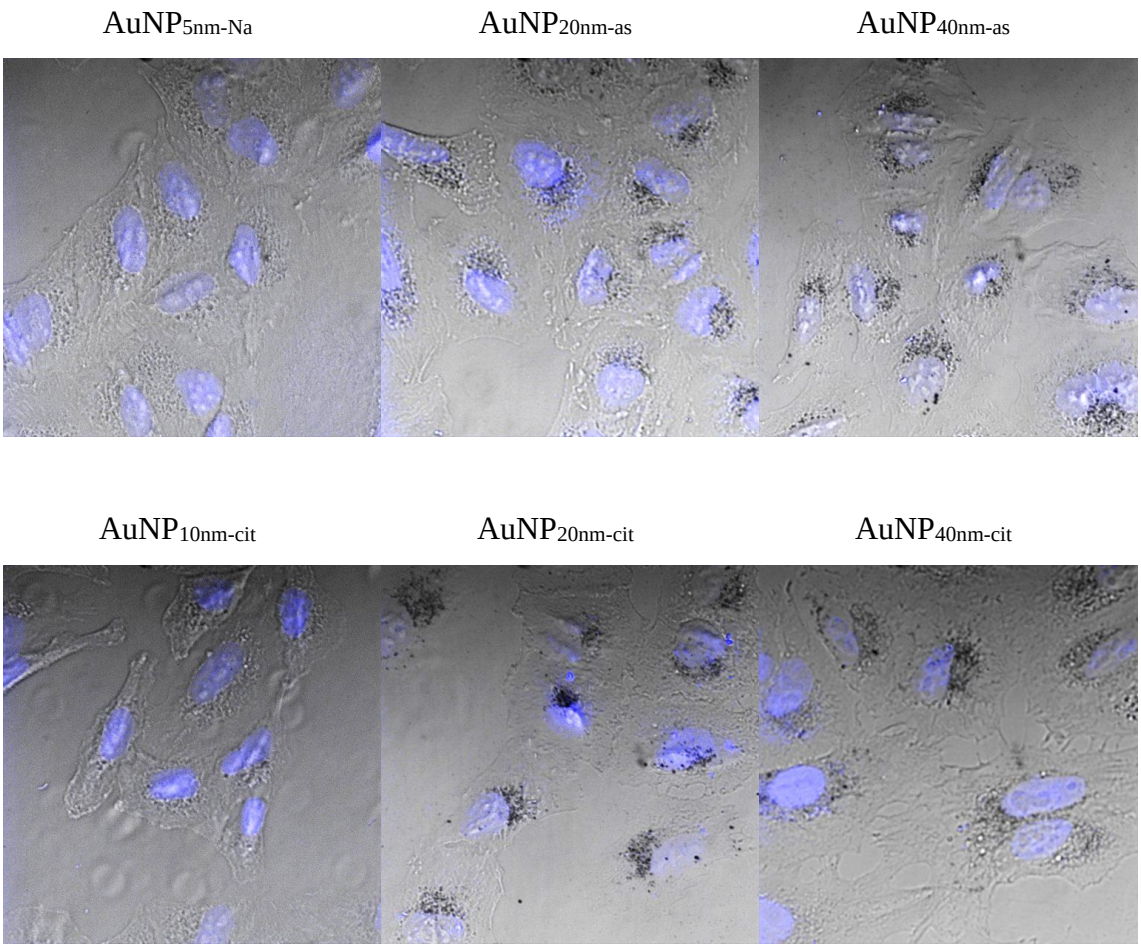

Figure 2.14. Confocal images of different AuNPs acquired after 24 hours incubation in H358 cells. DIC images represent with incubation 25 μM AuNPs obtained by using 40X objective. DAPI was used for nucleus staining.

It can be concluded from this study, bare gold nanoparticles whose surfaces were not decorated with any molecule can enter both A549 and H358 cells, and these particles can easily be visualized in cells by using DIC microscopy. Moreover, there was no difference in the distribution of gold nanoparticles within two different cancer cells.

When comparing A549 and H358 cells, any difference was observed from the point of cellular uptake and cellular distribution of gold nanoparticles within two different cancer cells. From these observations, it can be conclude that synthesized AuNPs can efficiently penetrate the both cell lines and localized at around nucleus.

2.5. Conclusion

In this part of study, six different gold nanoparticles were synthesized in between 5 and 40 nm sizes by using different reducing agents ($NaBH_4$, ascorbic acid, trisodium citrate). Physicochemical characterization of synthesized gold nanoparticles were performed by using UV-vis spectroscopy, dynamic light scattering (DLS), scanning electron microscopy (SEM) and transmission electron microscopy (TEM). ICP-MS was used for determination of concentrations (number of AuNPs/mL) and yield of synthesized gold nanoparticles.

A549 and H358 human lung cancer cells were used for cell studies. Viability of A549 and H358 cells were determined by MTT assay with different concentrations of gold nanoparticles for 24, 48 and 72 h. The toxic effects of these 6 different gold nanoparticles on lung cancer cells were examined and it was determined that there was no toxic effect even when the A549 cells were exposed to high doses up to 100 μM. According to MTT results, treated with gold nanoparticles up to concentration of 25 μM have no toxic effect on H358 cells. However, higher AuNPs concentration effected cell viability by 50% decrease.

In order to assess the amount of the uptake of AuNPs into A549 and H358 cells, the gold nanoparticle concentration in the cell culture media was determined by UV-Vis spectroscopy. As a result of the uptake study, it was determined that the 40 nm particles had the highest penetration into the cell. The uptake of gold nanoparticles into A549 and H358 cells gradually decreased in the order of 20 nm, 10 nm and 5 nm sizes. When two cell types were compared, there was no significant difference in cellular uptake depending on the size of gold nanoparticles.

In the microscope studies, gold nanoparticles displayed the best contrast under the DIC microscope. According to DIC images, gold nanoparticles were efficiently internalized into A549 and H358 cell lines. Synthesized AuNPs clearly seen as black dots in the cytoplasm at around the nucleus of both cells. All particles were found only in the cytoplasm of both cancer cells. The results were obtained by DIC images supported the results of cellular uptake of AuNPs by A549 and H358.

CHAPTER 3

OBSERVING INTRACELLULAR DISTRIBUTION OF PEPTIDE CONJUGATED GOLD NANOPARTICLES IN HUMAN LUNG CANCER CELLS USING LIVING CELL DARK FIELD IMAGING

3.1. Aim of the Study

It is great importance to develop and understanding of cellular uptake and distribution of gold nanoparticles in living system. If the particles are coated with a well-defined peptide before incubation, more controlled conditions are obtained. Targeting subcellular component leads to greater localization, which offers an effective method of enhanced imaging using plasmonic nanoparticles.

The aim of this study is to investigate and to compare the differences in cellular distribution and scattering properties of peptide conjugated and non-conjugated gold nanoparticles in the human lung cancer cells by using Dark field microscope. In order to investigate whether gold nanoparticles with different surface molecules have distinctive uptake processes, localization behavior and scattering properties in lung cancer cells, RGD coated gold nanoparticles with sizes of 20 and 40 nm were synthesized in this study.

3.2. Introduction

Plasmonic nanoparticles have been heavily utilized in the biomedical field due to their small size, and unique physical, optical, and chemical properties (Kelly et al. 2003, Dreaden et al. 2012). Gold nanoparticles are widely used in biotechnology and biomedical field because of their unique plasmonic properties, large surface area and high electron conductivity. Chemical adjustment of the nanoparticle surface is essential to provide biocompatibility and specificity to gold nanoparticles. AuNPs surface is one of the most stable and easily functionalized platforms for molecular conjugation.

Although many gold nanoparticle conjugates may exhibit a degree of intracellular penetration, particle size, charge and lipophilicity play a critical role in determining the degree of uptake. Cellular uptake predominantly depends on the specific surface chemistry of the particles. If the particles are coated with a well-defined ligand shell before incubation, more controlled conditions are obtained. Physical separation using hydrophilic polymer ligands is common practice and allows stable suspension of particles in both high ionic strength and serum concentration environments. Poly (ethylene glycol) (PEG) is the most common surface ligand used to stabilize biomedical nanoparticles and is particularly suited to gold surfaces by means of a thiol linker.

The most widely studied adhesive peptide in the biomaterials field is the tri-amino acid sequence, arginine-glycine-aspartate (RGD). The RGD sequence can bind to multiple integrin species, and synthetic RGD peptides offer several advantages for biomaterials applications. Integrin is composed of an α and β subunit, and the matching of these subunits determines the specificity for the ligand. For example, $\alpha_2\beta_1$ binds to selected collagen family members, $\alpha_5\beta_1$ binds to fibronectin, and $\alpha_v\beta_3$ binds to a range of ligands including fibronectin, vitronectin, and fibrinogen. In consequence, cells exposed to the material surfaces will perceive synthetic RGD in a background of synthetic integrin binding proteins (Bellis 2011). One strategy adopted by many investigators to minimize uncontrolled factors such as protein adsorption is to pattern RGD onto a material surface in combination with poly PEG (Xie et al. 2009, Kang, Mackey, and El-Sayed 2010, Austin, Kang, and El-Sayed 2013, Mackey et al. 2013).

The modification of nanometers is conducted to enhance the interaction of these nanoparticles with biological cells. The cellular uptake of particles and their distribution into the cell are specifically related to the surface chemistry of the particles. Targeted entry into cells is an increasingly important area of research.

Navita et al. demonstrated that citrate-capped gold particles were readily taken up by the cells and ended up in the endosome (Nativo, Prior, and Brust 2008). Citrate capped particles are quite densely packed, show clear signs of aggregation, and are strictly confined to the endosomes (Figure 3.1 right). However, ligand conjugated gold nanoparticles did not aggregate into cell due to ligand shell did prevent the particles from aggregation inside the cells (Figure 3.1 left).

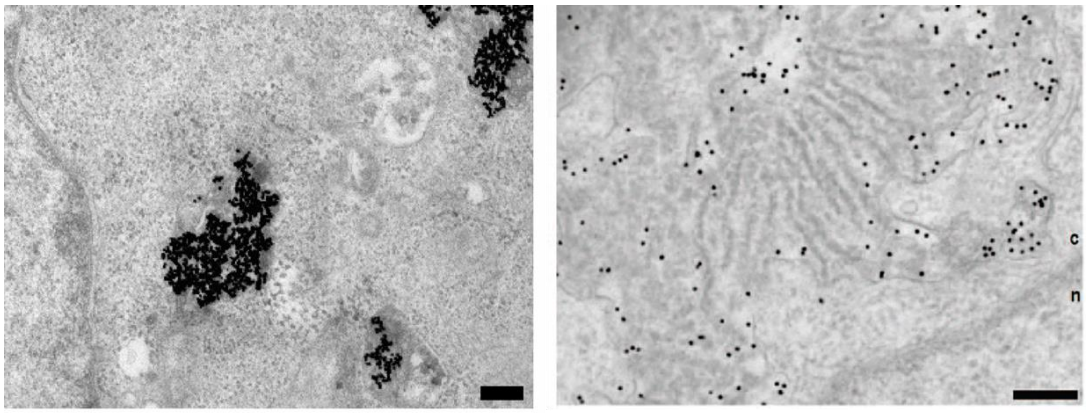

Figure 3.1. TEM images of citrate capped AuNPs (right) and peptide conjugated AuNPs (left) into HeLa cell

Plasmonic nanoparticles are especially useful for dark field imaging applications because of their enhanced resonant absorption and scattering properties. The nanoparticle, 30-100 nm in diameter, is intensely scattered and can be easily detected with a microscope under dark field illumination conditions.

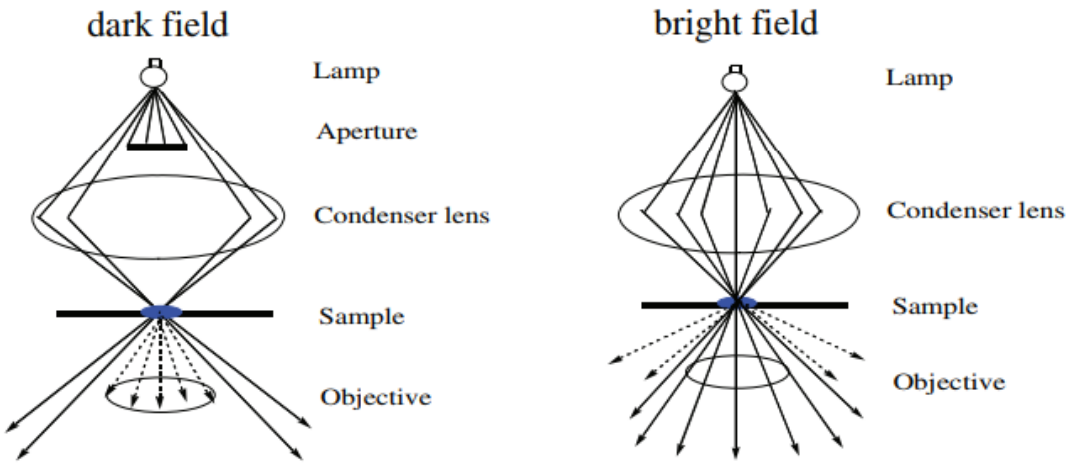

Figure 3.2. Schematic illustration the working principle of dark field and bright field microscope.

Dark-field, an illumination technique used to sharpen the contrast in unstained samples in optical microscopy, works by illuminating the sample with light that will not be collected by the objective lens, thus will not form part of an image. Thereby some bright objects are seen on a dark background. The high scattering features of AuNPs can enhance contrast in dark-field imaging. Dark-field microscopy was used for the successful selective detection of cancerous cells by El-Sayed et al. (El-Sayed, Huang, and

El-Sayed 2005), who conjugated 35-nm AuNPs with anti-EGFR antibodies to target two malignant epithelial cell lines. This is also helpful in monitoring the targeted delivery of nanorods conjugated with transferrin or cell-penetrating peptides (Oyelere et al. 2007). Figure 3.3 shows the dark field light scattering images of cells after incubation with CTAB capped nanorods and peptide conjugated gold nanorods for 2 h. It can be seen clearly that, while the CTAB-capped gold nanorods are not efficiently absorbed by the cells, the peptide conjugated gold nanorods enter into both cell lines with much higher efficiency. This result indicates that peptide conjugation enhances the cellular uptake of the gold nanorods. This enhanced gold nanorods uptake may be due to the receptor-mediated endocytosis.

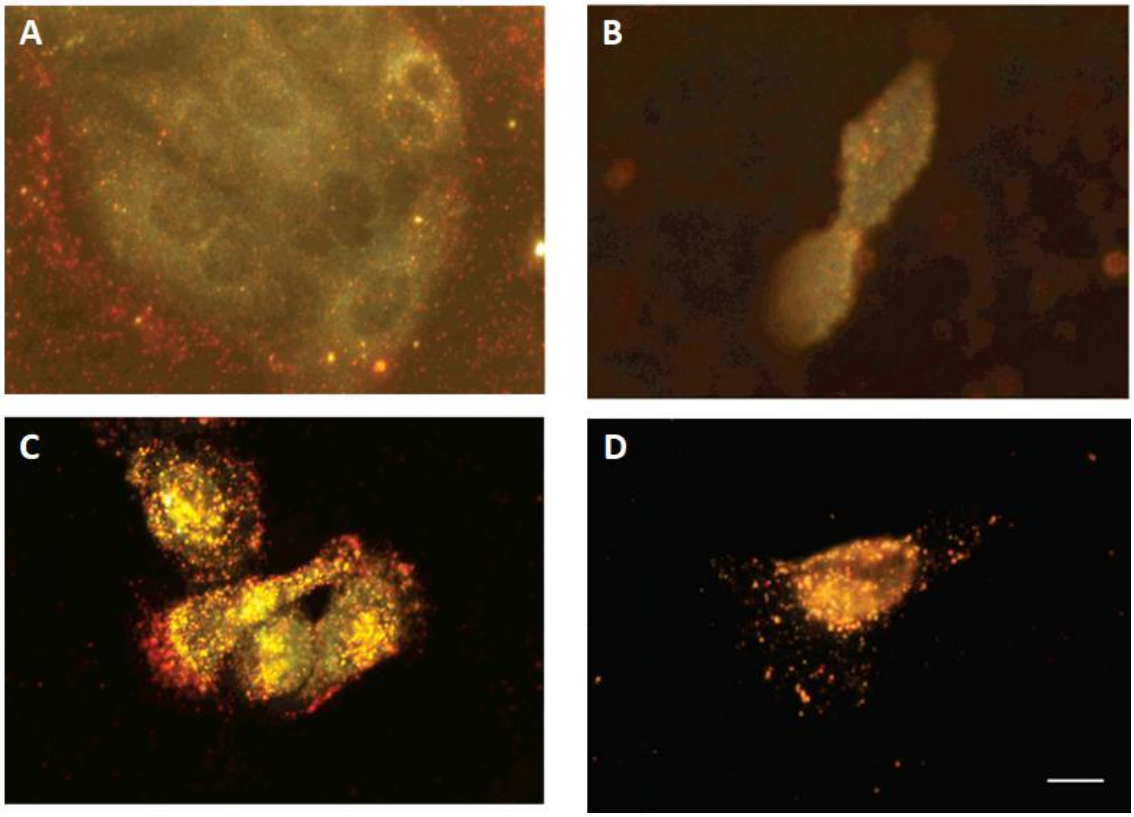

Figure 3.3. Dark field light scattering images of cells after incubation with gold nanorods and peptide-conjugated gold nanorods for 2 h. A. HaCat normal cells incubated with gold nanorods. B. HSC cancer cells incubated with gold nanorods. C. HaCat normal cells incubated with peptide-conjugated gold nanorods. D. HSC cancer cells incubated with peptide-conjugated gold nanorods. Peptide conjugation promotes the cellular uptake of gold nanorods. Scale bar: 10 μm (Source: Oyelere et al. 2007).

3.3. Experimenal Study

3.3.1. Synthesis of 20 nm 40 nm AuNPs

Gold nanoparticles synthesized with citrate reduction of $HAuCl_4$. Briefly, 50 mL of 0.50 mM $HAuCl_4$ are added to a 100 mL beaker on a stirring hot plate. A 1% solution (by mass) of trisodium citrate (0.25 ml for 40 nm, 0.50 ml for 20 nm AuNPs)) was mixed with this rapidly-stirred boiling solution. By changing the tri-sodium citrate amount 20 and 40 nm size of AuNPs were synthesized. Synthesized Au NPs were purified by centrifugation (14 000 rpm, 15 minutes).

3.3.2. AuNPs and Polyethyleneglycol Conjugation

Polyethylene glycol conjugation prevents aggregation of AuNPs before peptide conjugation. 0,2 mM solution of mPEG-SH 2000 (Laysan Bio) was prepared in DI water. The mPEG-SH solution was added in 10^3 times molar excess to AuNPs solution. The mPEG-AuNP solution was allowed to shake at room temperature overnight. Excess PEG was removed by centrifugation (4 000 rpm, 15 minutes) and peptide conjugated particles (PEG-AuNP) were redispersed in DI water.

3.3.3. RGD Peptide Conjugation of AuNPs

After PEGylation, gold nanoparticles were conjugated with RGD peptide (Sigma, Arg-Gly-Asp). 0.5 mM RGD was dissolved in DI water and was added to PEG-AuNPs solution in 10^5 times molar excess. RGD-AuNPs solution was allowed to shake 48 hours at room temperature. After the 48 hours, the excess amount of RGD peptides were removed by centrifugation (4000 rpm, 15 minutes). Particles were dispersed in DI water.

3.3.4. Cell Culture

A549 cancer epithelial cell line (human lung alveolar carcinoma cells), and H358 cancer epithelial cell line (human lung bronchioalveolar carcinoma cells) were used for this study. A549 cells were maintained in DMEM/F-12K medium and H358 cells were maintained in RPMI-1640 medium. All mediums were supplemented with 10% (v/v) fetal bovine serum (FBS), 1% (v/v) penicillin/streptomycin and 1% (v/v) L-glutamine. Cell cultures were kept at 37 ^{0}C in a 5% CO_2 humidified incubator.

3.3.5. Cytotoxicity Assay

A549 and H358 cells were seeded (10^5 cells/ml) in 96-well plates and incubated overnight to allow for cell attachment. After the overnight incubation, cell medium was removed and 100 µL/well of fresh complete medium, supplemented with AuNPs, were added to the cells. Cells were further incubated for 24, 48 and 72 h in the presence of AuNPs. Then, the medium was aspirated, cells washed three times with PBS. MTT solution (15µl, 5 mg/mL) was added to each well plate and incubated for 4 hours. After then, MTT medium was removed and DMSO was added which also used as positive control. The absorbance of each well was measured by spectrophotometry at 540 nm. Three replicates for each experiment were performed.

3.3.6. Living Cell Imaging

A549 and H358 cells ($5x10^4$ cells/ml) were seeded into 35 mm glass dish (µ-dish) and were incubated for overnight. After incubation, the medium was removed, cells were washed with PBS and fresh cell medium, containing 25 µM RGD conjugated AuNPs, were added to µ-dish. AuNPs containing cells were incubated at 37 ^{0}C for 24 h.

Cells were imaged using Olympus IX71 spinning disk confocal microscope. DAPI (4',6-Diamidino-2-Phenylindole, Dihydrochloride) was used to stain cell nuclei. Dark field condenser, used to deliver a narrow beam of white light from a halogen lamp, obtained the images. A 40X/0.6 objective was used to collect only the scattered light from

the sample. Thus, the samples with highly scattering characteristics were shown as a bright object on a dark background.

3.4. Results and Discussion

Monodisperse spherical gold nanoparticles, 10-100 nm in diameter, were synthesized by using Turkevich's method. The desired nanoparticles were obtained in water media by using auric acid as a gold precursor, sodium citrate as reducing agent and stabilizer. The size of nanoparticle was controlled by changing the concentration of sodium citrate reagent. Importantly, we used 20 and 40 nm gold nanoparticles due to their best contrast properties under DIC microscope in cells (see Part 2). 20 nm and 40 nm AuNPs were functionalized with PEG in order to prevent any aggregation. Furthers, PEG conjugated AuNPs were also conjugated with RGD peptides. Citrate-capped gold NPs are negatively charged due to a layer of negative citrate ions. When the antibody positively charged amino groups are attracted to the gold surface and sufficiently close for protein binding, the hydrophobic pockets of the protein will contact and bind to gold. RGD was used to increase nanoparticle endocytosis by targeting α and β integrin on the cell membrane and to increase scattering by localizing the plasmonic nanoparticles. Conjugated gold nanoparticles were characterized by using UV-vis spectroscopy, dynamic light scattering (DLS), scanning electron microscopy (SEM) and energy-dispersive X-ray spectroscopy (SEM-EDX).

Optical characterization of RGD conjugated AuNPs were carried out by using UV-vis spectrophotometer. UV-vis spectra of gold nanoparticles display a strong absorption at around 510-550 nm. Figure 3.4 shows the absorption spectrum of spherical gold nanoparticles before and after conjugation with RGD peptide. As we see in Figure 3.4, the characteristic absorption peak was observed at 525 nm for 20 nm bare AuNPs and 20 nm RGD-AuNPs (left), and 530 nm for bare 40 nm AuNPs and 40 nm RGD-AuNPs (right). The UV-vis spectrum shows that the maximum absorption wavelength value of both conjugated and non-conjugated AuNPs in both sizes did not change after conjugation and there was no change in the width of the wavelength. These results denoted that there was no agglomeration during conjugation and purification of nanoparticles.

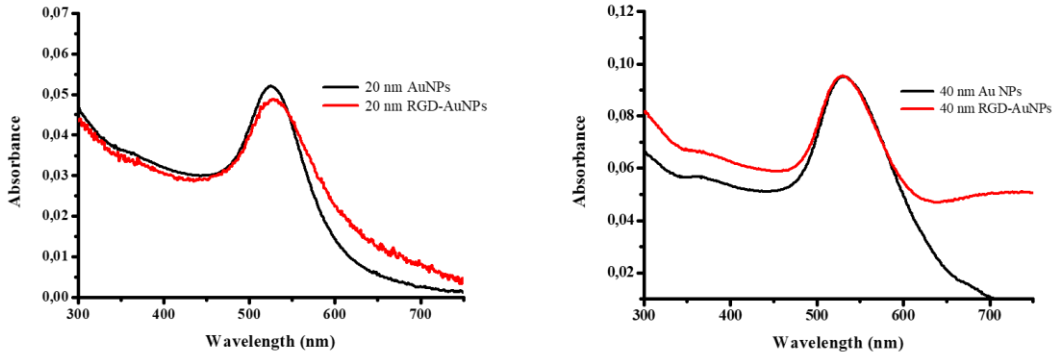

Figure 3.4. Uv-vis spectrum of 20 nm non conjugated and RGD conjugated AuNPs (left) and 40 nm non conjugated and RGD conjugated AuNPs (right)

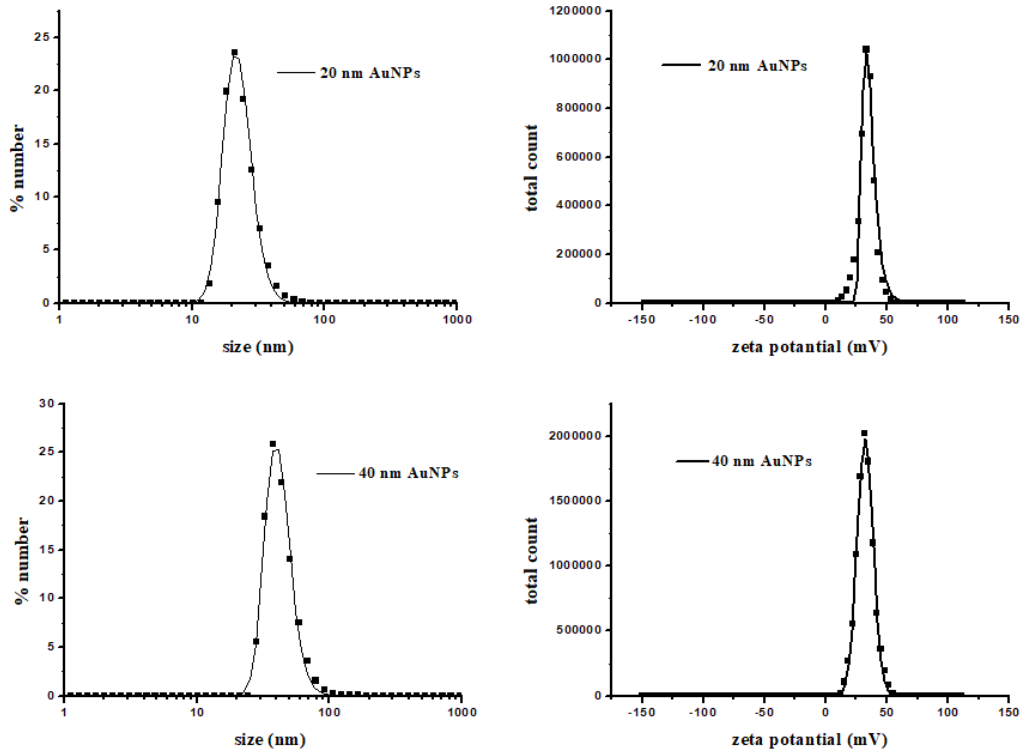

Figure 3.5. Size and zeta potentials of 20 nm and 40 nm non conjugated AuNPs. Size and zeta potential distribution was obtained by using DLS

Hydrodynamic diameters, and zeta potentials of non-conjugated and RGD conjugated gold nanoparticles were measured by using DLS (Dynamic light scattering, Malvern Nano-ZS). Figure 3.5 shows the size and zeta potential distribution of non-conjugated 20 nm and 40 nm AuNPs. According to the DLS results, gold nanoparticles were synthesized the desired size of 20 ±3 nm and 40 ±8 nm. Zeta potential distribution shows that synthesized gold nanoparticles exhibited the highly negative surface zeta

potential values of -28 ±14 mV and -33 ±15 mV for 20 nm and 40 nm in size, respectively. This result indicates that surface potentials of citrate reduced gold nanoparticles were negatively charged due to citrate were also coated on the surface of gold nanoparticles.

Size and zeta potential distribution of RGD conjugated 20 nm and 40 nm AuNPs were displayed in Figure 3.6. DLS results also indicate that the size of gold nanoparticles did not change after the RGD conjugation. In addition, the zeta potential measurements demonstrated that surface charge of RGD conjugated AuNPs increased to 0 ±8 mV for both sized RGD-AuNPs. This change in the surface potential of AuNPs proves that conjugation of RGD to AuNPs surface was carried out successfully. According to size and surface potential results, the conjugation of RGD peptides to AuNPs surface did not alter the diameter, but zeta potential further increased.

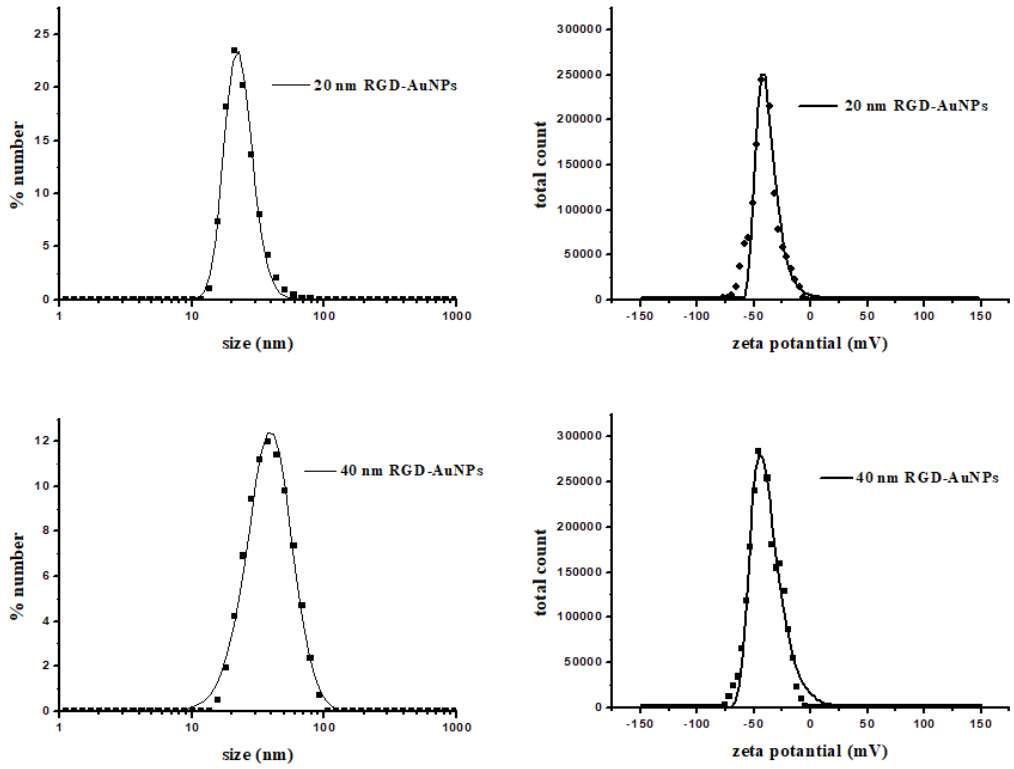

Figure 3.6. Measurements of particle size and zeta potentials of 20 nm and 40 nm RGD conjugated AuNPs. Size and zeta potential distribution was obtained by using DLS.

The size and morphology of RGD conjugated gold nanoparticles were investigated using a scanning electron microscope (SEM, Quanta 250FEG) at an accelerating voltage of 15 kV. Figure 3.7 shows the SEM images of RGD-conjugated 20

nm and 40 nm gold nanoparticles. According to SEM images, the shape and particle size of the RGD conjugate AuNPs did not change after conjugation, which supported the result of UV-vis graph and DLS measurement.

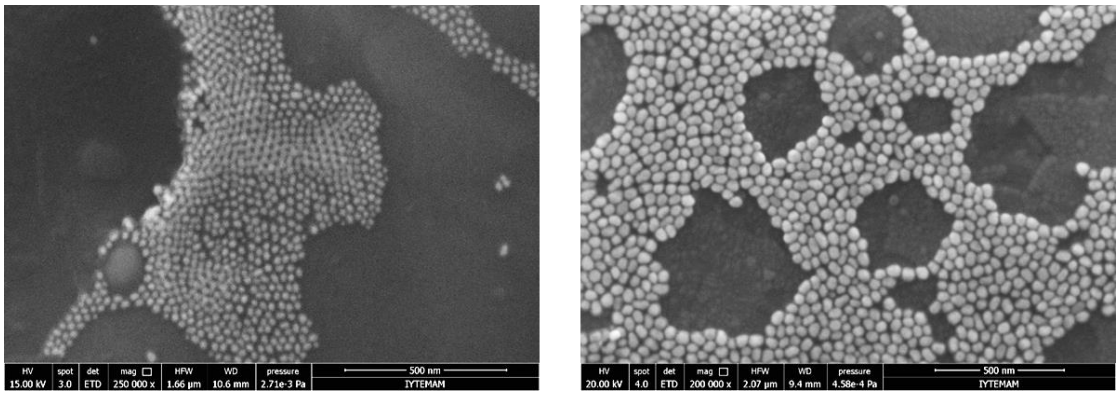

Figure 3.7. SEM images of 20 nm and 40 nm RGD- conjugated AuNPs.

To prove the conjugation of RGD on the gold nanoparticle surface, the elemental analysis of RGD-AuNPs were performed by using scanning electron microscope equipped with energy-dispersive X-ray spectroscopy (SEM-EDX). Energy dispersive X-ray analysis was performed for the characterization of the RGD conjugated gold nanoparticles Table 3.1 shows that the results of the EDX measurement. The presence of nitrogen (N) was attributed to amino acid residues of the RGD peptide on gold surface.

Table 3.1. EDX analysis results of AuNPs before and after conjugation

	Atomic %	
	Au	N
20 nm AuNP	100	0
20 nm RGD-AuNP	20	80
40 nm AuNP	100	0
40 nm RGD-AuNP	25	75

The cytotoxic of RGD conjugated AuNPs was assessed in two human lung cancer (A549 and H358) cell lines. MTT assay was used for the determination of cell viability.

As shown in Figure 3.8, RGD conjugated gold nanoparticles size with 20 nm and 40 nm display no toxic effect for A549 cell lines after the incubation for 24, 48 and 72h at concentrations range from 0.5 μM to 50 μM. Similar data were obtained in H358 cells,

with 0.5, 5, 50 μM for 20 nm RGD-AuNP and 40 nm RGD-AuNP. We did not observe any toxic effect on H358 cells (Figure 3.9). All these results show that RGD conjugated 20 nm and 40 nm sizes gold nanoparticles were non-toxic for human lung cancer A549 and H358 cell lines.

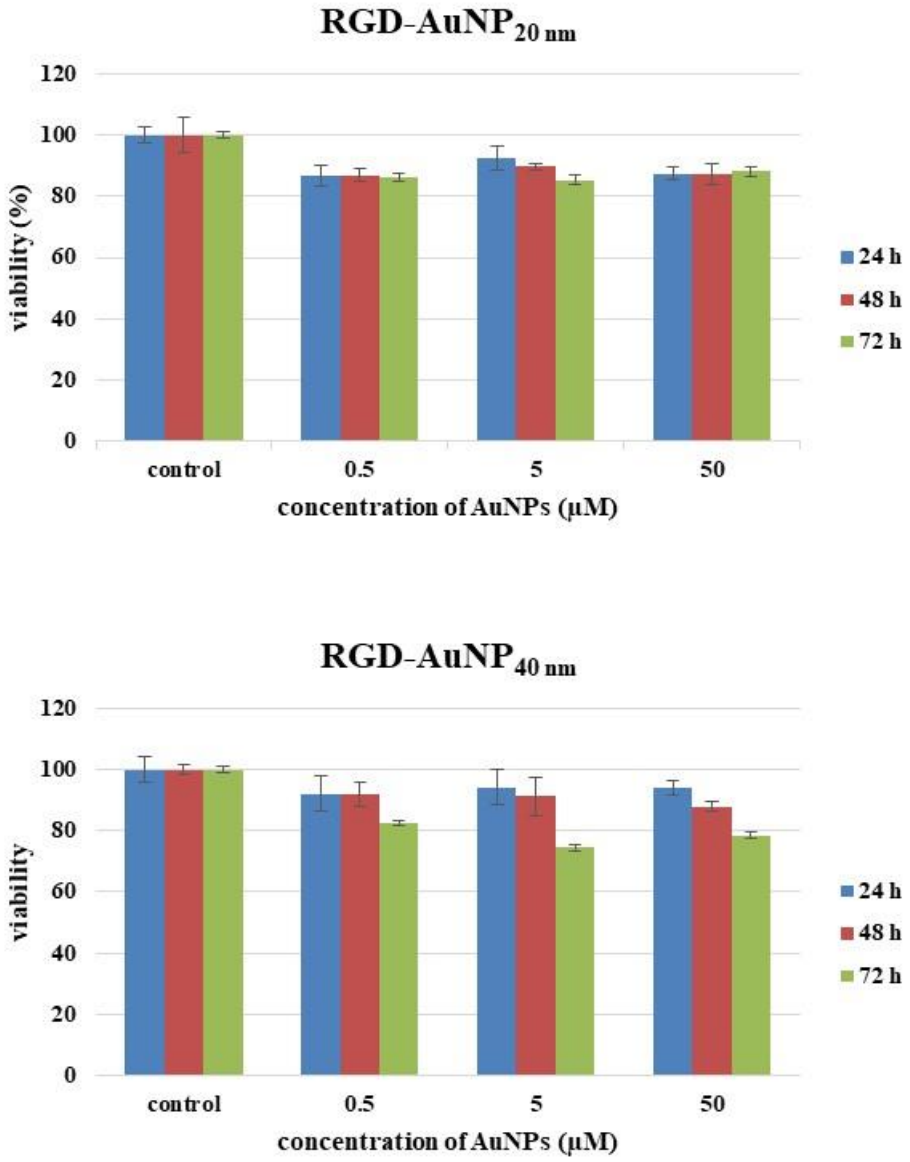

Figure 3.8. MTT assay of A549 cells treated with RGD conjugated 20 nm (top) and 40 nm (below) AuNPs at 0.5, 5, 50 μM after 24, 48 and 72 hours incubation.

Before getting dark field images of cells, A549 cells and H358 cells were treated with 25 μM 20 nm bare AuNPs, 40 nm bare AuNPs, 20 nm RGD-AuNPs and 40 nm RGD-AuNPs. After incubation for 24 hours, cell medium was removed, washed with PBS and fresh medium was added to cells.

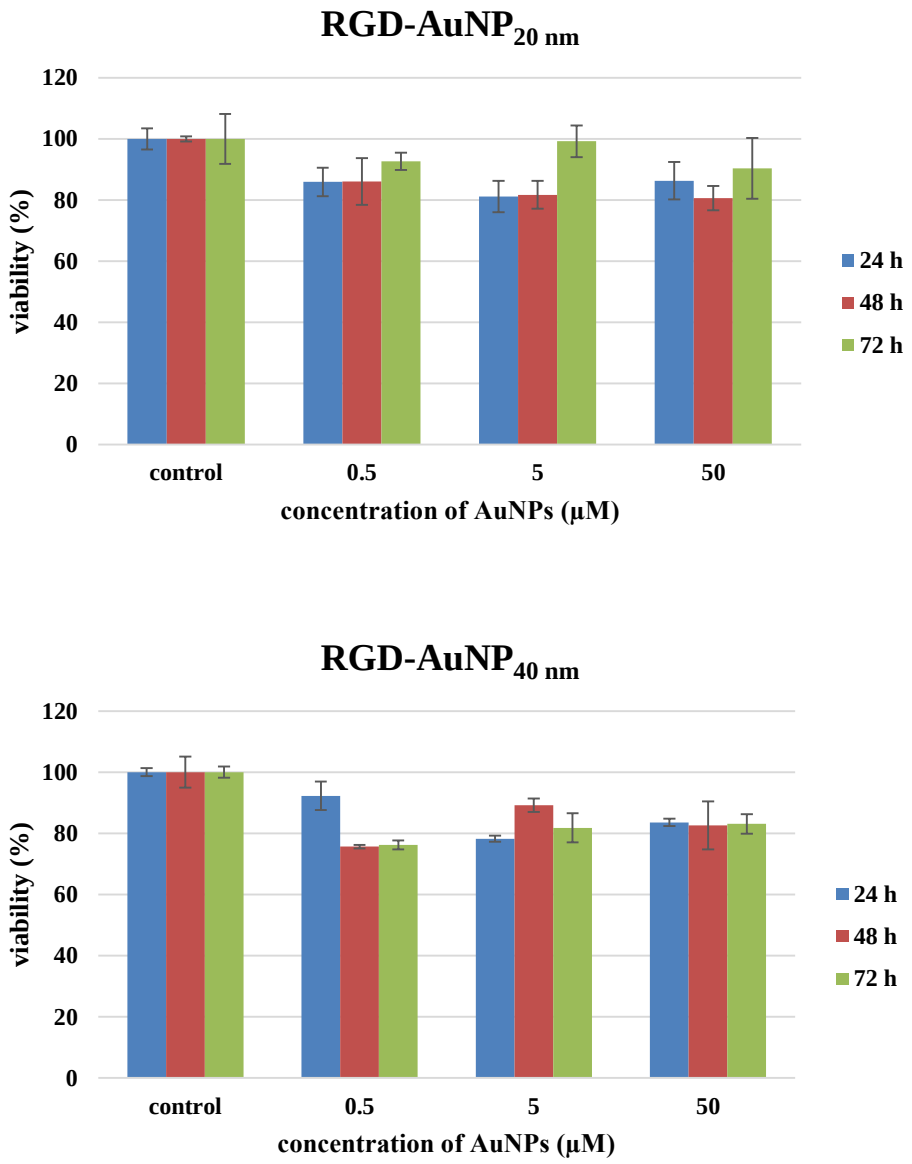

Figure 3.9. MTT assay of H358 cells treated with RGD conjugated 20 nm (top) and 40 nm (below) AuNPs at 0.5, 5, 50 µM after 24, 48 and 72 hours incubation.

The cell nuclei were stained blue with DAPI and cell images captured by the confocal microscope. An Olympus IX71 spinning disk confocal microscope was used to observe the internalization of different sizes (20 nm and 40 nm) and surface (bare and RGD conjugated AuNPs) of AuNPs by A549 and H358 human lung cancer cell lines.

Optical imaging techniques rely on scattering contrast to detect nanoparticles with or without targeting capability. Treated cells were monitored with dark field microscopy to observe the light scattering properties of bare and RGD peptide conjugated AuNPs. Dark field images of A549 and H358 control cell in Figure 3.10 and Figure 3.11 shows that control cells were seen almost dark.

Figure 3.10 shows the confocal bright field, fluorescence, dark field, and marge (dark field and fluorescence) images of A549 cells after incubation with 25 μM concentration of bare and RGD conjugated AuNPs for 24 h. Bright spots were observed into all treated cell, which referred gold nanoparticles. In the microscope image, it was clearly seen that non-conjugated and RGD conjugated AuNPs for both sizes were observed within the cytoplasm of A549 cells. RGD-conjugated AuNPs that dispersed into the cytoplasm of the cell were seen more bright compared to citrate stabilized AuNPs under the dark field microscope. This result indicated that peptide conjugation enhanced scattering intensity of the gold nanoparticles. The RGD peptide provides for receptor-mediated uptake of nanoparticles by cancer cells, as it mimics extracellular matrix proteins and targets; α and β integrin that are overexpressed on the cell surface. Uptake processes change the distribution of nanoparticles inside the cell. As shown in Figure 3.10 no significant scattering intensity changes were observed in the cell, which treated with 20 and 40 nm RGD-AuNPs.

H358 cancer cells were treated with gold nanoparticles of different size: 20 and 40 nm and surface chemistry: citrate and RGD peptide as shown in Figure 3.11. Same results were obtained in H358 cell lines. According to the Figure 3.11 non-conjugated and RGD conjugated gold nanoparticles are predominantly accumulated inside the cytoplasm of the H358 cells. Figure 3.11 shows that treated H358 cell with bare 20 and 40 nm AuNPs possess weak and disperse scattering. After RGD peptide conjugation, strong white scattering light was observed into H358 cancer cells. Large differences in the scattering intensity were observed due to the different surface modification of AuNPs. The light scattering pattern of gold nanoparticles is significantly different when RGD peptide was conjugated to AuNPs.

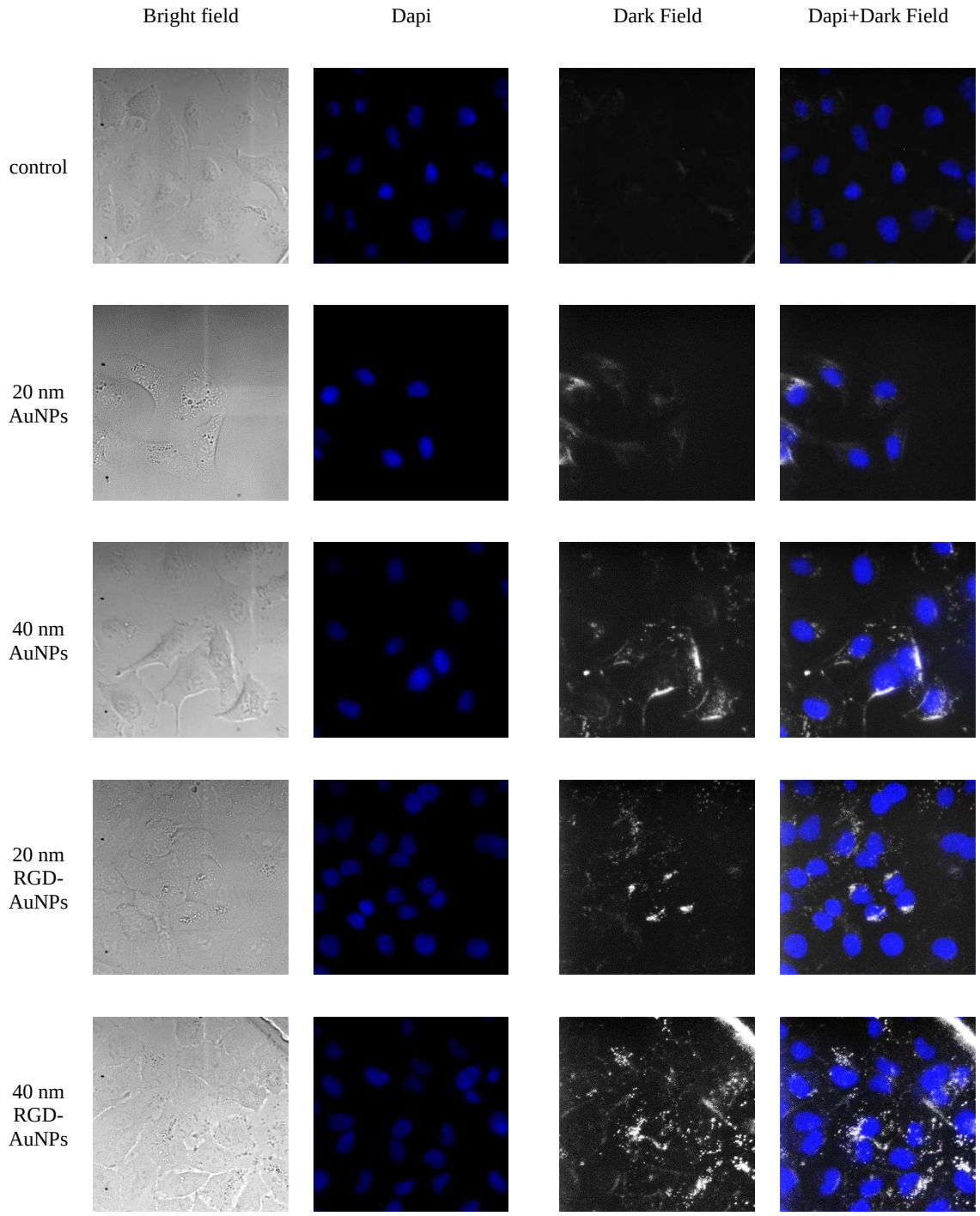

Figure 3.10. Confocal images of A549 living cells incubated with RGD conjugated and bare 20 and 40 nm AuNPs for 24 hours. Cells observed bright field, blue fluorescence images of nuclei and dark field by using spinning disk confocal microscopy. Nucleus were stained by DAPI (blue), merged images of dark field and blue fluorescence.

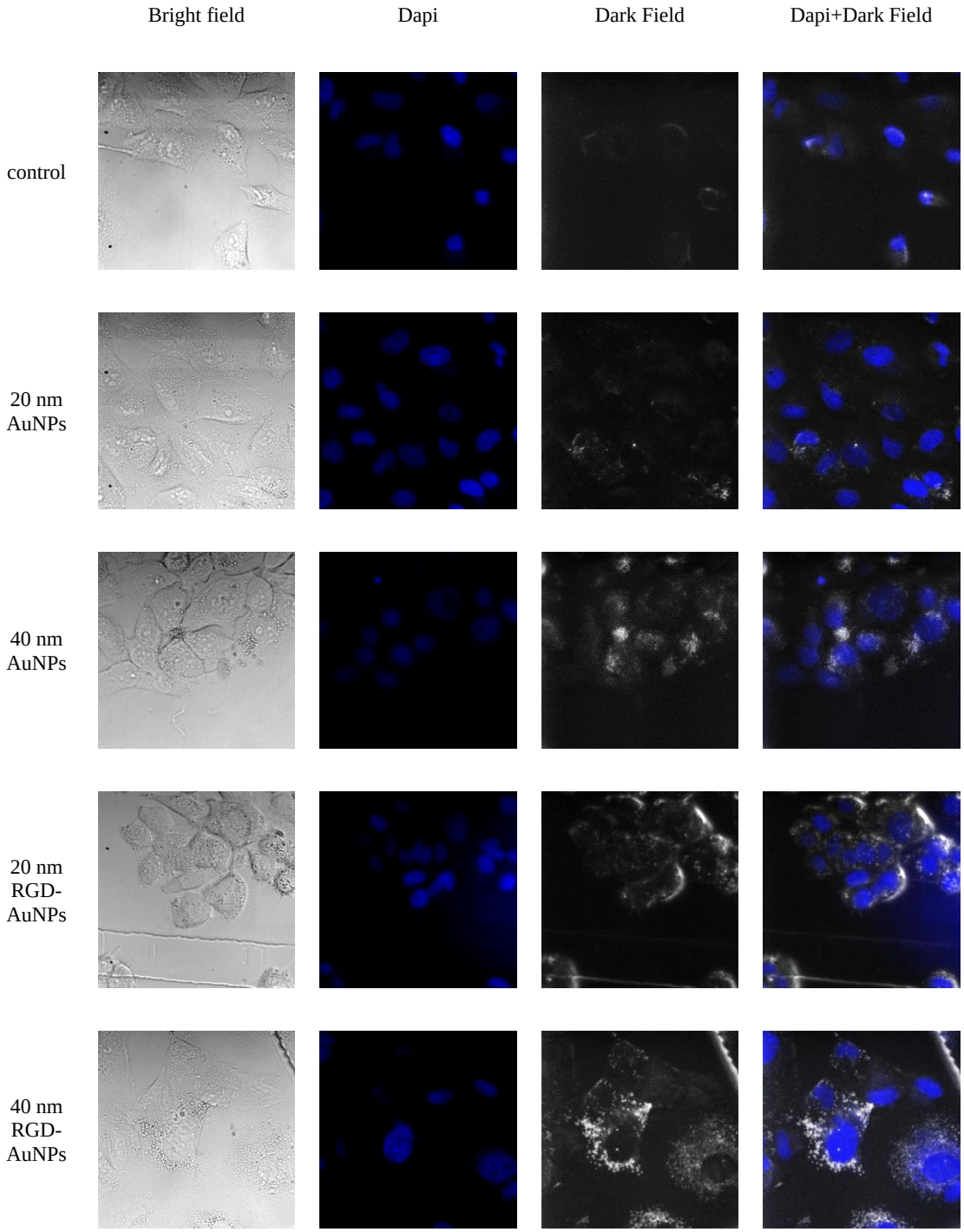

Figure 3.11. Confocal images of H358 living cells incubated with RGD conjugated and bare 20 and 40 nm AuNPs for 24 hours. Cells observed bright field, blue fluorescence images of nuclei and dark field by using spinning disk confocal microscopy. Nucleus were stained by DAPI (blue), merged images of dark field and blue fluorescence.

There is no doubt that particles can enter cells by a number of different routes. It is not yet clear which factors favor any particular uptake mechanism. The particles appear to enter the cytosol either directly through the cell membrane or receptor-mediated. The RGD conjugated AuNPs can be delivered into the cell by receptor-mediated endocytosis. Some articles reported that citrate capped gold nanoparticles are accumulated into the cell, however, peptide conjugated gold nanoparticles were stable against aggregation into cell (Chithrani and Chan 2007, Chithrani, Ghazani, and Chan 2006). It was clearly understood the dark field images, the non-conjugated gold nanoparticles were accumulated inside cells and scattering intensity was affected by these accumulations. The surface chemistry of AuNPs dictates their distribution within cells and, consequently, is responsible for their observed strong light-scattering properties.

3.5. Conclusions

We have synthesized Au nanospheres at the size of 20 and 40 nm and made these very suitable for scattering and absorption contrast enhancements in optical imaging with peptide conjugation. We have performed bioconjugation of these Au nanoparticles with RGD peptides, which bind with high efficiency to $\alpha_3\beta_1$ receptors expressed by A549 and H358 human lung carcinoma cells.

Using a confocal microscope in the dark field, we were able to image the intracellular localization of these AuNPs. After the 24 h of treatment with 0.25 mM bare and RGD conjugated AuNPs, the white spot appeared inside the cytoplasm of both cancer cells. After incubation with AuNPs and RGD-AuNPs, the cellular morphology did not change. The surface characterizations of AuNPs caused a change in the intensity of light scattered by the nanoparticles. RGD targeted AuNPs may be more effective as an imaging agent for biomedical application, due to their greater light scattering ability.

CHAPTER 4

INVESTIGATION OF THE NUCLEAR TARGETING EFFECT OF PEPTIDE CONJUGATED GOLD NANOPARTICLES IN LIVING HUMAN LUNG CELLS BY DIC MICROSCOPY

4.1. Aim of the Study

Au nanoparticles are being used in cancer research due to their biocompatibility and ability to act as a radiosensitizer and as a drug carrier in cancer therapy. Nucleus of the most important organelle in regulating reproduction, growth, metabolism, and death of cells through gene expression. The therapeutic response can be further enhanced if nanoparticles can be effectively targeted into the nucleus. Due to damage to the genome affects the viability of a cell, it is generally thought that GNPs have to localize within the cell nucleus.

The aim of this study is to prepare nuclear targeted gold nanoparticles and investigate their targeting ability in normal and cancer lung cells for this purpose, we synthesized 20 nm and 40 nm gold nanoparticles and these AuNPs was modified with two peptides. The first peptide (RGD) enhanced the uptake, the second peptide (NLS) enhanced the nuclear delivery. Peptide conjugated gold nanoparticles were explored to achieve nuclear targeting in cancer and normal lung cells (A549, H358 and BEAS2B).

4.2. Introduction

AuNPs are typical plasmonic materials that possess unique localized surface plasmon resonance (LSPR) properties. AuNPs display excellent biocompatibility, which allows them to be widely used for cellular studies, such as intracellular sensors, therapeutic agents, drug delivery carriers, and contrast agents for cellular imaging.

Fabrication of AuNPs can perform to have a different size from 2-150 nm. Their structural design enables the coating of the surfaces with a various targeting agent. In addition, the important properties are non-toxic and biocompatible.

Nuclear targeting of nanoparticles in living cells is generating widespread interest because of the possibility of developing new diagnostic and therapeutic strategies. The nucleus is a desirable target because the genetic information of the cell and transcription is found there. The nuclear membrane is a double-layer membrane marked with nuclear pores that allow diffusion of molecules and selective uptake into the nucleus. Cationic peptide sequences is that responsible for the transport of proteins into the nucleus from the cytoplasm. These sequences, known as nuclear localization signal sequence are very rich in basic amino acids. Nuclear localization signal peptides (NLS) such as the SV40 large T antigen, HIV-1 Tat protein NLS and adenoviral NLS are well-known for their role as a "Trojan horse", delivering cargo to the nucleus.

Targeted entry into cells is an increasingly important area of research. RGD and NLS peptides having the ability to target gold nanoparticles to the nucleus of cancer cells. There are lots of article about RGD and NLS peptides having the ability to target gold nanoparticles to the nucleus of cancer cells. Li et al. (Li et al. 2017), using confocal bright field microscopy, have demonstrated nuclear entry of 13 nm NLS conjugated gold nanospheres for MCF-7 cell line. They obtained the result that the proliferation of cells and the formation of a tumor in vivo were enormously inhibited after treatment with the nuclear-targeted nano carrier. Kang and colleagues prepared 24 nm RGD / NLS conjugated gold nanoparticles, which were located into the nucleus of HSC3 cells, and observed the effect of these particles on the cell cycle by using Dark field microscope and Rayleigh/Raman Spectroscopy (Kang, Austin, and El-Sayed 2012).

Table 4.1. Location of peptide-coated nanoparticles after 3 h incubation times with various cell lines

Peptide sequence	**HeLa**	**3T3/NIH**	**HepG2**
CGGGPKKKRKVGG	Cytoplasm	Cytoplasm	Cytoplasm
CGGRKKRRQRRRAP	Cytoplasm	No uptake	Cytoplasm
CGGFSTSLRARKA	Nucleus	Cytoplasm	No uptake
CKKKKKKGGRGDMFG	Nucleus	Cytoplasm	Nucleus

Tkachenko and co-workers published an article in 2003. They used four different peptide conjugate AuNPs and investigated the localization of this gold nanoparticles in 3 different cell lines (HeLa: human cervical epithelium cells, 3T3/NIH: murine fibroblastoma cells, and HepG2: human hepatocarcinoma) (Tkachenko et al. 2003). Table 4.1 summarizes the localization of peptide conjugated nanoparticles in living cells. According to this article, nuclear targeting effect of NLS conjugated gold nanoparticles depends not only the peptide sequence but also the cell type.

In another study, El- Sayed and co-workers used nuclear targeted AuNPs to selectively transport into the cancer cell nucleus (Kang, Mackey, and El-Sayed 2010). They prepared RGD and RGD/NLS conjugated AuNPs and investigated their uptake efficiency by HSC-3 (human oral squamous cell carcinoma), and one nonmalignant epithelial cell line, HaCat (human keratinocytes). Cancer and normal cells were incubated with these AuNPs at a concentration of 0.4 nM for 24 hours.

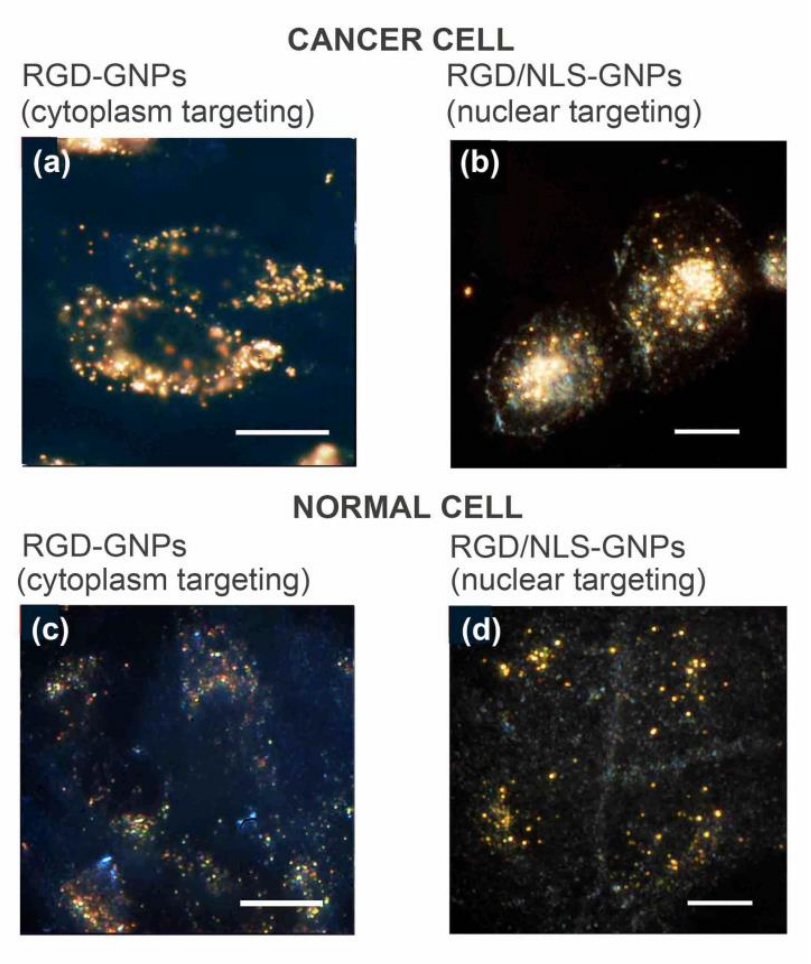

Figure 4.1. Dark field light scattering images of cytoplasm and nuclear targeting AuNPs.

Figure 4.1 clearly display the efficient uptake of AuNPs in cancer cells compared with normal cells. The RGD-AuNPs specifically target the cytoplasm of cancer cells over that of normal cells, and the RGD/NLS-AuNPs specifically target the nuclei of cancer cells over those of normal cells.

Table 4.2 summarizes literature studies related to gold nanoparticles targeted to the nucleus with peptides. It can be seen from the table that different sequence NLS peptides were used for different cell line and the different targeting effect was observed.

In this study, we used PKKKRKVEDPYC peptide sequence as a nuclear localization signal (NLS) peptides. Figure 4.2 shows that the molecular structure of NLS peptide, which has Pro-Lys-Lys-Lys-Arg-Lys-Val-Glu-Asp-Pro-Tyr-Cys amino acid sequence.

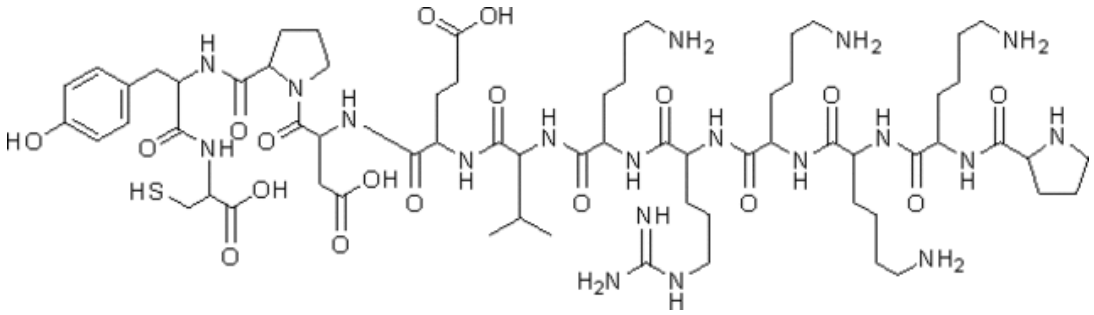

Figure 4.2. Molecular structure of NLS peptides

Through the SH part in the amino acid sequence, the NLS peptide can be quickly and easily attach to the surface of the gold nanoparticle.

Table 4.2. Literature summary of nucleus-targeted gold nanoparticles

	Cell	Peptide	Shape	Size	Instrument	Result	References
1	HSC HaCaT	RGD NLS (CGGGPKKKRKVGG)	Nanocubes Nanosphare	46 nm (edge) 42 nm	Dark field	Nanocubes internalized in nucleus of HSC more effectively	(Panikkanvalappil et al. 2014)
2	HSC-3	RGD (CGPDGRDGRDGRDGR) NLS (GGVKRKKKPGGC)	Spherical	25 nm	Raman-Dark field	Localized in nucleus	(Kang, Austin, and El-Sayed 2012)
3	HSC-3	RGD (CGPDGRDGRDGRDGR) NLS (GGVKRKKKPGGC)	Spherical	31nm	Dark field	Localized in nucleus	(Aioub, Austin, and El-Sayed 2014)
4	HeLa	NLS (KGGGPKKGRKVGG)	Spherical	20nm	TEM	Localized in nucleus	(Xie et al. 2009)
5	HSC-3	RGD (CGPDGRDGRDGRDGR) NLS (GGVKRKKKPGGC)	Spherical	31nm	Dark field	Localized in nucleus	(Aioub et al. 2014)

(Cont. on next page)

Table 4.2. (Cont.)

	Cell	Peptide	Shape	Size	Instrument	Result	References
6	HSC-3	RGD (CGPDGRDGRDGRDGR) NLS (GGVKRKKKPGGC)	Spherical	24nm	Rayleigh scattering	Localized in nucleus	(Austin, Kang, and El-Sayed 2013)
7	HSC-3	RGD (CGPDGRDGRDGRDGR) NLS (GGVKRKKKPGGC)	Spherical	21nm	Dark field	Localized in nucleus	(Kang, Austin, and El-Sayed 2014)
8	HSC-3	RGD (CGPDGRDGRDGRDGR) NLS (GGVKRKKKPGGC)	Spherical	28nm	Dark field	Localized in nucleus	(Kang et al. 2013)
9	HSC-3	RGD (CGPDGRDGRDGRDGR) NLS (CGGPKKKRKVGG)	Nanospheres Nanocages	35 nm 45 nm(edge)	Dark field	Nanocages localization in nucleus higher extend than nanospheres	(Mackey et al. 2013)

(Cont. on next page)

Table 4.2. (Cont.)

	Cell	Peptide	Shape	Size	Instrument	Result	References
10	HeLa	NLS (CGGGPKKKRKVGG) (CGGRKKRRQRRRAP) (CGGFSTSLRARKA)	Spherical	20 nm	VECDIC	cytoplasm, cytoplasm, nucleus	(Tkachenko et al. 2004)
11	3T3/NIH	NLS (CGGGPKKKRKVGG) (CGGRKKRRQRRRAP) (CGGFSTSLRARKA)	Spherical	20 nm	VECDIC	cytoplasm, no uptake, cytoplasm	(Tkachenko et al. 2004)
12	HepG2	NLS (CGGGPKKKRKVGG) (CGGRKKRRQRRRAP) (CGGFSTSLRARKA)	Spherical	20 nm	VECDIC	cytoplasm, cytoplasm, no uptake	(Tkachenko et al. 2004)
13	HEYA 8	RGD (CGPDGRDGRDGRDGR) NLS (GGVKRKKKPGGGC)	nanorods	25 x 5 nm	DIC	Localized in nucleus	(Ali et al. 2017)

(Cont. on next page)

Table 4.2. (Cont.)

	Cell	Peptide	Shape	Size	Instrument	Result	References
14	MCF 7	NLS	Spherical	13 nm	Confocal BF	Localized in nucleus	(Li et al. 2017)
15	HepG2	RGD (CGGGPKKKRKGC) NLS (GGVKRKKKPGGC)	nanorods	50 X10 nm	Dark field	Localized in nucleus	(Deng et al. 2017)
16	SH-SY5Y	NLS (CGTGPKKKRKVGGK)	Spherical	40 nm	Bright field	Localized in nucleus	(Huefner et al. 2013)
17	HSC 3 HaCat	NLS	nanorods	40 x 15 nm	Dark field	Localized in nucleus of both cells	(Oyelere et al. 2007)
18	HSC HaCat	RGD NLS (KKKRK)	Spherical	30 nm	Dark field	Conjugated AuNPs internalized in nucleus of HSC more effectively	(Kang, Mackey, and El-Sayed 2010)
19	SGC-7901	NLS (GGVKRKKKPGGC)	Nanorods	20 x 10 nm	Dark field	Localized in nucleus	(Liang et al. 2015)
20	HeLa	RGD NLS	Spherical	15 nm	TEM Dark field	Localized in nucleus	(Yang et al. 2014)

4.3. Experimental

4.3.1. Synthesis of Gold Nanoparticles

AuNPs were synthesized by using Turkevich`s method (Turkevich, Stevenson, and Hillier 1951) in which trisodium citrate acts as a reducing agent in aqueous solution. The experimental procedure is briefly explained below. Initially, 50 mL solution of HAuCl4 (0.25 mM) in a 100 mL beaker equipped with a magnetic stirrer heated to boiling temperature. Then, a 1% solution (by mass) of trisodium citrate (0.25 ml for 40 nm, 0.50 ml for 20 nm AuNPs) was added to this rapidly-stirred boiling solution. The color of the solution turned into the red within 10 minutes that indicated the formation of AuNPs. The reaction mixture was stirred for 1h at boiling temperature to ensure the completion of the reaction. By varying the amount of tri-sodium citrate, 20 and 40 nm of AuNPs were synthesized successfully. Synthesized Au NPs was purified by centrifugation (14 000 rpm, 15 minutes).

4.3.2. RGD/NLS and NLS Conjugation of AuNPs

The gold nanoparticles initially conjugated with polyethylene glycol to prevent the aggregation. To a solution of AuNPs, mPEG-SH 2000 (Laysan Bio) (0.2 mM in deionized water) was added in 10^3 times molar excess and shook at room temperature for overnight. Excess PEG was removed by centrifugation (4 000 rpm, 15 minutes) and peptide conjugated particles (PEG-AuNP) were re-dispersed in DI water.

After PEGylation, gold nanoparticles conjugated with RGD (arginine-glycine-aspartic acid) and NLS (PKKKRKVEDPYC) peptides. A 0.5 mM solution of RGD and 0.5 mM solution of NLS in DI water were added to PEG-AuNPs solution in DI water to achieve 10^3 and 10^4 times molar excess, respectively. For the conjugation of only NLS peptide to the PEG-AuNPs, 0.5 mM solution of NLS peptides was added to the PEG-AuNPs solution with a molar excess of 10^5. The solutions were left to shake at room temperature for 48 hours. Particles were purified by centrifugation at 4000 rpm for 15

minutes. RGD/NLS and NLS conjugated AuNPs were dispersed in DI water for further applications.

4.3.3. Cell Culture

All experiments were carried out three different human lung cell lines which were A549 (human lung, carcinoma) cells, others H358 (human lung bronchioalveolar, carcinoma) cells and BEAS2B (human lung bronchus, normal) cells. A549 cells were maintained in DMEM/F-12K medium and H358 cells were maintained in RPMI-1640 medium were supplemented with 10% (v/v) fetal bovine serum (FBS), 1% (v/v) penicillin/streptomycin and 1% (v/v) L-glutamine. BEAS2B were maintained in BEBM medium supplemented with BPE (2 ml), Hydrocortisone (0.5 ml), hEGF (0.5 ml), Epinephrine (0.5 ml), Transferrin (0.5 ml), Insulin (0.5 ml), Retinoic Acid (0.5 ml), Triiodothyronine (0.5 ml) GA-1000 (0.5 ml) in 500 ml basal medium. All cell cultures were kept at 37 ^{0}C in a 5% CO_2 humidified incubator.

4.3.4. Cell Viability

To assess the viability of A549, H358 and BEAS2B cells, MTT assay was performed. Cells were seeded in 96 well plate for overnight incubation. Then, the cell medium was removed and replaced with cell culture medium containing 0.5, 5 and 50 μM solution of AuNPs. Cells were left to incubation for 24, 48 and 72 hours. After indicated incubation times, the gold nanoparticle containing cell medium was replaced with MTT solution (PBS). Cells were incubated with the MTT solution for 4 hours. After that, DMSO (100 μL) was added to each well and absorbance measurement was taken by a multi plate reader (Thermo, vario scan) at 540 nm. Three replicates for each experiment were performed.

4.3.5. Cell Fixation

BEAS2B cells were seeded on the glass placed in 6 well plate and incubated for 24 hours. After the incubation time, the medium was removed, fresh BEBM medium, which contained 25 mM AuNPs, was added and cells incubated for further 24 h. Then, cell medium was removed and cells washed with PBS for three times. Fixation process was performed by using 4% paraformaldehyde (2ml/well) and incubated for 20 min at 37 ^{0}C. Then, PFA solution was removed and cells were washed three times with PBS solution. Double fixation was applied by using cold ethanol (at -20 ^{0}C), it was added to each well and further incubated for 20 min at that temperature. Finally, the fixed cells were taken from solution, dried and pasted on a microscope slide.

4.3.6. Living Cell Imaging

To obtain live cell images A549, H358 and BEAS2B cell lines seeded in μ-dish. After 24 h incubation of three cell lines, the cell mediums were removed and fresh medium that containing 20 nm and 40 nm sizes AuNPs, conjugated with RGD/NLS and NLS, were added and incubated for additional 24 h. Then, medium was removed and cells were washed with 1X PBS for three times. DAPI was used for the nucleus staining. Spinning disk confocal microscope (Andor Revolution with Olympus IX71 Inverted microscope) was used in this study. The DIC mode used with Nomarski prisms, 100X objective (1.2 NA) and Olympus 40X objective (0.6 NA). Andor IXON CCD camera was used to capture images in live cells.

4.4. Results and Discussion

In this study, we have prepared spherical gold nanoparticles with the diameter of 20 nm and 40 nm by using citrate reduction method. Different size of nanoparticles were obtained by varying the concentration of tri-sodium citrate. The main aim of this study is to investigate the internalization of peptide conjugated AuNPs (RGD/NLS and only NLS) into the nucleus. To do this purpose we used three different type of human lung cells

which were A549, H358 and BEAS2B cells. Firstly, the citrate-capped AuNPs were conjugated with polyethylene glycol thiol (mPEG-SH) to improve the biostability and prevent nonspecific interactions. For further modification two different AuNPs were designed: RGD/NLS-AuNPs and NLS-AuNPs. In these conjugations RGD (arginine-glycine-aspartic acid) was used for the increase nanoparticle endocytosis by targeting αβ integrins on the surface of cell membrane (Castel et al. 2001, Zitzmann, Ehemann, and Schwab 2002) and NLS (nuclear localizing sequence) was used to selectively target the nucleus. The characterization of synthesized conjugates was performed by using UV-vis spectroscopy, dynamic light scattering (DLS), scanning electron microscopy (SEM) and energy-dispersive X-ray spectroscopy (SEM-EDX) methods.

UV-vis absorption spectroscopy, a common method to characterize gold nanoparticles, was used to acquire the absorbance spectra of the nanoparticles before and after the peptide conjugations. As shown in Figure 4.3 (left), 20 nm AuNPs have an absorption band at 524, 526, and 526 nm for non-conjugated, RGD/NLS conjugated and only NLS conjugated particles, respectively. Similarly, in Figure 4.3 (right), 40 nm AuNPs, RGD/NLS-AuNPs and NLS-AuNPs showed an absorption maximum at 529, 530 and 532 nm, respectively. The obtained UV-Vis spectra confirmed that conjugation had no significant effect on absorption characteristics of particles such as red shift or broadening.

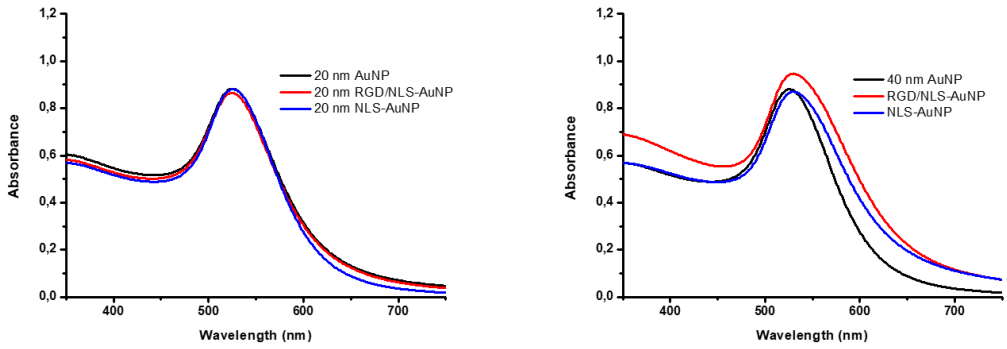

Figure 4.3. Uv-vis spectrum of 20 nm non conjugated (black), RGD/NLS conjugated (red) and NLS conjugated (blue) AuNPs (left); 40 nm non conjugated (black), RGD conjugated (red) and NLS conjugated (blue) AuNPs (right).

We further investigated the hydrodynamic size distribution of bare and conjugated gold nanoparticles by using DLS. As shown in Figure 4.4 (a) and Figure 4.4 (b), the conjugation of peptides has almost no significant effect on the size distribution of

particles. The conjugated particles have almost similar distribution curve as the non-conjugated particles.

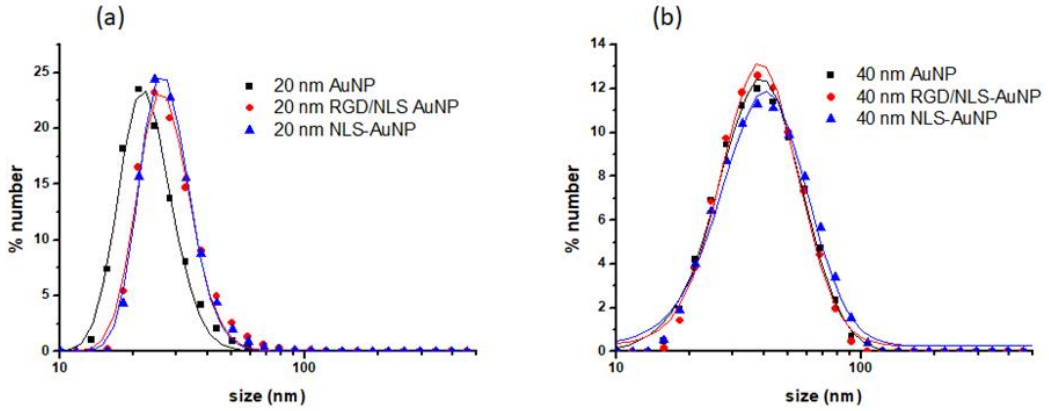

Figure 4.4. Size distribution of non conjugated and conjugated 20 nm (a) and 40 nm (b) AuNPs nanoparticles results obtained by using DLS.

In addition, the surface charge measurements were performed to get an idea of surface charge and conjugation by using Malvern Nano-ZS (Table 4.3). According to the zeta potential results, the surface potentials of citrate-reduced gold nanoparticles were -28±14 mV (20 nm) and -33±15 mV (40 nm). After the RGD and NLS peptide conjugation, zeta potentials of 20 nm gold nanoparticles changed dramatically to -4 ±10 mV for RGD/NLS-AuNPs and 6 ±12 mV for NLS-AuNPs. Another remarkable change occurred from -33 mV (40 nm AuNP) to 6 ±9 mV (RGD/NLS-AuNP) and 0 ±2 mV (NLS-AuNP) for 40 nm AuNPs. Zeta potential measurement demonstrated that after the RGD and NLS peptide conjugation, zeta potentials of gold nanoparticles were shifted to positively region.

Table 4.3. Characterizations of conjugated AuNPs.

	Size (nm)	Zeta potential (mV)	λ_{max} (nm)
20 nm AuNP	20 ±3	-28 ±14	524
20 nm RGD/NLS-AuNP	22 ±4	-4 ±10	526
20 nm NLS-AuNP	24 ±7	6 ±12	526
40 nm AuNP	40 ±8	-33 ±15	529
40 nm RGD/NLS-AuNP	43 ±12	6 ±9	530
40 nm NLS-AuNP	42 ±15	0 ±2	532

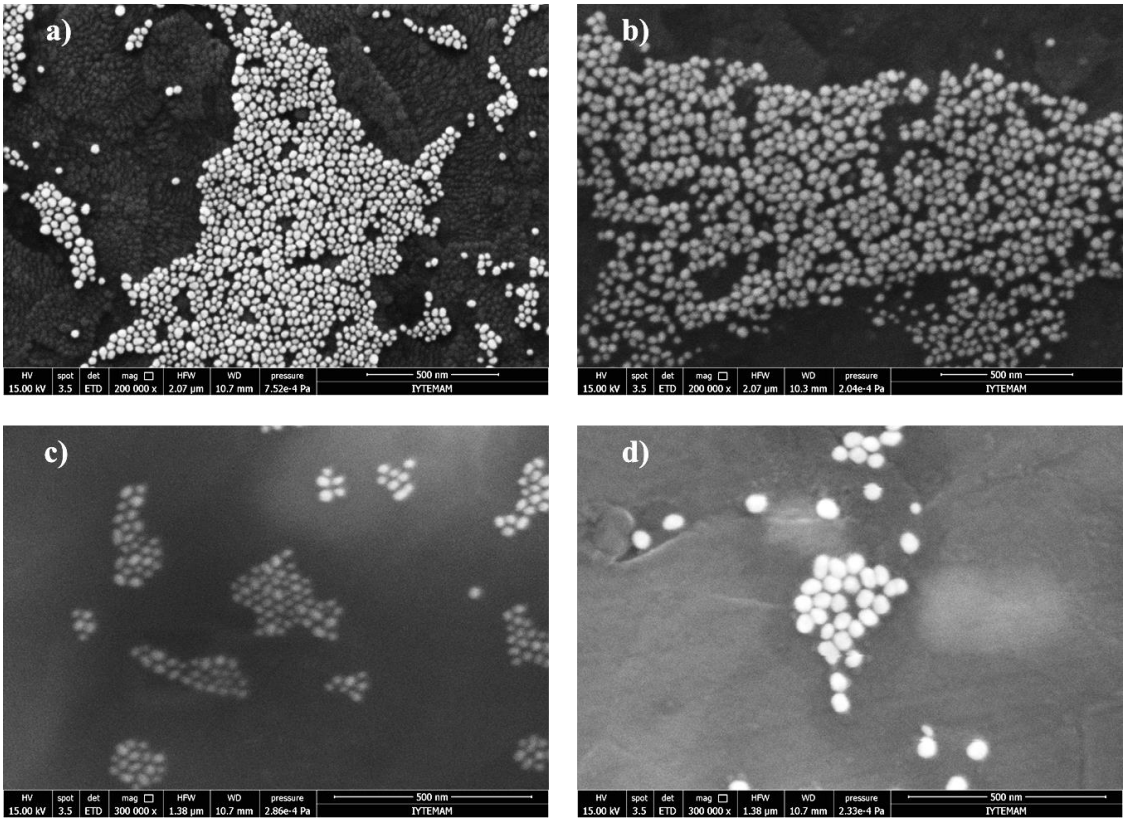

Figure 4.5. SEM images of conjugated AuNPs. a) 20 nm RGD/NLS-AuNP, b) 40 nm RGD/NLS-AuNP, c) 20 nm NLS-AuNP, d) 40 nm NLS-AuNP.

To complete characterization study of synthesized particles we also examined the surface morphology by using SEM (Scanning Electron Microscope). The results of SEM experiments also supported the DLS measurements. As shown in Figure 4.5, RGD/NLS and NLS conjugated particles have uniform spherical morphology and narrow size distribution.

Energy dispersive X-ray spectroscopy (EDX) analysis was performed to confirm the presence of peptide on the gold nanoparticle surface. The EDX results clearly shows the presence both S and N on the surface of gold nanoparticles

Table 4.4. EDX results of Conjugated AuNPs

	Atomic %		
	Au	N	S
20 nm NLS-AuNP	14	77	9
40 nm NLS-AuNP	32	62	6

In the subject of study, we aimed to investigate internalization of synthesized particles in human lung cancer cell lines. For such kind of biomedical study, cytotoxicity of nanomaterials is an important parameter. The viability assay were performed for all cell lines with different concentrations of NLS conjugated AuNPs ranging from 0.5 to 50 µM by using MTT assay (experimental section).

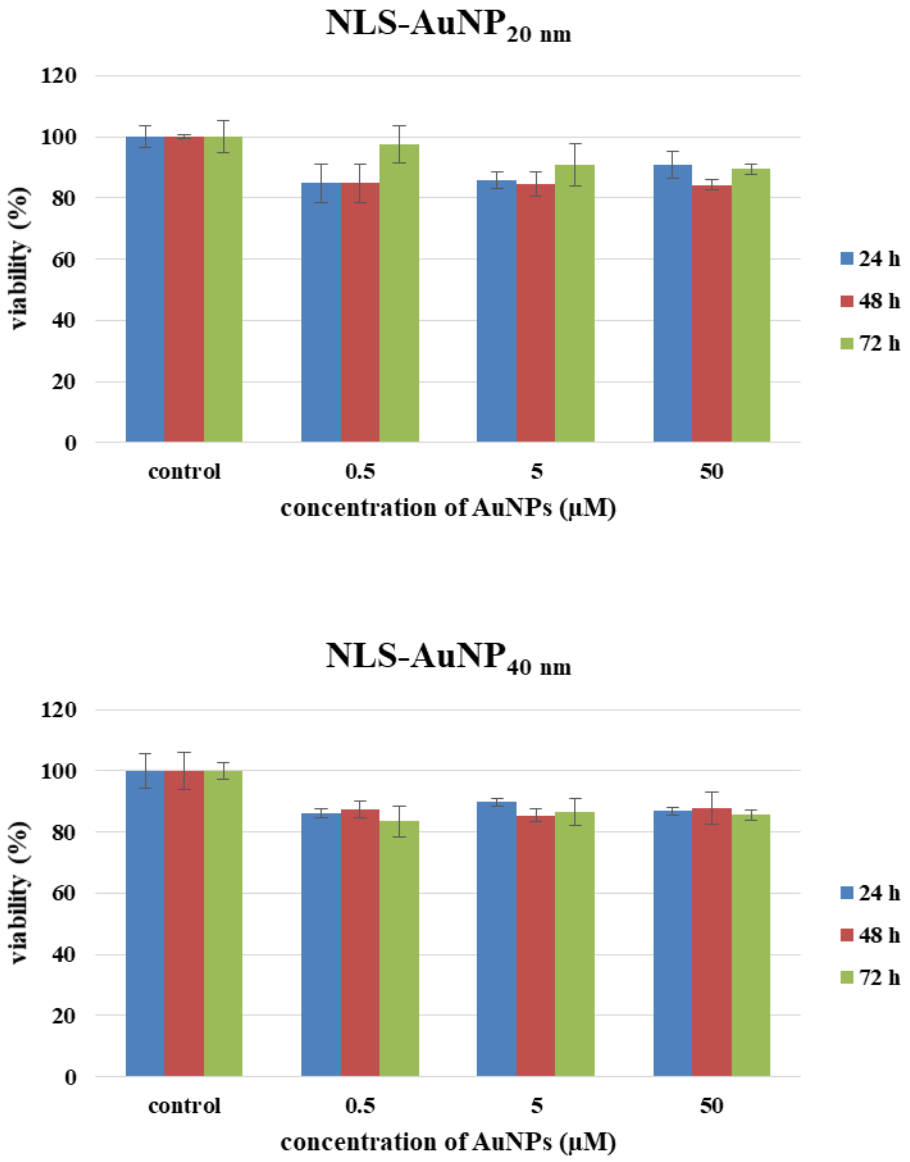

Figure 4.6. The cell viability of A549 cells that were treated with 25 µM NLS conjugated AuNPs for 24, 48 and 72 h.

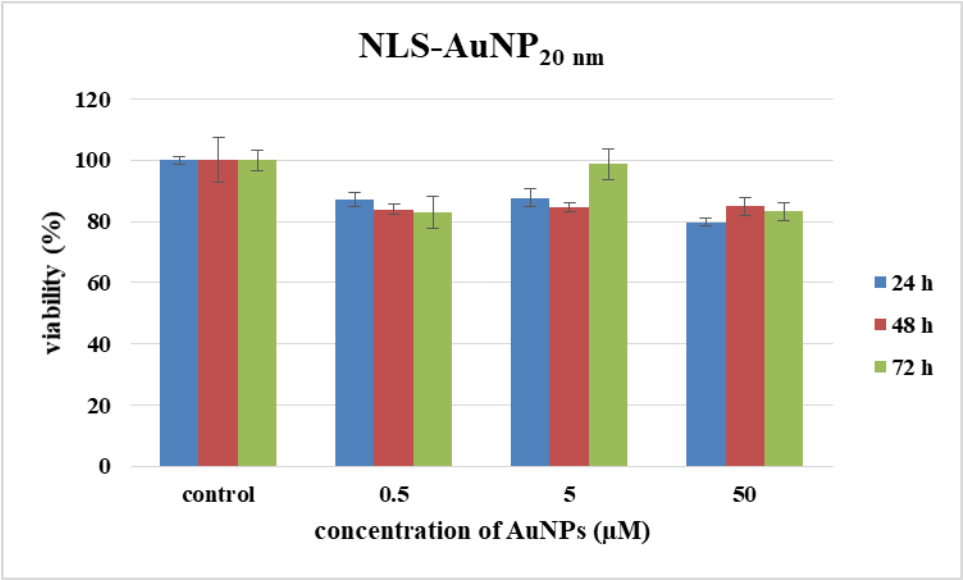

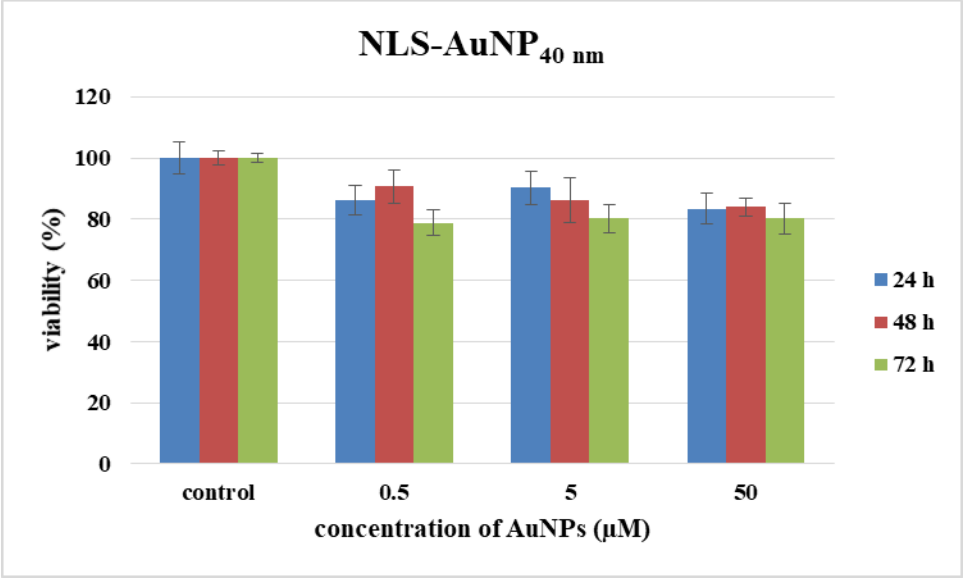

Figure 4.7. The cell viability of H358 cells that were treated with 25 µM NLS conjugated AuNPs for 24, 48 and 72 h.

The viability of A549 cancer cells (Figure 4.6) was still maintained approximately 85% and viability of H358 cancer cells (Figure 4.7) did not decrease below 80% up to 50 µM concentrations of gold nanoparticles. As shown in Figure 4.8, BEAS2B normal cells viability was more that 90% after treated with gold nanoparticles. It was clearly seen that no significant toxic effect was observed for 20 and 40 nm NLS-AuNPs on A549, H358 and BEAS2B cell lines.

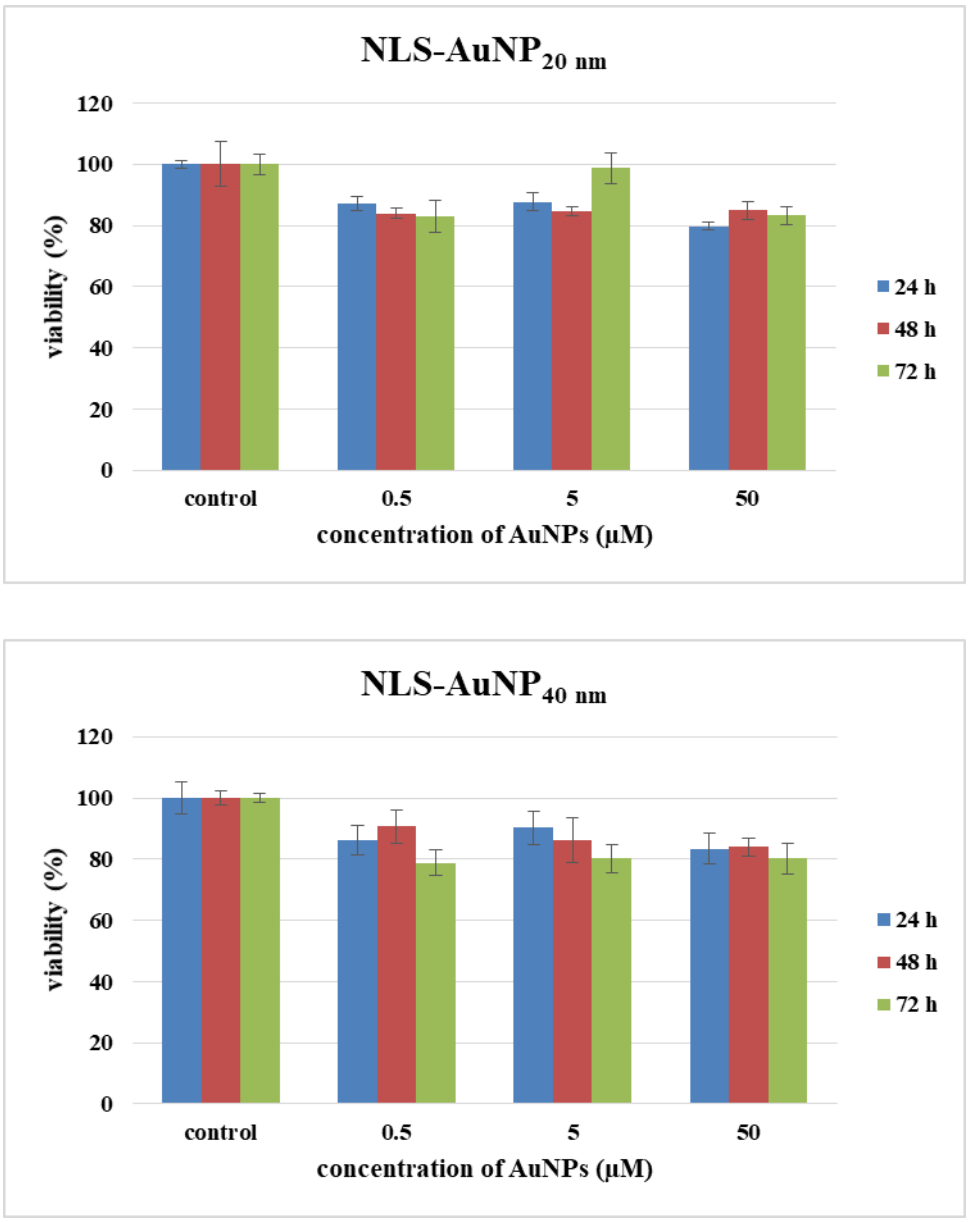

Figure 4.8. The cell viability of H358 cells that were treated with 25 µM NLS conjugated AuNPs for 24, 48 and 72 h.

A549 cells treated with 25 µM concentration of RGD/NLS-Au and NLS-Au nanoparticles for 24 hours. Then, live-cell DIC images of A549 cells were captured at 100X objective. As shown in Figure 4.9, the cell nuclei were stained blue with DAPI and the present of black dots inside the blue nuclei indicated the internalization of RGD/NLS-Au and NLS-Au nanoparticles. According to DIC images, all conjugated AuNPs internalized into nucleus of A549 cells and different surface conjugation of AuNPs with RGD/NLS and NLS peptides did not lead to significant difference in the internalization

of AuNPs by A549 cancer cell. It was observed that the morphology of the AuNPs treated cells did not change when compared to the control cell.

DIC images of H358 cancer cells treated with 25 μM RGD/NLS and NLS conjugated 20 and 40 nm AuNPs for 24 h were obtained within the living-cell in real time at. As shown in Figure 4.10, RGD/NLS-Au and NLS-Au nanoparticles was observed as a black dots into nucleus of H358 cancer cell. In addition, any change did not observed in morphology of H358 cell before and after treatment with gold nanoparticles. From these result, we conclude that both RGD/NLS and NLS conjugation were capable of entering the nucleus of H358 cancer cells.

In Figure 4.11, RGD/NLS and NLS conjugated 20 and 40 nm AuNPs treated BEAS2B normal cells and internalizations of particles were visualized by DIC microscopy at 100X objective. We did not observed black dots in nucleus of BEAS2B cells after the treated with RGD/NLS-Au -and NLS-Au NPs for 24 h.

In order to confirm the internalization of peptide conjugated gold nanoparticles, treated cells were fixed with paraformaldehyde. In the fixed cell imaging experiment, BEAS2B cell treated with 20 and 40 nm RGD/NLS and NLS conjugated AuNPs (Figure 4.12). Fixed-cell DIC imaging results revealed that all conjugated particles could interpenetrate the cell membrane and located in cytoplasm and none of them entered the nucleus of cell.

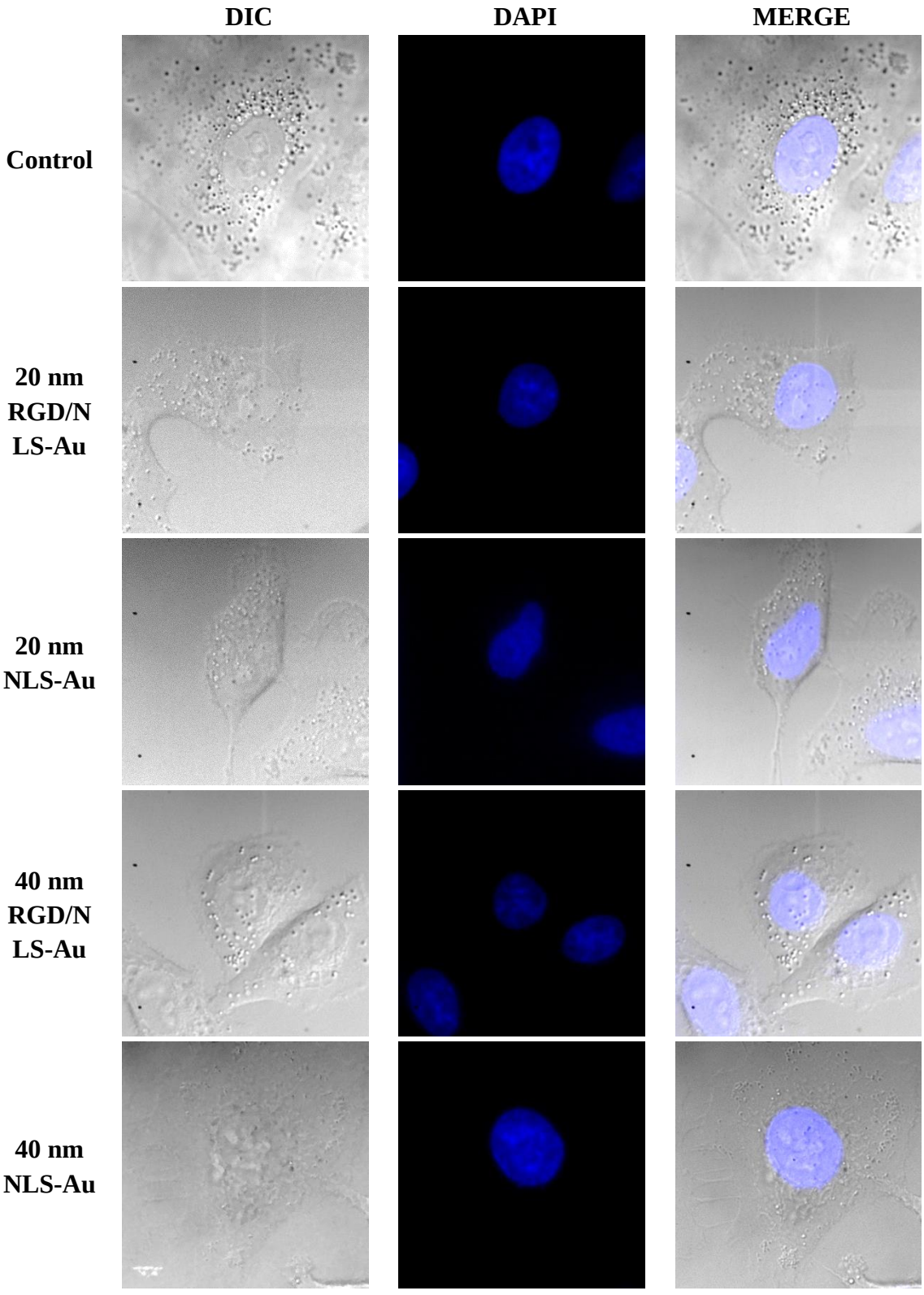

Figure 4.9. Live-cell confocal microscope images of A549 cell lines treated with 20 and 40 nm RGD/NLS and NLS conjugated AuNPs for 24 h. DIC images (left) were taken at 100X objective, nucleus were stained DAPI (middle) and merge images (right) were obtained using DIC and blue fluorescence images. Scale bar is 10 μm.

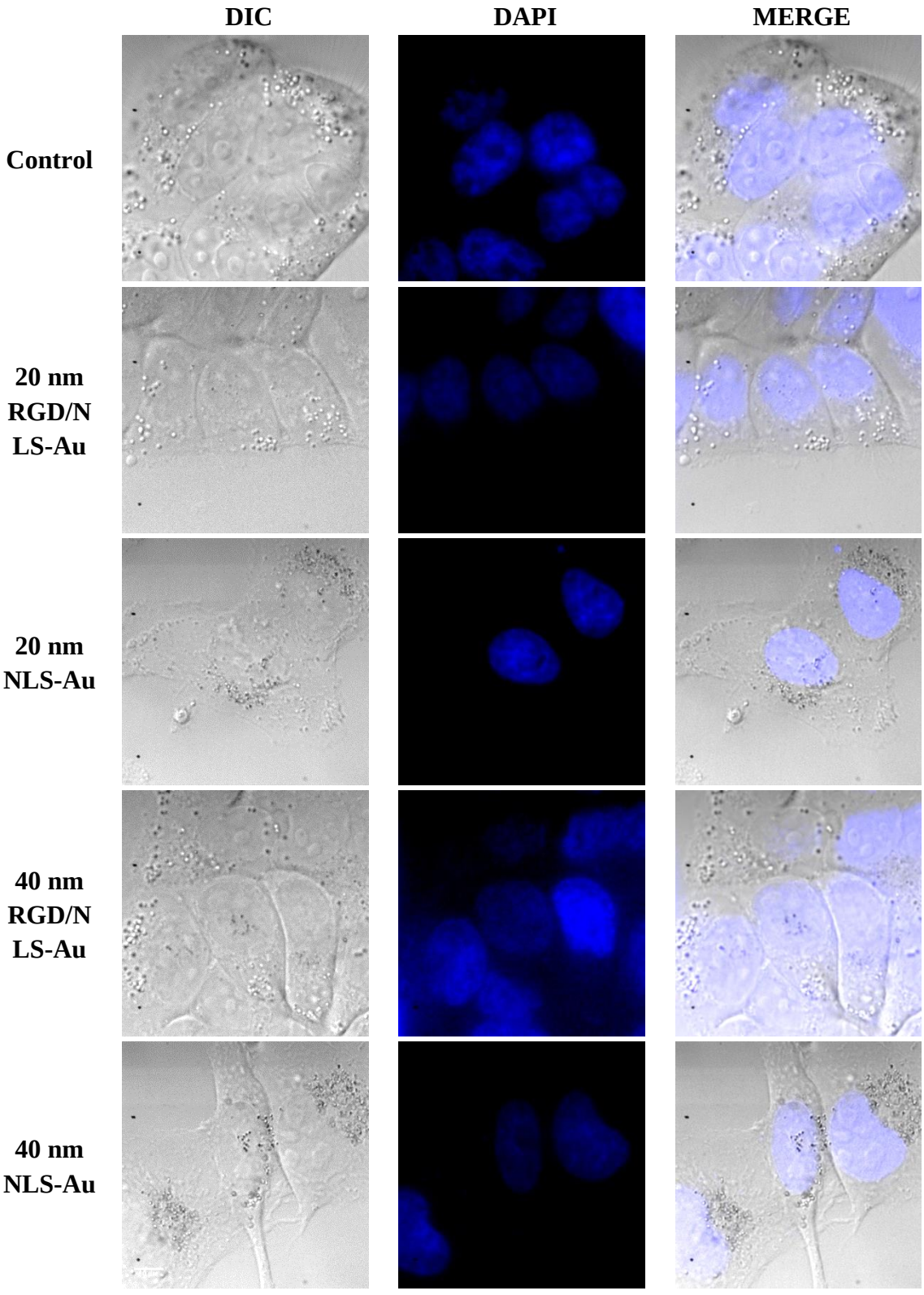

Figure 4.10. Live-cell confocal microscope images of H358 cell lines treated 20 and 40 nm RGD/NLS and NLS conjugated AuNPs for 24 h. DIC images (left) were taken at 100X objective, nucleus were stained DAPI (middle) and merge images (right) were obtained using DIC and blue fluorescence images. Scale bar is 10 μm.

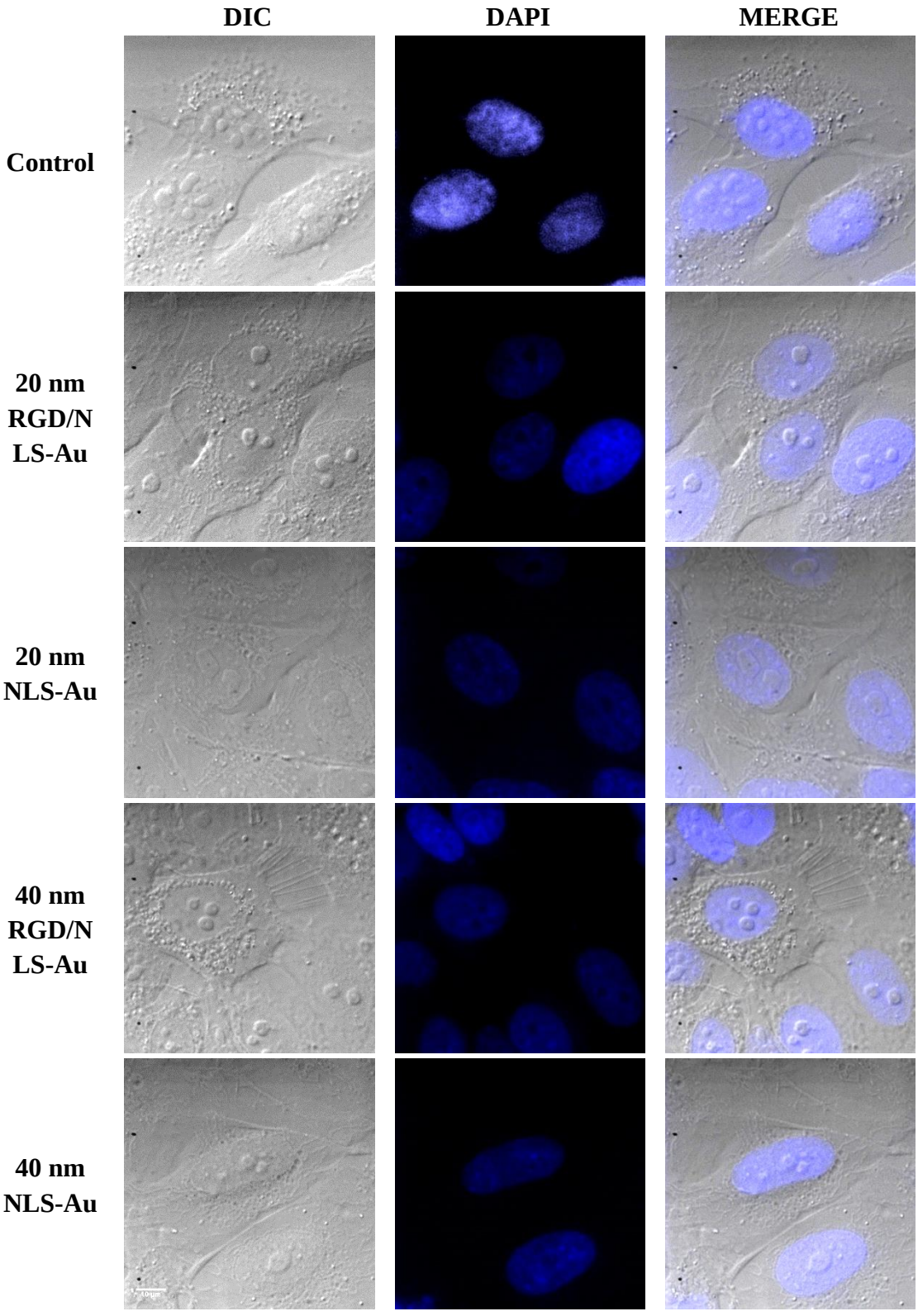

Figure 4.11. Live-cell confocal microscope images of BEAS2B cell lines treated 20 and 40 nm RGD/NLS and NLS conjugated AuNPs for 24 h. DIC images (left) were taken at 100X objective, nucleus were stained DAPI (middle) and merge images (right) were obtained using DIC and blue fluorescence images. Scale bar is 10 μm.

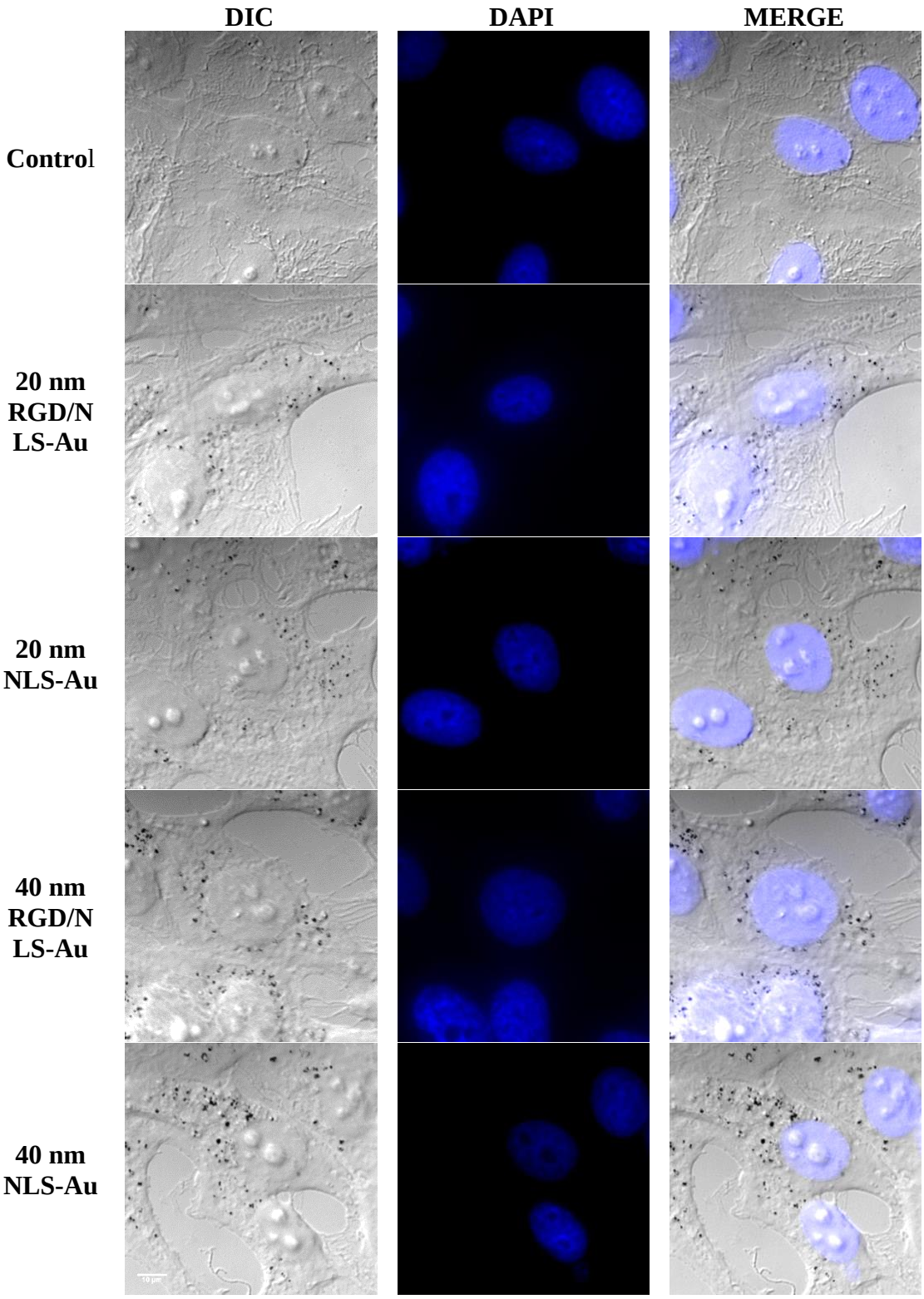

Figure 4.12. Fixed-cell DIC images of BEAS2B cell lines after treatment with 20 and 40 nm RGD/NLS and NLS conjugated AuNPs for 24 h. DIC images (left) were taken at 100X objective, nucleus were stained DAPI (middle) and merge images (right) were obtained using DIC and blue fluorescence images. Scale bar is 10 μm.

Table 4.5 summarized that number of cell contain particles into their nucleus from the number of total imaged cell (N_p: Number of cells contain particles in nucleus, N_c: Number of imaged cells). It was clearly seen that the ratio of cell contained particles into their nucleus was very high for both cancer cell lines. In addition, 167 BEAS2B cells were imaged and none of them contained AuNPs into their nucleus.

Table 4.5. Number of cells, which contained gold nanoparticles into nucleus cell

	A549 cell	H358 cells
	N_p/N_{tc}	N_p/N_{tc}
20 nm RGD/NLS-AuNP	5/6	19/33
20 nm NLS-AuNP	4/6	12/14
40 nm RGD/NLS-AuNP	8/11	18/37
40 nm NLS-AuNP	8/8	4/5
Total	**25/31**	53/89

A comparison of the function of RGD/NLS and NLS peptide when conjugated to gold nanoparticles, both of conjugate efficiently entered the nuclei of cells. Also, size of gold nanoparticles did not changed the efficiency of internalization into nucleus.

The NLS peptides, having a KKKRK (lysine-lysine-lysine-arginine-lysine) sequence, provides for nuclear localization of nanoparticles, by binding importin α in the cytoplasm of the cell, which subsequently binds importin β located on the cytoplasmic side of the nuclear membrane (Zhou et al. 2013). α_3 integrin was strongly expressed in A549, H358 and BEAS2B cells (Koukoulis et al. 1997). Also, $\alpha_6\beta_1$ and $\alpha_v\beta_1$ integrin were expressed in A549 cancer cell lines. $\alpha_3\beta_1$ integrin were expressed in all two types of lung cancer (A549 and H358) (Guo et al. 2009). In addition, H358 cell lines have $\alpha_1\beta_1$ and $\alpha_v\beta_6$ integrin intensely (Eberlein et al. 2012). Conjugated gold nanoparticles were reached into nucleus of A549 and H358 cancer cell lines by way of αβ integrin and NLS interaction.

4.5. Conclusions

The surfaces of the Au nanoparticles were modified to contain poly(ethylene glycol) (PEG) to ensure stability in a biological environment and reduce nonspecific binding of proteins. Following PEGylation, RGD and nuclear localizing signal (NLS) peptides were conjugated to the particle surface to exploit the overexpression of α and β integrins on the cell membrane and increase internalization of the particles, as well as selectively deliver the AuNPs to the nucleus of cell.

The combination of RGD peptide and NLS peptide allowed efficient nuclear targeting. The internalizations of different gold nanoparticles (20 nm RGD/NLS-AuNP, 40 nm RGD/NLS-AuNP, 20 nm NLS-AuNPs and 40 nm NLS-AuNPs) by A549 (cancer), H358 (cancer) and BEAS2B (normal) cells were visualized by DIC microscopy.

RGD/NLS and NLS conjugated AuNPs were targeted into nucleus of A549 and H358 cancer cells. None of the conjugated gold nanoparticles did not enter the nucleus of BEAS2B normal cell line. According to the fixed cell images, RGD/NLS and NLS conjugated AuNPs entered the cytoplasm of normal cell, but none of them did not target the nucleus of BEAS2B cell lines. The significant morphological changes of all cell lines did not observed after treatment of conjugated AuNPs.

Our results demonstrated that the entry of peptide targeted gold nanoparticles into the cell nucleus are critically dependent on the nuclear targeting peptide on the surface of gold nanoparticles.

CHAPTER 5

CONCLUSIONS

Gold nanoparticles are among one of the most extensively studied nanomaterials. Due to their optical properties, plasmonic nanoparticles have been utilized in a wide range of biomedical applications such as imaging, sensing, and photothermal therapy. The cellular delivery of therapeutic agents and their localization within cells is currently a great challenge in medicinal chemistry. In this thesis study, six different gold nanoparticles were synthesized in between 5 and 40 nm sizes by using different reducing agents, which are $NaBH_4$, ascorbic acid, trisodium citrate. Physicochemical characterization of 5 nm-Na, 20 nm-as, 40 nm-as, 10 nm-cit, 20 nm-cit, and 40 nm-cit gold nanoparticles were performed by using UV-vis spectroscopy, dynamic light scattering (DLS), scanning electron microscopy (SEM) and transmission electron microscopy (TEM). ICP-MS was used for determination of concentrations (number of AuNPs/mL) and yield of synthesized gold nanoparticles. It was determined that, the shape of synthesized Au nanoparticles were spherical and size distribution were monodisperse. Gold nanoparticles were obtained with high efficiency. The yield of reactions were determined by using ICP-MS. The reduction from gold (III) to gold atoms was at least 80% up to 97%.

A549 and H358 human lung cancer cells were used for cell studies. Cytotoxicity effect of synthesized gold nanoparticles on A549 and H358 cells were determined by MTT assay with different concentrations of gold nanoparticles for 24, 48 and 72 h. The viability of lung cancer cells after treated with these 6 different gold nanoparticles were examined and it was determined that there was no toxic effect even when the A549 cells were exposed to high concentration up to 100 μM, with an average survival rate of 70%. MTT results shows that there was no toxic effect on H358 cells treated with gold nanoparticles up to 25 μM concentration. However, higher AuNPs concentration effected cell viability by 50% decrease.

In order to assess the amount of the uptake of AuNPs into A549 and H358 cells, optical spectroscopic method was used. As a result of the uptake measurement, it was determined that the 20 nm and 40 nm particles had the highest cellular uptake by A549

and H358 cells. When we compared the two cancer cell lines, there was no significant difference in cellular uptake of gold nanoparticles.

Gold nanoparticles displayed the best contrast under the DIC microscope due to their plasmonic properties. Synthesized AuNPs clearly seen as black dots into the cells. Cytotoxicity assay indicated that RGD peptide conjugated gold nanoparticles did not show toxic effect on A549 and H358 cell lines. According to DIC images, gold nanoparticles were efficiently internalized into A549 and H358 cell lines. All sized gold nanoparticles entered into cytoplasm and localized at around the nucleus of both cells. According the DIC images 20 and 40 nm AuNPs were seen more efficiently other sized. The results obtained with DIC images are consistent with cellular uptake results obtained the spectroscopic measurement.

Because of their high cellular uptake and best contrast properties under DIC microscope, we have synthesized Au nanospheres at the size of 20 and 40 nm. We have performed bioconjugation of these Au nanoparticles with RGD peptides, which bind with high efficiency to $\alpha_3\beta_1$ receptors expressed by A549 and H358 human lung carcinoma cells. According to optical and structural characterizations, the size and shape of particle did not change after RGD conjugation. Cellular localization, distribution and scattering properties of RGD conjugated gold nanoparticles into A549 and H358 cells were investigated by using dark field microscopy.

After the 24 h of treatment with 0.25 mM bare and RGD conjugated AuNPs, white spots indicated to gold nanoparticles were observed in the cell. In the microscope image, it is clearly seen that non-conjugated and RGD conjugated AuNPs for both size were observed within the cytoplasm of A549 and H358 cells. Following incubation time with bare AuNPs and RGD-AuNPs, the cellular morphology did not change. The surface characterizations of AuNPs caused a change in the intensity of light scattered by the nanoparticles. The light scattering pattern of gold nanoparticles is significantly different when RGD peptide were conjugated to AuNPs. RGD-conjugated AuNPs that dispersed into cytoplasm of cell were seen more bright compared to citrate stabilized AuNPs under dark field microscope.

20 and 40 nm gold nanoparticles were conjugated with specific peptide to target the nuclei of lung cancer cell and investigated their targeting efficiency. Firstly, the surfaces of AuNPs were modified with PEG to increase biocompatibility and prevent nonspecific interactions under physiological conditions. After PEGylation, AuNPs were modified with RGD and NLS peptides. The RGD peptide and NLS peptides were

conjugated to the particle surface to exploit the overexpression of α and β integrins on the cell membrane and increase internalization of the particles, as well as selectively deliver the AuNPs to the nucleus of cell. For this purpose, four different conjugation: 20 nm RGD/NLS-AuNPs, 40 nm RGD/NLS-AuNPs, 20 nm NLS-AuNPs and 40 nm NLS-AuNPs were prepared. Optical and structural characterizations of peptide conjugated AuNPs were perform by using UV-Vis spectroscopy, DLS, SEM, SEM-EDX. According the result peptide conjugation were archived successfully and after the conjugation, particles size and shape did not change. Peptide conjugated gold nanoparticles showed no cytotoxicity to lung cancer and normal cells. The internalizations of this gold nanoparticles by A549 (cancer), H358 (cancer) and BEAS2B (normal) cells were visualized by DIC microscopy.

Gold nanoparticles were easily observed under DIC microscope as black dots, due to the difference in the refractive index between gold and cell. According to live cell DIC images, RGD/NLS and NLS conjugated AuNPs were enter into nucleus of A549 and H358 cancer cells. None of the conjugated gold nanoparticles did not enter the nucleus of BEAS2B normal cell line. The fixed cell DIC images shows that RGD/NLS and NLS conjugated AuNPs entered the cell and localized into cytoplasm of normal cell, but none of them did not reach the nucleus of BEAS2B cell lines.

Compared with the previous study, bare gold nanoparticles aggregated around the nucleus and they cannot entered the nuclei of cells. In addition, RGD conjugated gold nanoparticles spread in the cytoplasm of cells. Gold nanoparticles conjugated with nuclear localization signal were thought to be able to internalize into the nucleus of cancer cell. The nucleus is a desirable target because the genetic information of the cell and transcription machinery reside there. The preparation of nuclei targeted gold nanoparticles, which especially targets the nucleus of the cancer cell, were archived. Thus, the prepared peptide conjugated gold nanoparticles in this thesis can be used in the diagnosis and treatment of human lung cancer cells.

REFERENCES

Ackerson, Christopher J., Pablo D. Jadzinsky, Jonathan Z. Sexton, David A. Bushnell, and Roger D. Kornberg. 2010. "Synthesis and Bioconjugation of 2 and 3 nm-Diameter Gold Nanoparticles." *Bioconjugate Chemistry* 21 (2):214-218. doi: 10.1021/bc900135d.

Aden, Arthur L., and Milton Kerker. 1951. "Scattering of Electromagnetic Waves from Two Concentric Spheres." *Journal of Applied Physics* 22 (10):1242-1246. doi: 10.1063/1.1699834.

Agasti, Sarit S., Apiwat Chompoosor, Chang-Cheng You, Partha Ghosh, Chae Kyu Kim, and Vincent M. Rotello. 2009. "Photoregulated Release of Caged Anticancer Drugs from Gold Nanoparticles." *Journal of the American Chemical Society* 131 (16):5728-5729. doi: 10.1021/ja900591t.

Ahmed, Naveed, Hatem Fessi, and Abdelhamid Elaissari. 2012. "Theranostic applications of nanoparticles in cancer." *Drug Discovery Today* 17 (17):928-934. doi: https://doi.org/10.1016/j.drudis.2012.03.010.

Aioub, Mena, Lauren A. Austin, and Mostafa A. El-Sayed. 2014. "Determining Drug Efficacy Using Plasmonically Enhanced Imaging of the Morphological Changes of Cells upon Death." *The Journal of Physical Chemistry Letters* 5 (20):3514-3518. doi: 10.1021/jz501866g.

Aioub, Mena, Bin Kang, Megan A. Mackey, and Mostafa A. El-Sayed. 2014. "Biological Targeting of Plasmonic Nanoparticles Improves Cellular Imaging via the Enhanced Scattering in the Aggregates Formed." *The Journal of Physical Chemistry Letters* 5 (15):2555-2561. doi: 10.1021/jz501091x.

Ali, M. R. K., Y. Wu, D. Ghosh, B. H. Do, K. Chen, M. R. Dawson, N. Fang, T. A. Sulchek, and M. A. El-Sayed. 2017. "Nuclear Membrane-Targeted Gold Nanoparticles Inhibit Cancer Cell Migration and Invasion." *Acs Nano* 11 (4):3716-3726. doi: 10.1021/acsnano.6b08345.

Alkilany, Alaaldin M., and Catherine J. Murphy. 2010. "Toxicity and cellular uptake of gold nanoparticles: what we have learned so far?" *Journal of Nanoparticle Research* 12 (7):2313-2333. doi: 10.1007/s11051-010-9911-8.

Alkilany, Alaaldin M., Pratik K. Nagaria, Cole R. Hexel, Timothy J. Shaw, Catherine J. Murphy, and Michael D. Wyatt. 2009. "Cellular Uptake and Cytotoxicity of Gold Nanorods: Molecular Origin of Cytotoxicity and Surface Effects." *Small* 5 (6):701-708. doi: 10.1002/smll.200801546.

Alkilany, Alaaldin M., Pratik K. Nagaria, Michael D. Wyatt, and Catherine J. Murphy. 2010. "Cation Exchange on the Surface of Gold Nanorods with a Polymerizable

Surfactant: Polymerization, Stability, and Toxicity Evaluation." *Langmuir* 26 (12):9328-9333. doi: 10.1021/la100253k.

Austin, Lauren A., Bin Kang, and Mostafa A. El-Sayed. 2013. "A New Nanotechnology Technique for Determining Drug Efficacy Using Targeted Plasmonically Enhanced Single Cell Imaging Spectroscopy." *Journal of the American Chemical Society* 135 (12):4688-4691. doi: 10.1021/ja4011145.

Bain, Colin D., E. Barry Troughton, Yu Tai Tao, Joseph Evall, George M. Whitesides, and Ralph G. Nuzzo. 1989. "Formation of monolayer films by the spontaneous assembly of organic thiols from solution onto gold." *Journal of the American Chemical Society* 111 (1):321-335. doi: 10.1021/ja00183a049.

Balmain, Allan, Joe Gray, and Bruce Ponder. 2003. "The genetics and genomics of cancer." 33:238-244. *Nat Genet*. doi:10.1038/ng1107.

Bardhan, Rizia, Surbhi Lal, Amit Joshi, and Naomi J. Halas. 2011. "Theranostic Nanoshells: From Probe Design to Imaging and Treatment of Cancer." *Accounts of Chemical Research* 44 (10):936-946. doi: 10.1021/ar200023x.

Beddoes, Charlotte M., C. Patrick Case, and Wuge H. Briscoe. 2015. "Understanding nanoparticle cellular entry: A physicochemical perspective." *Advances in Colloid and Interface Science* 218 (Supplement C):48-68. doi: https://doi.org /10.1016/j.cis.2015.01.007.

Bellis, Susan L. 2011. "Advantages of RGD peptides for directing cell association with biomaterials." *Biomaterials* 32 (18):4205-4210. doi: https://doi.org/10.1016 /j.biomaterials.2011.02.029.

Berciaud, Stéphane, Laurent Cognet, Gerhard A. Blab, and Brahim Lounis. 2004. "Photothermal Heterodyne Imaging of Individual Nonfluorescent Nanoclusters and Nanocrystals." *Physical Review Letters* 93 (25):257402.

Bouhelier, Alexandre, Michael R. Beversluis, and Lukas Novotny. 2003. "Characterization of nanoplasmonic structures by locally excited photoluminescence." *Applied Physics Letters* 83 (24):5041-5043. doi: 10.1063 /1.1634383.

Boyd, G. T., Z. H. Yu, and Y. R. Shen. 1986. "Photoinduced luminescence from the noble metals and its enhancement on roughened surfaces." *Physical Review B* 33 (12):7923-7936.

Boyer, David, Philippe Tamarat, Abdelhamid Maali, Brahim Lounis, and Michel Orrit. 2002. "Photothermal Imaging of Nanometer-Sized Metal Particles Among Scatterers." *Science* 297 (5584):1160-1163. doi: 10.1126/science.1073765.

Brown, Sarah D., Paola Nativo, Jo-Ann Smith, David Stirling, Paul R. Edwards, Balaji Venugopal, David J. Flint, Jane A. Plumb, Duncan Graham, and Nial J. Wheate. 2010. "Gold Nanoparticles for the Improved Anticancer Drug Delivery of the Active Component of Oxaliplatin." *Journal of the American Chemical Society* 132 (13):4678-4684. doi: 10.1021/ja908117a.

Brusnichkin, Anton V., Dmitry A. Nedosekin, Mikhail A. Proskurnin, and Vladimir P. Zharov. 2007. "Photothermal Lens Detection of Gold Nanoparticles: Theory and Experiments." *Applied Spectroscopy* 61 (11):1191-1201. doi: 10.1366/000370207782597175.

Brust, Mathias, Merryl Walker, Donald Bethell, David J. Schiffrin, and Robin Whyman. 1994. "Synthesis of thiol-derivatised gold nanoparticles in a two-phase Liquid-Liquid system." *Journal of the Chemical Society, Chemical Communications* (7):801-802. doi: 10.1039/C39940000801.

Burda, Clemens, Xiaobo Chen, Radha Narayanan, and Mostafa A. El-Sayed. 2005. "Chemistry and Properties of Nanocrystals of Different Shapes." *Chemical Reviews* 105 (4):1025-1102. doi: 10.1021/cr030063a.

Cai, Weibo, Ting Gao, Hao Hong, and Jiangtao Sun. 2008. "Applications of gold nanoparticles in cancer nanotechnology." *Nanotechnology, science and applications* 2008 (1):10.2147/NSA.S3788. doi: 10.2147/NSA.S3788.

Carbo-Argibay, E., B. Rodriguez-Gonzalez, J. Pacifico, I. Pastoriza-Santos, J. Perez-Juste, and L. M. Liz-Marzan. 2007. "Chemical sharpening of gold nanorods: the rod-to-octahedron transition." *Angew Chem Int Ed Engl* 46 (47):8983-7. doi: 10.1002/anie.200703259.

Castel, Susanna, Roser Pagan, Francesc Mitjans, Jaume Piulats, Simon Goodman, Alfred Jonczyk, Florian Huber, Senén Vilaró, and Manuel Reina. 2001. "RGD Peptides and Monoclonal Antibodies, Antagonists of αv-Integrin, Enter the Cells by Independent Endocytic Pathways." *Laboratory Investigation* 81:1615. doi: 10.1038/labinvest.3780375.

Cedervall, Tommy, Iseult Lynch, Martina Foy, Tord Berggård, Seamas C Donnelly, Gerard Cagney, Sara Linse, and Kenneth A Dawson. 2007. "Detailed Identification of Plasma Proteins Adsorbed on Copolymer Nanoparticles." *Angewandte Chemie International Edition* 46 (30):5754-5756. doi: 10.1002/anie.200700465.

Chen, Jingyi, Joseph M. McLellan, Andrew Siekkinen, Yujie Xiong, Zhi-Yuan Li, and Younan Xia. 2006. "Facile Synthesis of Gold−Silver Nanocages with Controllable Pores on the Surface." *Journal of the American Chemical Society* 128 (46):14776-14777. doi: 10.1021/ja066023g.

Cheng, Yu, Joseph D. Meyers, Ann-Marie Broome, Malcolm E. Kenney, James P. Basilion, and Clemens Burda. 2011. "Deep Penetration of a PDT Drug into

Tumors by Noncovalent Drug-Gold Nanoparticle Conjugates." *Journal of the American Chemical Society* 133 (8):2583-2591. doi: 10.1021/ja108846h.

Cheng, Yu, Anna C. Samia, Jun Li, Malcolm E. Kenney, Andrew Resnick, and Clemens Burda. 2010. "Delivery and Efficacy of a Cancer Drug as a Function of the Bond to the Gold Nanoparticle Surface." *Langmuir* 26 (4):2248-2255. doi: 10.1021 /la902390d.

Chithrani, B. Devika, and Warren C. W. Chan. 2007. "Elucidating the Mechanism of Cellular Uptake and Removal of Protein-Coated Gold Nanoparticles of Different Sizes and Shapes." *Nano Letters* 7 (6):1542-1550. doi: 10.1021/nl070363y.

Chithrani, B. Devika, Arezou A. Ghazani, and Warren C. W. Chan. 2006. "Determining the Size and Shape Dependence of Gold Nanoparticle Uptake into Mammalian Cells." *Nano Letters* 6 (4):662-668. doi: 10.1021/nl052396o.

Cho, Wan-Seob, Minjung Cho, Jinyoung Jeong, Mina Choi, Beom Seok Han, Hyung-Seon Shin, Jin Hong, Bong Hyun Chung, Jayoung Jeong, and Myung-Haing Cho. 2010. "Size-dependent tissue kinetics of PEG-coated gold nanoparticles." *Toxicology and Applied Pharmacology* 245 (1):116-123. doi: https://doi.org /10.1016/j.taap.2010.02.013.

Connor, Ellen E, Judith Mwamuka, Anand Gole, Catherine J Murphy, and Michael D Wyatt. 2005. "Gold Nanoparticles Are Taken Up by Human Cells but Do Not Cause Acute Cytotoxicity." *Small* 1 (3):325-327. doi: 10.1002/smll.200400093.

Daniel, Marie-Christine, and Didier Astruc. 2004. "Gold Nanoparticles: Assembly, Supramolecular Chemistry, Quantum-Size-Related Properties, and Applications toward Biology, Catalysis, and Nanotechnology." *Chemical Reviews* 104 (1):293-346. doi: 10.1021/cr030698+.

Davis, Mark E., Zhuo Chen, and Dong M. Shin. 2008. "Nanoparticle therapeutics: an emerging treatment modality for cancer." *Nat Rev Drug Discov* 7 (9):771-782.

De Brabander, M., R. Nuydens, G. Geuens, M. Moeremans, and J. De Mey. 1986. "The use of submicroscopic gold particles combined with video contrast enhancement as a simple molecular probe for the living cell." *Cell Motility and the Cytoskeleton* 6 (2):105-113. doi: 10.1002/cm.970060207.

Deng, Rong, Huixin Qu, Lijia Liang, Jing Zhang, Biying Zhang, Dianshuai Huang, Shuping Xu, Chongyang Liang, and Weiqing Xu. 2017. "Tracing the Therapeutic Process of Targeted Aptamer/Drug Conjugate on Cancer Cells by Surface-Enhanced Raman Scattering Spectroscopy." *Analytical Chemistry* 89 (5):2844-2851. doi: 10.1021/acs.analchem.6b03971.

Deraedt, Christophe, Lionel Salmon, Sylvain Gatard, Roberto Ciganda, Ricardo Hernandez, Jaime Ruiz, and Didier Astruc. 2014. "Sodium borohydride stabilizes

very active gold nanoparticle catalysts." *Chemical Communications* 50 (91): 14194-14196. doi: 10.1039/C4CC05946H.

Dhar, Shanta, Weston L. Daniel, David A. Giljohann, Chad A. Mirkin, and Stephen J. Lippard. 2009. "Polyvalent Oligonucleotide Gold Nanoparticle Conjugates as Delivery Vehicles for Platinum(IV) Warheads." *Journal of the American Chemical Society* 131 (41):14652-14653. doi: 10.1021/ja9071282.

Dickerson, Erin B., Erik C. Dreaden, Xiaohua Huang, Ivan H. El-Sayed, Hunghao Chu, Sujatha Pushpanketh, John F. McDonald, and Mostafa A. El-Sayed. 2008. "Gold nanorod assisted near-infrared plasmonic photothermal therapy (PPTT) of squamous cell carcinoma in mice." *Cancer Letters* 269 (1):57-66. doi: https://doi.org/10.1016/j.canlet.2008.04.026.

Doorley, Gerard W., and Christine K. Payne. 2011. "Cellular binding of nanoparticles in the presence of serum proteins." *Chemical Communications* 47 (1):466-468. doi: 10.1039/C0CC02618B.

Dreaden, Erik C., Alaaldin M. Alkilany, Xiaohua Huang, Catherine J. Murphy, and Mostafa A. El-Sayed. 2012. "The golden age: gold nanoparticles for biomedicine." *Chemical Society Reviews* 41 (7):2740-2779. doi: 10.1039 /C1CS15237H.

Dreaden, Erik C., Sandra C. Mwakwari, Quaovi H. Sodji, Adegboyega K. Oyelere, and Mostafa A. El-Sayed. 2009. "Tamoxifen−Poly(ethylene glycol)−Thiol Gold Nanoparticle Conjugates: Enhanced Potency and Selective Delivery for Breast Cancer Treatment." *Bioconjugate Chemistry* 20 (12):2247-2253. doi: 10.1021 /bc9002212.

Dupuy, D. E., and S. N. Goldberg. 2001. "Image-guided radiofrequency tumor ablation: Challenges and opportunities - Part II." *Journal of Vascular and Interventional Radiology* 12 (10):1135-1148. doi: 10.1016/s1051-0443(07)61670-4.

Durr, Nicholas J., Timothy Larson, Danielle K. Smith, Brian A. Korgel, Konstantin Sokolov, and Adela Ben-Yakar. 2007. "Two-Photon Luminescence Imaging of Cancer Cells Using Molecularly Targeted Gold Nanorods." *Nano Letters* 7 (4):941-945. doi: 10.1021/nl062962v.

Eberlein, C., J. Kendrew, K. McDaid, A. Alfred, J. S. Kang, V. N. Jacobs, S. J. Ross, C. Rooney, N. R. Smith, J. Rinkenberger, A. Cao, A. Churchman, J. F. Marshall, H. M. Weir, V. Bedian, D. C. Blakey, I. N. Foltz, and S. T. Barry. 2012. "A human monoclonal antibody 264RAD targeting αvβ6 integrin reduces tumour growth and metastasis, and modulates key biomarkers in vivo." *Oncogene* 32:4406. doi: 10.1038/onc.2012.460

Edwards, Peter P, and John Meurig Thomas. 2007. "Gold in a Metallic Divided State From Faraday to Present-Day Nanoscience." *Angewandte Chemie International Edition* 46 (29):5480-5486. doi: 10.1002/anie.200700428.

El-Sayed, Ivan H., Xiaohua Huang, and Mostafa A. El-Sayed. 2005. "Surface Plasmon Resonance Scattering and Absorption of anti-EGFR Antibody Conjugated Gold Nanoparticles in Cancer Diagnostics: Applications in Oral Cancer." *Nano Letters* 5 (5):829-834. doi: 10.1021/nl050074e.

El-Sayed, Mostafa A. 2001. "Some Interesting Properties of Metals Confined in Time and Nanometer Space of Different Shapes." *Accounts of Chemical Research* 34 (4):257-264. doi: 10.1021/ar960016n.

Eustis, Susie, and Mostafa A. El-Sayed. 2006. "Why gold nanoparticles are more precious than pretty gold: Noble metal surface plasmon resonance and its enhancement of the radiative and nonradiative properties of nanocrystals of different shapes." *Chemical Society Reviews* 35 (3):209-217. doi: 10.1039/B514191E.

Faraday, Michael. 1857. "The Bakerian Lecture: Experimental Relations of Gold (and Other Metals) to Light." *Philosophical Transactions of the Royal Society of London* 147:145-181. doi: 10.1098/rstl.1857.0011.

Flynn, Nolan T., Thanh Nga T. Tran, Michael J. Cima, and Robert Langer. 2003. "Long-Term Stability of Self-Assembled Monolayers in Biological Media." *Langmuir* 19 (26):10909-10915. doi: 10.1021/la035331e.

Frens, G. 1973. "Controlled Nucleation for the Regulation of the Particle Size in Monodisperse Gold Suspensions." *Nature Physical Science* 241 (105):20-22. doi: doi:10.1038/physci241020a0.

Fujimoto, J. G., M. E. Brezinski, G. J. Tearney, S. A. Boppart, B. Bouma, M. R. Hee, J. F. Southern, and E. A. Swanson. 1995. "Optical Biopsy And Imaging Using Optical Coherence Tomography." *Nature Medicine* 1 (9):970-972. doi: 10.1038 /nm0995-970.

Ghitescu, L., and A. Fixman. 1984. "Surface charge distribution on the endothelial cell of liver sinusoids." *The Journal of Cell Biology* 99 (2):639.

Ghosh, Partha S., Chae-Kyu Kim, Gang Han, Neil S. Forbes, and Vincent M. Rotello. 2008. "Efficient Gene Delivery Vectors by Tuning the Surface Charge Density of Amino Acid-Functionalized Gold Nanoparticles." *ACS Nano* 2 (11):2213-2218. doi: 10.1021/nn800507t.

Gibson, Jacob D., Bishnu P. Khanal, and Eugene R. Zubarev. 2007. "Paclitaxel-Functionalized Gold Nanoparticles." *Journal of the American Chemical Society* 129 (37):11653-11661. doi: 10.1021/ja075181k.

Goldberg, S. Nahum. 2001. "Radiofrequency tumor ablation: principles and techniques." *European Journal of Ultrasound* 13 (2):129-147. doi: https://doi.org/10.1016/S0929-8266(01)00126-4.

Gole, Anand, and Catherine J. Murphy. 2008. "Azide-Derivatized Gold Nanorods: Functional Materials for "Click" Chemistry." *Langmuir* 24 (1):266-272. doi: 10.1021/la7026303.

Goodman, Catherine M., Catherine D. McCusker, Tuna Yilmaz, and Vincent M. Rotello. 2004. "Toxicity of Gold Nanoparticles Functionalized with Cationic and Anionic Side Chains." *Bioconjugate Chemistry* 15 (4):897-900. doi: 10.1021/bc049951i.

Gu, Yan-Juan, Jinping Cheng, Chun-Chi Lin, Yun Wah Lam, Shuk Han Cheng, and Wing-Tak Wong. 2009. "Nuclear penetration of surface functionalized gold nanoparticles." *Toxicology and Applied Pharmacology* 237 (2):196-204. doi: http://dx.doi.org/10.1016/j.taap.2009.03.009.

Gu, Yan, Wei Sun, Gufeng Wang, and Ning Fang. 2011. "Single Particle Orientation and Rotation Tracking Discloses Distinctive Rotational Dynamics of Drug Delivery Vectors on Live Cell Membranes." *Journal of the American Chemical Society* 133 (15):5720-5723. doi: 10.1021/ja200603x.

Guo, Linlang, Fan Zhang, Yingqian Cai, and Tengfei Liu. 2009. "Expression profiling of integrins in lung cancer cells." *Pathology - Research and Practice* 205 (12):847-853. doi: https://doi.org/10.1016/j.prp.2009.07.005.

Hanahan, Douglas, and Robert A. Weinberg. 2000. "The Hallmarks of Cancer." *Cell* 100 (1):57-70. doi: https://doi.org/10.1016/S0092-8674(00)81683-9.

Hardman, Ron. 2006. "A Toxicologic Review of Quantum Dots: Toxicity Depends on Physicochemical and Environmental Factors." *Environmental Health Perspectives* 114 (2):165-172. doi: 10.1289/ehp.8284.

Harris, J. Milton, and Robert B. Chess. 2003. "Effect of pegylation on pharmaceuticals." *Nat Rev Drug Discov* 2 (3):214-221.

Hauck, Tanya S, Arezou A Ghazani, and Warren C W Chan. 2008. "Assessing the Effect of Surface Chemistry on Gold Nanorod Uptake, Toxicity, and Gene Expression in Mammalian Cells." *Small* 4 (1):153-159. doi: 10.1002/smll.200700217.

Heo, Dong Nyoung, Dae Hyeok Yang, Ho-Jin Moon, Jung Bok Lee, Min Soo Bae, Sang Cheon Lee, Won Jun Lee, In-Cheol Sun, and Il Keun Kwon. 2012. "Gold nanoparticles surface-functionalized with paclitaxel drug and biotin receptor as theranostic agents for cancer therapy." *Biomaterials* 33 (3):856-866. doi: https://doi.org/10.1016/j.biomaterials.2011.09.064.

Hostetler, Michael J., Allen C. Templeton, and Royce W. Murray. 1999. "Dynamics of Place-Exchange Reactions on Monolayer-Protected Gold Cluster Molecules." *Langmuir* 15 (11):3782-3789. doi: 10.1021/la981598f.

Hou, Wenbo, Mita Dasog, and Robert W. J. Scott. 2009. "Probing the Relative Stability of Thiolate- and Dithiolate-Protected Au Monolayer-Protected Clusters." *Langmuir* 25 (22):12954-12961. doi: 10.1021/la9018053.

Hu, Kai, and Allen J. Bard. 1998. "In Situ Monitoring of Kinetics of Charged Thiol Adsorption on Gold Using an Atomic Force Microscope." *Langmuir* 14 (17):4790-4794. doi: 10.1021/la971363o.

Huang, X. H., P. K. Jain, I. H. El-Sayed, and M. A. El-Sayed. 2007. "Gold nanoparticles: interesting optical properties and recent applications in cancer diagnostic and therapy." *Nanomedicine* 2 (5):681-693. doi: 10.2217/17435889.2.5.681.

Huefner, Anna, Wei-Li Kuan, Roger A. Barker, and Sumeet Mahajan. 2013. "Intracellular SERS Nanoprobes For Distinction Of Different Neuronal Cell Types." *Nano Letters* 13 (6):2463-2470. doi: 10.1021/nl400448n.

Huff, Terry B., Matthew N. Hansen, Yan Zhao, Ji-Xin Cheng, and Alexander Wei. 2007. "Controlling the Cellular Uptake of Gold Nanorods." *Langmuir* 23 (4):1596-1599. doi: 10.1021/la062642r.

Imura, Kohei, Tetsuhiko Nagahara, and Hiromi Okamoto. 2004. "Plasmon Mode Imaging of Single Gold Nanorods." *Journal of the American Chemical Society* 126 (40):12730-12731. doi: 10.1021/ja047836c.

Jain, P. K., K. S. Lee, I. H. El-Sayed, and M. A. El-Sayed. 2006a. "Calculated absorption and scattering properties of gold nanoparticles of different size, shape, and composition: Applications in biological imaging and biomedicine." *Journal of Physical Chemistry B* 110 (14):7238-7248. doi: 10.1021/jp057170o.

Jain, Prashant K., Kyeong Seok Lee, Ivan H. El-Sayed, and Mostafa A. El-Sayed. 2006b. "Calculated Absorption and Scattering Properties of Gold Nanoparticles of Different Size, Shape, and Composition: Applications in Biological Imaging and Biomedicine." *The Journal of Physical Chemistry B* 110 (14):7238-7248. doi: 10.1021/jp057170o.

Jana, N. R., L. Gearheart, and C. J. Murphy. 2001. "Seed-Mediated Growth Approach for Shape-Controlled Synthesis of Spheroidal and Rod-like Gold Nanoparticles Using a Surfactant Template." *Advanced Materials* 13 (18):1389-1393. doi: 10.1002/1521-4095(200109)13:18<1389::AID-ADMA1389>3.0.CO;2-F.

Jiang, W., B. Y. S. Kim, J. T. Rutka, and W. C. W. Chan. 2008. "Nanoparticle-mediated cellular response is size-dependent." *Nature Nanotechnology* 3 (3):145-150. doi: 10.1038/nnano.2008.30.

Jing, Chao, Zhen Gu, Yi-Lun Ying, Da-Wei Li, Lei Zhang, and Yi-Tao Long. 2012. "Chrominance to Dimension: A Real-Time Method for Measuring the Size of Single Gold Nanoparticles." *Analytical Chemistry* 84 (10):4284-4291. doi: 10.1021/ac203118g.

Jokerst, Jesse V., Adam J. Cole, Dominique Van de Sompel, and Sanjiv S. Gambhir. 2012. "Gold Nanorods for Ovarian Cancer Detection with Photoacoustic Imaging and Resection Guidance via Raman Imaging in Living Mice." *ACS Nano* 6 (11):10366-10377. doi: 10.1021/nn304347g.

Joshi, Hrushikesh, Pravin S. Shirude, Vipul Bansal, K. N. Ganesh, and Murali Sastry. 2004. "Isothermal Titration Calorimetry Studies on the Binding of Amino Acids to Gold Nanoparticles." *The Journal of Physical Chemistry B* 108 (31):11535-11540. doi: 10.1021/jp048766z.

Kang, Bin, Marwa M. Afifi, Lauren A. Austin, and Mostafa A. El-Sayed. 2013. "Exploiting the Nanoparticle Plasmon Effect: Observing Drug Delivery Dynamics in Single Cells via Raman/Fluorescence Imaging Spectroscopy." *ACS Nano* 7 (8):7420-7427. doi: 10.1021/nn403351z.

Kang, Bin, Lauren A. Austin, and Mostafa A. El-Sayed. 2012. "Real-Time Molecular Imaging throughout the Entire Cell Cycle by Targeted Plasmonic-Enhanced Rayleigh/Raman Spectroscopy." *Nano Letters* 12 (10):5369-5375. doi: 10.1021 /nl3027586.

Kang, Bin, Lauren A. Austin, and Mostafa A. El-Sayed. 2014. "Observing Real-Time Molecular Event Dynamics of Apoptosis in Living Cancer Cells using Nuclear-Targeted Plasmonically Enhanced Raman Nanoprobes." *ACS Nano* 8 (5):4883-4892. doi: 10.1021/nn500840x.

Kang, Bin, Megan A. Mackey, and Mostafa A. El-Sayed. 2010. "Nuclear Targeting of Gold Nanoparticles in Cancer Cells Induces DNA Damage, Causing Cytokinesis Arrest and Apoptosis." *Journal of the American Chemical Society* 132 (5):1517-1519. doi: 10.1021/ja9102698.

Kelly, K. Lance, Eduardo Coronado, Lin Lin Zhao, and George C. Schatz. 2003. "The Optical Properties of Metal Nanoparticles: The Influence of Size, Shape, and Dielectric Environment." *The Journal of Physical Chemistry B* 107 (3):668-677. doi: 10.1021/jp026731y.

Khan, Jameel Ahmad, Beena Pillai, Taposh Kumar Das, Yogendra Singh, and Souvik Maiti. 2007. "Molecular Effects of Uptake of Gold Nanoparticles in HeLa Cells." *ChemBioChem* 8 (11):1237-1240. doi: 10.1002/cbic.200700165.

Khlebtsov, Nikolai, and Lev Dykman. 2011. "Biodistribution and toxicity of engineered gold nanoparticles: a review of in vitro and in vivo studies." *Chemical Society Reviews* 40 (3):1647-1671. doi: 10.1039/C0CS00018C.

Kim, Byoungjin, Gang Han, Bhushan J. Toley, Chae-kyu Kim, Vincent M. Rotello, and Neil S. Forbes. 2010. "Tuning payload delivery in tumour cylindroids using gold nanoparticles." *Nat Nano* 5 (6):465-472. doi: http://www.nature.com/nnano /journal/v5/n6/abs/nnano.2010.58.html#supplementary-information.

Kim, Chae Kyu, Partha Ghosh, Chiara Pagliuca, Zheng-Jiang Zhu, Stefano Menichetti, and Vincent M. Rotello. 2009. "Entrapment of Hydrophobic Drugs in Nanoparticle Monolayers with Efficient Release into Cancer Cells." *Journal of the American Chemical Society* 131 (4):1360-1361. doi: 10.1021/ja808137c.

Kim, Chulhong, Hyon-Min Song, Xin Cai, Junjie Yao, Alexander Wei, and Lihong V. Wang. 2011. "In vivo photoacoustic mapping of lymphatic systems with plasmon-resonant nanostars." *Journal of materials chemistry* 21 (9):2841-2844. doi: 10.1039/C0JM04194G.

Kim, Dongkyu, Sangjin Park, Jae Hyuk Lee, Yong Yeon Jeong, and Sangyong Jon. 2007. "Antibiofouling Polymer-Coated Gold Nanoparticles as a Contrast Agent for in Vivo X-ray Computed Tomography Imaging." *Journal of the American Chemical Society* 129 (24):7661-7665. doi: 10.1021/ja071471p.

Kim, F., S. Connor, H. Song, T. Kuykendall, and P. Yang. 2004. "Platonic gold nanocrystals." *Angew Chem Int Ed Engl* 43 (28):3673-7. doi: 10.1002 /anie.200454216.

Kneipp, Janina, Harald Kneipp, Burghardt Wittig, and Katrin Kneipp. "Novel optical nanosensors for probing and imaging live cells." *Nanomedicine: Nanotechnology, Biology and Medicine* 6 (2):214-226. doi: 10.1016 /j.nano.2009.07.009.

Knoll, M., and E. Ruska. 1932. "Das Elektronenmikroskop." *Zeitschrift für Physik* 78 (5):318-339. doi: 10.1007/bf01342199.

Koukoulis, George K., William H. Warren, Ismo Virtanen, and Victor E. Gould. 1997. "Immunolocalization of integrins in the normal lung and in pulmonary carcinomas." *Human Pathology* 28 (9):1018-1025. doi: 10.1016/S00468177 (97)90054-X.

Leduc, Cécile, Jin-Mi Jung, Randy R. Carney, Francesco Stellacci, and Brahim Lounis. 2011. "Direct Investigation of Intracellular Presence of Gold Nanoparticles via Photothermal Heterodyne Imaging." *ACS Nano* 5 (4):2587-2592. doi: 10.1021 /nn1023285.

Lee, Kyeong-Seok, and Mostafa A. El-Sayed. 2005. "Dependence of the Enhanced Optical Scattering Efficiency Relative to That of Absorption for Gold Metal Nanorods on Aspect Ratio, Size, End-Cap Shape, and Medium Refractive Index." *The Journal of Physical Chemistry B* 109 (43):20331-20338. doi: 10.1021 /jp054385p.

Li, Jing-Liang, and Min Gu. 2010. "Surface plasmonic gold nanorods for enhanced two-photon microscopic imaging and apoptosis induction of cancer cells." *Biomaterials* 31 (36):9492-9498. doi: https://doi.org/10.1016/j.biomaterials.2010.08.068.

Li, Na, Huijun Yang, Zhengze Yu, Yanli Li, Wei Pan, Hongyu Wang, and Bo Tang. 2017. "Nuclear-targeted siRNA delivery for long-term gene silencing." *Chemical Science* 8 (4):2816-2822. doi: 10.1039/C6SC04293G.

Li, Yang, Chao Jing, Lei Zhang, and Yi-Tao Long. 2012. "Resonance scattering particles as biological nanosensors in vitro and in vivo." *Chemical Society Reviews* 41 (2):632-642. doi: 10.1039/C1CS15143F.

Liang, Han-Pu, Li-Jun Wan, Chun-Li Bai, and Li Jiang. 2005. "Gold Hollow Nanospheres: Tunable Surface Plasmon Resonance Controlled by Interior-Cavity Sizes." *The Journal of Physical Chemistry B* 109 (16):7795-7800. doi: 10.1021/jp045006f.

Liang, Lijia, Dianshuai Huang, Hailong Wang, Haibo Li, Shuping Xu, Yixin Chang, Hui Li, Ying-Wei Yang, Chongyang Liang, and Weiqing Xu. 2015. "In Situ Surface-Enhanced Raman Scattering Spectroscopy Exploring Molecular Changes of Drug-Treated Cancer Cell Nucleus." *Analytical Chemistry* 87 (4):2504-2510. doi: 10.1021/ac504550w.

Liang, Zhijian, Andrei Susha, and Frank Caruso. 2003. "Gold Nanoparticle-Based Core−Shell and Hollow Spheres and Ordered Assemblies Thereof." *Chemistry of Materials* 15 (16):3176-3183. doi: 10.1021/cm031014h.

Loumaigne, Matthieu, Alain Richard, Julien Laverdant, Daniele Nutarelli, and Anne Débarre. 2010. "Ligand-Induced Anisotropy of the Two-Photon Luminescence of Spherical Gold Particles in Solution Unraveled at the Single Particle Level." *Nano Letters* 10 (8):2817-2824. doi: 10.1021/nl100737y.

Love, J. Christopher, Lara A. Estroff, Jennah K. Kriebel, Ralph G. Nuzzo, and George M. Whitesides. 2005. "Self-Assembled Monolayers of Thiolates on Metals as a Form of Nanotechnology." *Chemical Reviews* 105 (4):1103-1170. doi: 10.1021/cr0300789.

Love, Sara A., Bryce J. Marquis, and Christy L. Haynes. 2008. "Recent Advances in Nanomaterial Plasmonics: Fundamental Studies and Applications." *Applied Spectroscopy* 62 (12):346A-362A. doi: 10.1366/000370208786822331.

Lu, Xianmao, Leslie Au, Joseph McLellan, Zhi-Yuan Li, Manuel Marquez, and Younan Xia. 2007. "Fabrication of Cubic Nanocages and Nanoframes by Dealloying Au/Ag Alloy Nanoboxes with an Aqueous Etchant Based on Fe(NO3)3 or NH4OH." *Nano Letters* 7 (6):1764-1769. doi: 10.1021/nl070838l.

Lundqvist, Martin, Johannes Stigler, Giuliano Elia, Iseult Lynch, Tommy Cedervall, and Kenneth A. Dawson. 2008. "Nanoparticle size and surface properties determine the protein corona with possible implications for biological impacts." *Proceedings of the National Academy of Sciences* 105 (38):14265-14270. doi: 10.1073/pnas.0805135105.

Lynch, Iseult, Tommy Cedervall, Martin Lundqvist, Celia Cabaleiro-Lago, Sara Linse, and Kenneth A. Dawson. 2007. "The nanoparticle–protein complex as a biological entity; a complex fluids and surface science challenge for the 21st century." *Advances in Colloid and Interface Science* 134 (Supplement C):167-174. doi: https://doi.org/10.1016/j.cis.2007.04.021.

Lynch, Iseult, and Kenneth A. Dawson. 2008. "Protein-nanoparticle interactions." *Nano Today* 3 (1):40-47. doi: https://doi.org/10.1016/S1748-0132(08)70014-8.

Ma, Y., Q. Kuang, Z. Jiang, Z. Xie, R. Huang, and L. Zheng. 2008. "Synthesis of trisoctahedral gold nanocrystals with exposed high-index facets by a facile chemical method." *Angew Chem Int Ed Engl* 47 (46):8901-4. doi: 10.1002 /anie.200802750.

Mackey, Megan A., Farhat Saira, Mahmoud A. Mahmoud, and Mostafa A. El-Sayed. 2013. "Inducing Cancer Cell Death by Targeting Its Nucleus: Solid Gold Nanospheres versus Hollow Gold Nanocages." *Bioconjugate Chemistry* 24 (6):897-906. doi: 10.1021/bc300592d.

Magnussen, O. M. 2002. "Ordered Anion Adlayers on Metal Electrode Surfaces." *Chemical Reviews* 102 (3):679-726. doi: 10.1021/cr000069p.

Male, Keith B., Bernard Lachance, Sabahudin Hrapovic, Geoff Sunahara, and John H. T. Luong. 2008. "Assessment of Cytotoxicity of Quantum Dots and Gold Nanoparticles Using Cell-Based Impedance Spectroscopy." *Analytical Chemistry* 80 (14):5487-5493. doi: 10.1021/ac8004555.

Marquis, Bryce J., Sara A. Love, Katherine L. Braun, and Christy L. Haynes. 2009. "Analytical methods to assess nanoparticle toxicity." *Analyst* 134 (3):425-439. doi: 10.1039/B818082B.

Martin, Benjamin R., Daniel J. Dermody, Brian D. Reiss, Mingming Fang, L. Andrew Lyon, Michael J. Natan, and Thomas E. Mallouk. 1999. "Orthogonal Self-Assembly on Colloidal Gold-Platinum Nanorods." *Advanced Materials* 11 (12):1021-1025. doi: 10.1002/(SICI)1521-4095(199908)11:12<1021::AID-ADMA1021>3.0.CO;2-S.

Mie, Gustav. 1908. "Beiträge zur Optik trüber Medien, speziell kolloidaler Metallösungen." *Annalen der Physik* 330 (3):377-445. doi: 10.1002/andp. 19083300302.

Millstone, Jill E., Sungho Park, Kevin L. Shuford, Lidong Qin, George C. Schatz, and Chad A. Mirkin. 2005. "Observation of a Quadrupole Plasmon Mode for a Colloidal Solution of Gold Nanoprisms." *Journal of the American Chemical Society* 127 (15):5312-5313. doi: 10.1021/ja043245a.

Ming, Tian, Wei Feng, Qin Tang, Feng Wang, Lingdong Sun, Jianfang Wang, and Chunhua Yan. 2009. "Growth of Tetrahexahedral Gold Nanocrystals with High-Index Facets." *Journal of the American Chemical Society* 131 (45):16350-16351. doi: 10.1021/ja907549n.

Mirkin, Chad A., Robert L. Letsinger, Robert C. Mucic, and James J. Storhoff. 1996. "A DNA-based method for rationally assembling nanoparticles into macroscopic materials." *Nature* 382 (6592):607-609.

Mirza, A. N., B. D. Fornage, N. Sneige, H. M. Kuerer, L. A. Newman, F. C. Ames, and S. E. Singletary. 2001. "Radiofrequency ablation of solid tumors." *Cancer journal (Sudbury, Mass.)* 7 (2):95-102.

Monteiro-Riviere, N. A., A. O. Inman, and L. W. Zhang. 2009. "Limitations and relative utility of screening assays to assess engineered nanoparticle toxicity in a human cell line." *Toxicology and Applied Pharmacology* 234 (2):222-235. doi: https://doi.org/10.1016/j.taap.2008.09.030.

Muñoz Javier, Almudena, Oliver Kreft, Alicia Piera Alberola, Christian Kirchner, Bernd Zebli, Andrei S Susha, Elias Horn, Susanne Kempter, Andre G Skirtach, Andrey L Rogach, Joachim Rädler, Gleb B Sukhorukov, Martin Benoit, and Wolfgang J Parak. 2006. "Combined Atomic Force Microscopy and Optical Microscopy Measurements as a Method To Investigate Particle Uptake by Cells." *Small* 2 (3):394-400. doi: 10.1002/smll.200500282.

Murphy, Catherine J., Anand M. Gole, John W. Stone, Patrick N. Sisco, Alaaldin M. Alkilany, Edie C. Goldsmith, and Sarah C. Baxter. 2008. "Gold Nanoparticles in Biology: Beyond Toxicity to Cellular Imaging." *Accounts of Chemical Research* 41 (12):1721-1730. doi: 10.1021/ar800035u.

Nativo, Paola, Ian A. Prior, and Mathias Brust. 2008. "Uptake and Intracellular Fate of Surface-Modified Gold Nanoparticles." *ACS Nano* 2 (8):1639-1644. doi: 10.1021/nn800330a.

Niidome, Takuro, Masato Yamagata, Yuri Okamoto, Yasuyuki Akiyama, Hironobu Takahashi, Takahito Kawano, Yoshiki Katayama, and Yasuro Niidome. 2006. "PEG-modified gold nanorods with a stealth character for in vivo applications." *Journal of Controlled Release* 114 (3):343-347. doi: https://doi.org/10.1016/j.jconrel.2006.06.017.

Nikoobakht, Babak, and Mostafa A. El-Sayed. 2003. "Preparation and Growth Mechanism of Gold Nanorods (NRs) Using Seed-Mediated Growth Method." *Chemistry of Materials* 15 (10):1957-1962. doi: 10.1021/cm020732l.

Nitin, Nitin, David J. Javier, and Rebecca Richards-Kortum. 2007. "Oligonucleotide-Coated Metallic Nanoparticles as a Flexible Platform for Molecular Imaging Agents." *Bioconjugate Chemistry* 18 (6):2090-2096. doi: 10.1021/bc0701242.

Niu, Wenxin, Shanliang Zheng, Dawei Wang, Xiaoqing Liu, Haijuan Li, Shuang Han, Jiuan Chen, Zhiyong Tang, and Guobao Xu. 2009. "Selective Synthesis of Single-Crystalline Rhombic Dodecahedral, Octahedral, and Cubic Gold Nanocrystals." *Journal of the American Chemical Society* 131 (2):697-703. doi: 10.1021 /ja804115r.

Oh, E., K. Susumu, J. B. Blanco-Canosa, I. L. Medintz, P. E. Dawson, and H. Mattoussi. 2010. "Preparation of Stable Maleimide-Functionalized Au Nanoparticles and Their Use in Counting Surface Ligands." *Small* 6 (12):1273-1278. doi: 10.1002 /smll.201000279.

Oldenburg, Amy L., Matthew N. Hansen, Tyler S. Ralston, Alexander Wei, and Stephen A. Boppart. 2009. "Imaging gold nanorods in excised human breast carcinoma by spectroscopic optical coherence tomography." *Journal of Materials Chemistry* 19 (35):6407-6411. doi: 10.1039/B823389F.

Oldenburg, Amy L., Matthew N. Hansen, Daniel A. Zweifel, Alexander Wei, and Stephen A. Boppart. 2006. "Plasmon-resonant gold nanorods as low backscattering albedo contrast agents." *Optics Express* 14 (15):6724-6738. doi: 10.1364/OE.14.006724.

Oldenburg, S. J., R. D. Averitt, S. L. Westcott, and N. J. Halas. 1998. "Nanoengineering of optical resonances." *Chemical Physics Letters* 288 (2):243-247. doi: http:// dx.doi.org/10.1016/S0009-2614(98)00277-2.

Orendorff, C. J., S. C. Baxter, E. C. Goldsmith, and C. J. Murphy. 2005. "Light scattering from gold nanorods: tracking material deformation." *Nanotechnology* 16 (11): 2601-2605. doi: 10.1088/0957-4484/16/11/022.

Oyelere, Adegboyega K., Po C. Chen, Xiaohua Huang, Ivan H. El-Sayed, and Mostafa A. El-Sayed. 2007. "Peptide-Conjugated Gold Nanorods for Nuclear Targeting." *Bioconjugate Chemistry* 18 (5):1490-1497. doi: 10.1021/bc070132i.

Pan, Yu, Annika Leifert, David Ruau, Sabine Neuss, Jörg Bornemann, Günter Schmid, Wolfgang Brandau, Ulrich Simon, and Willi Jahnen-Dechent. 2009. "Gold Nanoparticles of Diameter 1.4 nm Trigger Necrosis by Oxidative Stress and Mitochondrial Damage." *Small* 5 (18):2067-2076. doi: 10.1002/smll.200900466.

Pan, Yu, Sabine Neuss, Annika Leifert, Monika Fischler, Fei Wen, Ulrich Simon, Günter Schmid, Wolfgang Brandau, and Willi Jahnen-Dechent. 2007. "Size-Dependent Cytotoxicity of Gold Nanoparticles." *Small* 3 (11):1941-1949. doi: 10.1002 /smll.200700378.

Panikkanvalappil, Sajanlal R., Steven M. Hira, Mahmoud A. Mahmoud, and Mostafa A. El-Sayed. 2014. "Unraveling the Biomolecular Snapshots of Mitosis in Healthy and Cancer Cells Using Plasmonically-Enhanced Raman Spectroscopy." *Journal of the American Chemical Society* 136 (45):15961-15968. doi: 10.1021/ja506289u.

Patra, Hirak K., Shuvojit Banerjee, Utpal Chaudhuri, Prabir Lahiri, and Anjan Kr Dasgupta. 2007. "Cell selective response to gold nanoparticles." *Nanomedicine: Nanotechnology, Biology and Medicine* 3 (2):111-119. doi: https://doi.org/10.1016/j.nano.2007.03.005.

Peckys, Diana B., and Niels de Jonge. 2011. "Visualizing Gold Nanoparticle Uptake in Live Cells with Liquid Scanning Transmission Electron Microscopy." *Nano Letters* 11 (4):1733-1738. doi: 10.1021/nl200285r.

Peer, D., J. M. Karp, S. Hong, O. C. FaroKhzad, R. Margalit, and R. Langer. 2007. "Nanocarriers as an emerging platform for cancer therapy." *Nature Nanotechnology* 2 (12):751-760. doi: 10.1038/nnano.2007.387.

Pernodet, Nadine, Xiaohua Fang, Yuan Sun, Asya Bakhtina, Aditi Ramakrishnan, Jonathan Sokolov, Abraham Ulman, and Miriam Rafailovich. 2006. "Adverse Effects of Citrate/Gold Nanoparticles on Human Dermal Fibroblasts." *Small* 2 (6):766-773. doi: 10.1002/smll.200500492.

Personick, M. L., M. R. Langille, J. Zhang, N. Harris, G. C. Schatz, and C. A. Mirkin. 2011. "Synthesis and isolation of {110}-faceted gold bipyramids and rhombic dodecahedra." *J Am Chem Soc* 133 (16):6170-3. doi: 10.1021/ja201826r.

Polizzi, Mark A., Nathan A. Stasko, and Mark H. Schoenfisch. 2007. "Water-Soluble Nitric Oxide-Releasing Gold Nanoparticles." *Langmuir* 23 (9):4938-4943. doi: 10.1021/la0633841.

Ponder, B. A. J. 2001. "Cancer genetics." *Nature* 411 (6835) : 336-341. doi: 10.1038/35077207.

Pong, Boon-Kin, Hendry I. Elim, Jian-Xiong Chong, Wei Ji, Bernhardt L. Trout, and Jim-Yang Lee. 2007. "New Insights on the Nanoparticle Growth Mechanism in the Citrate Reduction of Gold(III) Salt: Formation of the Au Nanowire Intermediate and Its Nonlinear Optical Properties." *The Journal of Physical Chemistry C* 111 (17):6281-6287. doi: 10.1021/jp068666o.

Prado, Adilson R., Jairo P. Oliveira, Wanderson J. Keijok, Bárbara Altoé Milaneze, Breno V. Nogueira, Marco C. C. Guimarães, Maria J. Pontes, and Moises R. N. Ribeiro. 2014. "Comparison between the synthesis of gold nanoparticles with sodium citrate and sodium tetraboreto." *BMC Proceedings* 8 (Suppl 4):P252-P252. doi: 10.1186/1753-6561-8-S4-P252.

Radwan, S. H., and H. M. E. Azzazy. 2009. "Gold nanoparticles for molecular diagnostics." *Expert Review of Molecular Diagnostics* 9 (5):511-524. doi: 10.1586/erm.09.33.

Roduner, Emil. 2006. "Size matters: why nanomaterials are different." *Chemical Society Reviews* 35 (7):583-592. doi: 10.1039/B502142C.

Rosi, N. L., and C. A. Mirkin. 2005. "Nanostructures in biodiagnostics." *Chemical Reviews* 105 (4):1547-1562. doi: 10.1021/cr030067f.

Rosi, Nathaniel L., David A. Giljohann, C. Shad Thaxton, Abigail K. R. Lytton-Jean, Min Su Han, and Chad A. Mirkin. 2006. "Oligonucleotide-Modified Gold Nanoparticles for Intracellular Gene Regulation." *Science* 312 (5776):1027-1030. doi: 10.1126/science.1125559.

Ryan, Joseph A., K. Wesley Overton, Molly E. Speight, Christine N. Oldenburg, LiNa Loo, Wayne Robarge, Stefan Franzen, and Daniel L. Feldheim. 2007. "Cellular Uptake of Gold Nanoparticles Passivated with BSA−SV40 Large T Antigen Conjugates." *Analytical Chemistry* 79 (23):9150-9159. doi: 10.1021/ac0715524.

Sardar, Rajesh, Alison M. Funston, Paul Mulvaney, and Royce W. Murray. 2009. "Gold Nanoparticles: Past, Present, and Future." *Langmuir* 25 (24):13840-13851. doi: 10.1021/la9019475.

Sau, Tapan K., and Catherine J. Murphy. 2004. "Seeded High Yield Synthesis of Short Au Nanorods in Aqueous Solution." *Langmuir* 20 (15):6414-6420. doi: 10.1021 /la049463z.

Saxton, Michael J., and Ken Jacobson. 1997. "SINGLE-PARTICLE TRACKING: Applications to Membrane Dynamics." *Annual Review of Biophysics and Biomolecular Structure* 26 (1):373-399. doi: 10.1146/ annurev.biophys.26.1.373.

Schmid, Guenter. 1992. "Large clusters and colloids. Metals in the embryonic state." *Chemical Reviews* 92 (8):1709-1727. doi: 10.1021/cr00016a002.

Schmid, Günter, Reinhard Pfeil, Roland Boese, Friedhelm Bandermann, Sonja Meyer, Gijs H. M. Calis, and Jan W. A. van der Velden. 1981. "Au55[P(C6H5)3]12CI6 — ein Goldcluster ungewöhnlicher Größe." *Chemische Berichte* 114 (11):3634-3642. doi: 10.1002/cber.19811141116.

Seferos, Dwight S., David A. Giljohann, Haley D. Hill, Andrew E. Prigodich, and Chad A. Mirkin. 2007. "Nano-Flares: Probes for Transfection and mRNA Detection in Living Cells." *Journal of the American Chemical Society* 129 (50):15477-15479. doi: 10.1021/ja0776529.

Shankar, S. Shiv, Akhilesh Rai, Balaprasad Ankamwar, Amit Singh, Absar Ahmad, and Murali Sastry. 2004. "Biological synthesis of triangular gold nanoprisms." *Nat Mater* 3 (7):482-488.

Shimizu, Takami, Toshiharu Teranishi, Satoshi Hasegawa, and Mikio Miyake. 2003. "Size Evolution of Alkanethiol-Protected Gold Nanoparticles by Heat Treatment in the Solid State." *The Journal of Physical Chemistry B* 107 (12):2719-2724. doi: 10.1021/jp026920g.

Shukla, Ravi, Vipul Bansal, Minakshi Chaudhary, Atanu Basu, Ramesh R. Bhonde, and Murali Sastry. 2005. "Biocompatibility of Gold Nanoparticles and Their Endocytotic Fate Inside the Cellular Compartment: A Microscopic Overview." *Langmuir* 21 (23):10644-10654. doi: 10.1021/la0513712.

Singh, Amit, Ravi Shukla, Shabir Hassan, R. R. Bhonde, and Murali Sastry. 2011. "Cytotoxicity and Cellular Internalization Studies of Biogenic Gold Nanotriangles in Animal Cell Lines." *International Journal of Green Nanotechnology* 3 (4):251-263. doi: 10.1080/19430892.2011.633479.

Skrabalak, Sara E., Jingyi Chen, Yugang Sun, Xianmao Lu, Leslie Au, Claire M. Cobley, and Younan Xia. 2008. "Gold Nanocages: Synthesis, Properties, and Applications." *Accounts of Chemical Research* 41 (12):1587-1595. doi: 10.1021 /ar800018v.

Sperling, Ralph A., Pilar Rivera Gil, Feng Zhang, Marco Zanella, and Wolfgang J. Parak. 2008. "Biological applications of gold nanoparticles." *Chemical Society Reviews* 37 (9):1896-1908. doi: 10.1039/B712170A.

Sun, T., and G. J. Diebold. 1992. "generation of ultrasonic-waves from a layered photoacoustic source." *Nature* 355 (6363):806-808. doi: 10.1038/355806a0.

Sun, W., N. Fang, B. G. Trewyn, M. Tsunoda, Slowing, II, V. S. Y. Lin, and E. S. Yeung. 2008. "Endocytosis of a single mesoporous silica nanoparticle into a human lung cancer cell observed by differential interference contrast microscopy." *Analytical and Bioanalytical Chemistry* 391 (6):2119-2125. doi: 10.1007/s00216-008-2162-1.

Sun, Wei, Gufeng Wang, Ning Fang, and Edward S. Yeung. 2009. "Wavelength-Dependent Differential Interference Contrast Microscopy: Selectively Imaging Nanoparticle Probes in Live Cells." *Analytical Chemistry* 81 (22):9203-9208. doi: 10.1021/ac901623b.

Takahashi, Hironobu, Yasuro Niidome, Takuro Niidome, Kenji Kaneko, Hideya Kawasaki, and Sunao Yamada. 2006. "Modification of Gold Nanorods Using Phosphatidylcholine to Reduce Cytotoxicity." *Langmuir* 22 (1):2-5. doi: 10.1021 /la0520029.

Templeton, Allen C., W. Peter Wuelfing, and Royce W. Murray. 2000. "Monolayer-Protected Cluster Molecules." *Accounts of Chemical Research* 33 (1):27-36. doi: 10.1021/ar9602664.

Tkachenko, Alexander G., Huan Xie, Donna Coleman, Wilhelm Glomm, Joseph Ryan, Miles F. Anderson, Stefan Franzen, and Daniel L. Feldheim. 2003. "Multifunctional Gold Nanoparticle−Peptide Complexes for Nuclear Targeting." *Journal of the American Chemical Society* 125 (16):4700-4701. doi: 10.1021 /ja0296935.

Tkachenko, Alexander G., Huan Xie, Yanli Liu, Donna Coleman, Joseph Ryan, Wilhelm R. Glomm, Mathew K. Shipton, Stefan Franzen, and Daniel L. Feldheim. 2004. "Cellular Trajectories of Peptide-Modified Gold Particle Complexes: Comparison of Nuclear Localization Signals and Peptide Transduction Domains." *Bioconjugate Chemistry* 15 (3):482-490. doi: 10.1021/bc034189q.

Troutman, Timothy S., Jennifer K. Barton, and Marek Romanowski. 2007. "Optical coherence tomography with plasmon resonant nanorods of gold." *Optics Letters* 32 (11):1438-1440. doi: 10.1364/OL.32.001438.

Tsoli, Maria, Hubert Kuhn, Wolfgang Brandau, Helmut Esche, and Günter Schmid. 2005. "Cellular Uptake and Toxicity of Au55 Clusters." *Small* 1 (8-9):841-844. doi: 10.1002/smll.200500104.

Tsunoda, M., D. Isailovic, and E. S. Yeung. 2008. "Real-time three-dimensional imaging of cell division by differential interference contrast microscopy." *Journal of Microscopy* 232 (2):207-211. doi: 10.1111/j.1365-2818.2008.02091.x.

Turkevich, John, Peter Cooper Stevenson, and James Hillier. 1951. "A study of the nucleation and growth processes in the synthesis of colloidal gold." *Discussions of the Faraday Society* 11 (0):55-75. doi: 10.1039/DF9511100055.

Turner, Mark, Vladimir B. Golovko, Owain P. H. Vaughan, Pavel Abdulkin, Angel Berenguer-Murcia, Mintcho S. Tikhov, Brian F. G. Johnson, and Richard M. Lambert. 2008. "Selective oxidation with dioxygen by gold nanoparticle catalysts derived from 55-atom clusters." *Nature* 454 (7207):981-983. doi: http:// www.nature.com/nature/journal/v454/n7207/suppinfo/nature07194_S1.html.

Vartholomeos, Panagiotis, Matthieu Fruchard, Antoine Ferreira, and Constantinos Mavroidis. 2011. "MRI-Guided Nanorobotic Systems for Therapeutic and Diagnostic Applications." *Annual Review of Biomedical Engineering* 13 (1):157-184. doi: 10.1146/annurev-bioeng-071910-124724.

Verma, Ayush, and Francesco Stellacci. 2010. "Effect of Surface Properties on Nanoparticle–Cell Interactions." *Small* 6 (1):12-21. doi: 10.1002/smll. 200901158.

Verma, Ayush, Oktay Uzun, Yuhua Hu, Ying Hu, Hee-Sun Han, Nicki Watson, Suelin Chen, Darrell J. Irvine, and Francesco Stellacci. 2008. "Surface-structure-regulated cell-membrane penetration by monolayer-protected nanoparticles." *Nat Mater* 7 (7):588-595. doi: http://www.nature.com/nmat/journal/v7/n7/suppinfo/nmat2202_S1.html.

Villiers, Christian L., Heidi Freitas, Rachel Couderc, Marie-Bernadette Villiers, and Patrice N. Marche. 2010. "Analysis of the toxicity of gold nano particles on the immune system: effect on dendritic cell functions." *Journal of Nanoparticle Research* 12 (1):55-60. doi: 10.1007/s11051-009-9692-0.

von Maltzahn, Geoffrey, Ji-Ho Park, Amit Agrawal, Nanda Kishor Bandaru, Sarit K. Das, Michael J. Sailor, and Sangeeta N. Bhatia. 2009. "Computationally Guided Photothermal Tumor Therapy Using Long-Circulating Gold Nanorod Antennas." *Cancer Research* 69 (9):3892-3900. doi: 10.1158/0008-5472.can-08-4242.

Walter, Michael, Jaakko Akola, Olga Lopez-Acevedo, Pablo D. Jadzinsky, Guillermo Calero, Christopher J. Ackerson, Robert L. Whetten, Henrik Grönbeck, and Hannu Häkkinen. 2008. "A unified view of ligand-protected gold clusters as superatom complexes." *Proceedings of the National Academy of Sciences* 105 (27):9157-9162. doi: 10.1073/pnas.0801001105.

Wang, Haifeng, Terry B. Huff, Daniel A. Zweifel, Wei He, Philip S. Low, Alexander Wei, and Ji-Xin Cheng. 2005. "In vitro and in vivo two-photon luminescence imaging of single gold nanorods." *Proceedings of the National Academy of Sciences of the United States of America* 102 (44):15752-15756. doi: 10.1073/pnas.0504892102.

Wang, Hui, Daniel W. Brandl, Peter Nordlander, and Naomi J. Halas. 2007. "Plasmonic Nanostructures: Artificial Molecules." *Accounts of Chemical Research* 40 (1):53-62. doi: 10.1021/ar0401045.

Wang, Shuguang, Wentong Lu, Oleg Tovmachenko, Uma Shanker Rai, Hongtao Yu, and Paresh Chandra Ray. 2008. "Challenge in Understanding Size and Shape Dependent Toxicity of Gold Nanomaterials in Human Skin Keratinocytes." *Chemical physics letters* 463 (1-3):145-149. doi: 10.1016/j.cplett.2008.08.039.

Wang, Z. L., M. B. Mohamed, S. Link, and M. A. El-Sayed. 1999. "Crystallographic facets and shapes of gold nanorods of different aspect ratios." *Surface Science* 440 (1):L809-L814. doi: http://dx.doi.org/10.1016/S0039-6028(99)00865-1.

Wax, A., and K. Sokolov. 2009. "Molecular imaging and darkfield microspectroscopy of live cells using gold plasmonic nanoparticles." *Laser & Photonics Reviews* 3 (1-2):146-158. doi: 10.1002/lpor.200810011.

Weare, Walter W., Scott M. Reed, Marvin G. Warner, and James E. Hutchison. 2000. "Improved Synthesis of Small (dCORE ≈ 1.5 nm) Phosphine-Stabilized Gold

Nanoparticles." *Journal of the American Chemical Society* 122 (51):12890-12891. doi: 10.1021/ja002673n.

Willets, Katherine A., and Richard P. Van Duyne. 2007. "Localized Surface Plasmon Resonance Spectroscopy and Sensing." *Annual Review of Physical Chemistry* 58 (1):267-297. doi: 10.1146/annurev.physchem.58.032806.104607.

Xie, Wei, Li Wang, Yuying Zhang, Le Su, Aiguo Shen, Jinquan Tan, and Jiming Hu. 2009. "Nuclear Targeted Nanoprobe for Single Living Cell Detection by Surface-Enhanced Raman Scattering." *Bioconjugate Chemistry* 20 (4):768-773. doi: 10.1021/bc800469g.

Yang, C., J. Uertz, D. Yohan, and B. D. Chithrani. 2014. "Peptide modified gold nanoparticles for improved cellular uptake, nuclear transport, and intracellular retention." *Nanoscale* 6 (20):12026-12033. doi: 10.1039/C4NR02535K.

Yang, Xinmai, Erich W. Stein, S. Ashkenazi, and Lihong V. Wang. 2009. "Nanoparticles for photoacoustic imaging." *Wiley Interdisciplinary Reviews: Nanomedicine and Nanobiotechnology* 1 (4):360-368. doi: 10.1002/wnan.42.

Yee, Chanel K., Abraham Ulman, Julia D. Ruiz, Atul Parikh, Henry White, and Miriam Rafailovich. 2003. "Alkyl Selenide- and Alkyl Thiolate-Functionalized Gold Nanoparticles: Chain Packing and Bond Nature." *Langmuir* 19 (22):9450-9458. doi: 10.1021/la020628i.

Yguerabide, Juan, and Evangelina E. Yguerabide. 1998a. "Light-Scattering Submicroscopic Particles as Highly Fluorescent Analogs and Their Use as Tracer Labels in Clinical and Biological Applications: I. Theory." *Analytical Biochemistry* 262 (2):137-156. doi: https://doi.org/10.1006/abio.1998.2759.

Yguerabide, Juan, and Evangelina E. Yguerabide. 1998b. "Light-Scattering Submicroscopic Particles as Highly Fluorescent Analogs and Their Use as Tracer Labels in Clinical and Biological Applications: II. Experimental Characterization." *Analytical Biochemistry* 262 (2):157-176. doi: https:// doi.org /10.1006/abio.1998.2760.

Yu, C. X., H. Nakshatri, and J. Irudayaraj. 2007. "Identity profiling of cell surface markers by multiplex gold nanorod probes." *Nano Letters* 7 (8):2300-2306. doi: 10.1021/nl070894m.

Zagaynova, E. V., M. V. Shirmanova, M. Yu Kirillin, B. N. Khlebtsov, A. G. Orlova, I. V. Balalaeva, M. A. Sirotkina, M. L. Bugrova, P. D. Agrba, and V. A. Kamensky. 2008. "Contrasting properties of gold nanoparticles for optical coherence tomography: phantom, in vivo studies and Monte Carlo simulation." *Physics in Medicine & Biology* 53 (18):4995.

Zhang, Jian, Mark R. Langille, Michelle L. Personick, Ke Zhang, Shuyou Li, and Chad A. Mirkin. 2010. "Concave Cubic Gold Nanocrystals with High-Index Facets." *Journal of the American Chemical Society* 132 (40):14012-14014. doi: 10.1021 /ja106394k.

Zhang, L., Y. Li, D. W. Li, C. Jing, X. Y. Chen, M. Lv, Q. Huang, Y. T. Long, and I. Willner. 2011. "Single Gold Nanoparticles as Real-Time Optical Probes for the Detection of NADH-Dependent Intracellular Metabolic Enzymatic Pathways." *Angewandte Chemie-International Edition* 50 (30):6789-6792. doi: 10.1002 /anie.201102151.

Zhao, Yan, Waleska Pérez-Segarra, Qicun Shi, and Alexander Wei. 2005. "Dithiocarbamate Assembly on Gold." *Journal of the American Chemical Society* 127 (20):7328-7329. doi: 10.1021/ja050432f.

Zheng, Ming, Fredric Davidson, and Xueying Huang. 2003. "Ethylene Glycol Monolayer Protected Nanoparticles for Eliminating Nonspecific Binding with Biological Molecules." *Journal of the American Chemical Society* 125 (26):7790-7791. doi: 10.1021/ja0350278.

Zhou, Wang, Hao Cao, Xinghai Yang, Kan Cong, Wei Wang, Tianrui Chen, Huabin Yin, Zhipeng Wu, Xiaopan Cai, Tielong Liu, and Jianru Xiao. 2013. "Characterization of Nuclear Localization Signal in the N Terminus of Integrin-linked Kinase-associated Phosphatase (ILKAP) and Its Essential Role in the Down-regulation of RSK2 Protein Signaling." *Journal of Biological Chemistry* 288 (9):6259-6271. doi: 10.1074/jbc.M112.432195.

Zitzmann, Sabine, Volker Ehemann, and Manfred Schwab. 2002. "Arginine-Glycine-Aspartic Acid (RGD)-Peptide Binds to Both Tumor and Tumor-Endothelial Cells <strong>in Vivo</strong&gt." *Cancer Research* 62 (18):5139.

Zysk, A. M., F. T. Nguyen, A. L. Oldenburg, D. L. Marks, and S. A. Boppart. 2007. "Optical coherence tomography: a review of clinical development from bench to bedside." *Journal of Biomedical Optics* 12 (5). doi: 10.1117/1.2793736.

VITA

PERSONAL INFORMATION

Surname, Name: ÜÇÜNCÜ Melek
Nationality: Turkish (T.C.)
Date and Place of Birth: 01.07.1986, Gebze
Marital Status: Married
Phone: (+90) 543 535 33 14
E-mail: mlkzkn@gmail.com

EDUCATION

Degree	Institution	Year of Graduation
PhD	İzmir Institute of Technology	2018
MSc	Ege University	2011
BSc	Ege University	2008

PUBLICATIONS

1. Hakan Akat, Melek Ozkan, Expresspolymer Letters, 2011, 5(4), 318-326.
2. Yeliz Yıldırım, Buket Doğan, Sinem Muğlalı, Fehmi Saltan, Melek Özkan, Hakan Akat, Journal of Applied Polymer Science, 2012, 126(4), 1236-1246.
3. Hakan Akat, Melek Özkan, Fehmi Saltan, Asian Journal of Chemistry, 2012, 24(10), 4558-4562.
4. Melek Özkan, Hahan Akat, Asian Journal of Chemistry, 2012, 24(10), 4313-4316.
5. Fırat B. Barlas, Didem Ag Seleci, Melek Ozkan, Bilal Demir, Muharrem Seleci, Mutlu Aydin, Mehmet A. Tasdelen, Hadi M. Zareie, Suna Timur, Serdar Ozcelik, Yusuf Yagci, Journal of Materials Chemistry B, 2014, 2, 6412-6421.
6. Betul Unal, Esra Evrim Yalcinkaya, Sila Gumustas, Burak Sonmez, Melek Ozkan, Mehmet Balcan, Dilek Odaci Demirkol, Suna Timur, New Journal of Chemistry, 2017, 41, 9371.
7. Gokhan Yilmaz, Emine Guler, Caner Geyik, Bilal Demir, Dilek Odaci, Serdar Ozcelik, Melek Ozkan, Suna Timur, C. Remzi Becer, Molecular Systems Design & Engineering, 2017, 0,1-3.

CONFERENCES

1. International Symposium on CANCER NANOMEDİCİNE (November 2013), İZMİR
2. Advanced Materials World Congress (16-19 September 2013), İZMİR
3. VIII. Nanoscience and Nanotechnology Conference (25-29 Haziran 2012), ANKARA
4. 24. National Chemistry Congress (Haziran 2010), ZONGULDAK